Experimental Measurement of Graphite Wear in Helium at Elevated Temperatures and the Discrete Element Modelling of Graphite Dust Production Inside the Pebble Bed Modular Reactor

by

Charel Daniël Wilke

Thesis presented in partial fulfilment of the requirements for the degree of Master of Engineering (Mechanical) in the Faculty of Engineering at Stellenbosch University

Supervisor: Dr C Coetzee

Co-supervisor: Mr RT Dobson

March 2013

DECLARATION

By submitting this thesis electronically, I declare that the entirety of the work contained therein is my own, original work, that I am the sole author thereof (save to the extent explicitly otherwise stated), that reproduction and publication thereof by Stellenbosch University will not infringe any third party rights and that I have not previously in its entirety or in part submitted it for obtaining any qualification.

Date: .....

ABSTRACT

Experimental Measurement of Graphite Wear in Helium at Elevated Temperatures and the Discrete Element Modelling of Graphite Dust Production Inside the Pebble Bed Modular Reactor

CD Wilke

Department of Mechanical and Mechatronic Engineering,
University of Stellenbosch,
Private Bag X1, Matieland 7602, South Africa.

Thesis: M.Sc.Eng. (Mech)

March 2013

Production of graphite dust inside the Pebble Bed Modular Reactor (PBMR) influences the reactor operation negatively. Graphite is used as a moderator in the reactor core and the formation and transportation of graphite dust away from the reactor core decreases the amount of moderator which in turn has a negative impact on the reactor operation. High levels of radioactive dust may also contaminate reactor components which may pose a health risk to maintenance personnel.

In this study a pressure vessel was designed and used to measure the wear of a graphite pebble in helium at elevated temperatures. By means of a multi-linear regression analysis a proper mathematical function was established in order to relate graphite wear to certain tribological parameters. These parameters were identified through a literature study.

Discrete Element Modelling (DEM) was used to simulate the gravitational flow of graphite pebbles through the reactor core. The experimentally determined mathematical function was incorporated into the DEM simulation to estimate the annual mass of graphite dust to be produced by the PBMR pebble bed as a result of pebble-pebble interaction and pebble-wall interaction during refuelling.

UITTREKSEL

Eksperimentele Meting van Grafiet Slytasie in Helium by Verhoogde Temperature en die Diskrete Element Modellering van Grafiet Stof Produksie Binne die Korrel Bed Modulêre Reaktor

CD Wilke

Departement Meganiese en Megatroniese Ingenieurswese,
Universiteit van Stellenbosch,
Privaatsak X1, Matieland 7602, Suid-Afrika.

Tesis: M.Sc. Ing. (Meg)

Maart 2013

Die vorming van grafiet stof binne die korrelbed-modulêre reaktor (PBMR) beïnvloed die werking daarvan negatief. Grafiet word gebruik as 'n moderator in die reaktor kern en die vorming en vervoer van grafietstof weg van die reaktor kern lei tot 'n afname in die hoeveelheid moderator en dit het 'n negatiewe impak op die werking van die reaktor. Hoë vlakke van radioaktiewe grafietstof kontamineer ook reaktorkomponente wat 'n gesondheidsrisiko vir onderhoudspersoneel inhou.

In hierdie studie was 'n drukvat ontwerp en gebruik om die slytasie van 'n grafietkorrel in helium by verhoogde temperature te meet. 'n Multi-lineêre regressie analise is dan gebruik om 'n wiskundige funksie daar te stel wat die verband tussen grafietslytasie en die eksperimentele parameters vas stel. Hierdie parameters was met behulp van 'n literatuurstudie geïdentifiseer.

Diskrete Element Modellering (DEM) was gebruik om die gravitasionele vloei van grafietkorrels in die reaktor te modelleer. Die eksperimenteel bepaalde wiskundige funksie word in die DEM simulasie ge-inkorporeer om 'n skatting te maak van die jaarlikse massa grafietstof wat gevorm sal word in die PBMR korrelbed as 'n gevolg van korrel-korrel interaksie en korrel-wand interaksie gedurende hersirkulasie.

CONTENTS

Page Number

LIST OF FIGURES

Page Number

LIST OF TABLES

Page Number

NOMENCLATURE

Constants		[Unit]
A_{Bed}	Annular reactor area	[m^2]
b	Bulk shear strength	[Pa]
c	Inner and outer reactor wall pressure ratio	[]
$F_{pressure}$	Force due to pressure drop in core	[N]
g	Gravitational constant	[m/s^2]
H	Indentation hardness	[Pa]
k_{adh}	Archard's adhesive wear constant	[m^3/Nm]
k_{abr}	Archard's abrasive wear constant	[m^3/Nm]
k	Ratio of horizontal to vertical Pressure	[]
m_p	Pebble mass	[kg]
m_{bed}	Pebble bed mass	[kg]
$m_{pressure}$	Mass equivalent of pressure drop in core	[kg]
m_{total}	Total mass of all pebbles and pressure drop	[kg]
R_p	Pebble radius	[m]
V_{Bed}	Total pebble bed volume	[m^3]
υ	Relative contact velocity	[m/s]
v_s	Helium specific volume	[m^3/kg]

Variables

A_r	Real area of contact	[m^2]
a	Hertz contact radius	[m]
CR	Pebbles circulation rate	[/hour]
D	Effective reactor diameter	[m]
D_i	Reactor inner diameter	[m]
D_o	Reactor outer diameter	[m]
E^*	Effective Modulus of Elasticity	[GPa]
L	Normal load	[N]
P	Pressure	[Pa]
P_D	Helium pressure drop	[Pa]
P_e	Electric power output	[MWe]
P_H	Reactor horizontal pressure profile	[Pa]
P_t	Thermal power output	[MWth]
P_v	Reactor vertical pressure profile	[Pa]
R	Correlation factor	[]
R^*	Effective curvature	[m]
R_c	Asperity contact radius	[m]
R_G	Individual Gas Constant	[J/kgK]
S	Shear force	[N]
SF	Reactor geometry scale factor	[]
T	Temperature	[ºC]
t	Time	[s]
V	Worn volume	[m^3]
W	Wear extent	[g]

Variables

		[Unit]
x	Worn distance	[m]
z	Reactor height	[m]

Vectors

$\bar{b}$	Pebble centre global position	[m]
$\bar{c}_n$	Local contact position (normalized)	[m]
$\bar{c}$	Global contact position	[m]
$\bar{r}$	Pebble radius	[m]
$\bar{v}$	Pebble contact velocity	[m/s]
$\bar{\upsilon}_r$	Pebble contact relative velocity	[m/s]
$\bar{v}_{tl}$	Pebble contact translational velocity	[m/s]
$\bar{\omega}$	Pebble angular velocity	[rad/s]

Greek Letters

β	Abrasive grain angle	[º]
δ	Pebble deformation distance	[m]
ρ	Density	[kg/m^3]
ρ_p	Actual pebble density	[kg/m^3]
ρ_{Bed}	Modified pebble density	[kg/m^3]
μ	Dynamic Coulomb friction	[]
σ	Standard deviation	[]
σ_x, σ_y, σ_z	Principle stresses	[Pa]
τ	Average shear stress	[Pa]
τ_{max}	Maximum shear stress	[Pa]

1. INTRODUCTION

The Pebble Bed Modular Reactor (PBMR) is a fourth generation 400 MW_{th} High Temperature Gas Reactor (HTGR) and its core consists of side, centre, top and bottom reflectors. Figure 1 (b) illustrates the overall reactor layout. The most important component is the Core Structure Ceramics (CSC) which are manufactured of individual graphite blocks. The main function of the CSC is to protect the metallic components from high temperature neutron fluency levels and support the weight of fuel spheres ('pebbles'). The PBMR utilizes 450 000 low enriched uranium TRIple coated ISOtropic (TRISO) pebbles (J. Slabber, 2006).

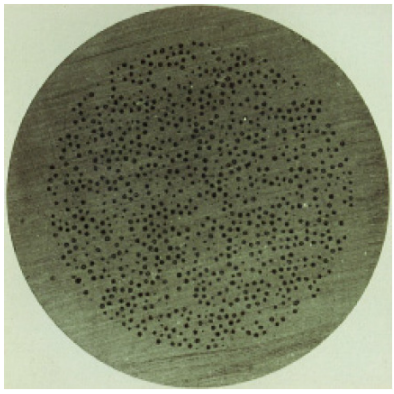

(a) - Section of PBMR fuel sphere (Hrovat and Grosse, 2006)

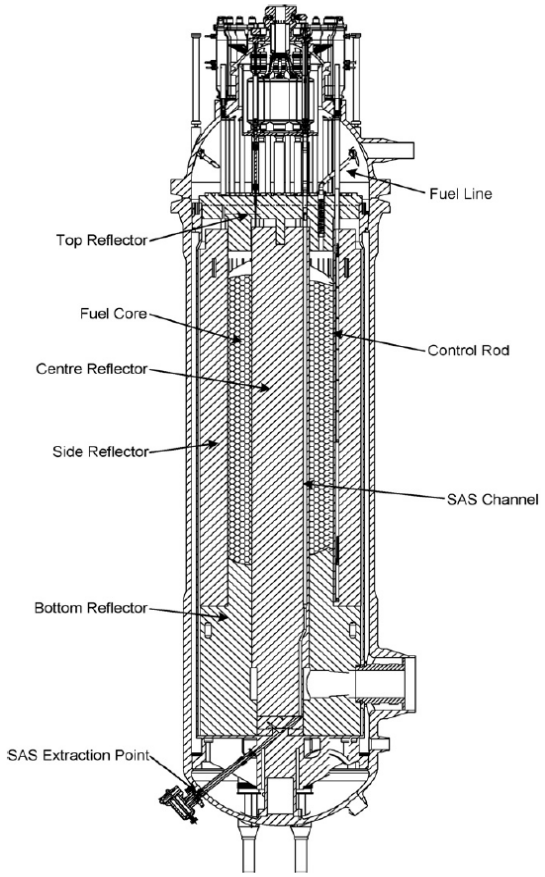

(b) - PBMR layout (Mitchell and Polson, 2006)

Figure 1: PBMR fuel sphere and the PBMR layout

The 60 mm diameter pebbles, as shown in Figure 1 (a), are made of a A3-graphite matrix. Each pebble consists of a 5 mm thick shell and 50 mm diameter core. The shell and core graphite are identical and consists of mostly natural graphite (72.9%), petroleum coke (18.2%) and binder coke (9.1%). The fabrication of these pebbles consists of moulding and different heat treatment stages. Resinated graphite matrix powder and coated fuel particles are moulded together which is treated with a first stage of heat treatment (few hundred degrees) to ensure the correct quality. After the pebble is compacted, the graphitization process is established by the second heat treatment stage (up to 3000ºC). The second heat treatment ensures dimensional stability and mechanical integrity. The pebbles are moulded in a silicone die to obtain the required isotropic and crystalline structure. Lastly the pebbles are moulded in vacuum in a third rubber die to the required density of 1730 kg/m^3 (Hrovat and Grosse, 2006) . The pebbles in the cavity of the reactor are constantly in motion during cyclic refuelling. Since the outer shell of the pebbles are in contact, friction and wear generates graphite dust.

The German Arbeitsgemeinschaft VersuchsReacktor (AVR) operated from 1960 for 21 years during which time 3 kg of graphite dust per Full Power Year (FPY) was produced. Another pebble bed reactor, the Chinese Thorium High Temperature Reactor-300 (THTR-300) operated between 1983 and 1988 and produced 16 kg of dust per FPY of which 6 kg was produced in the core (Wahsweiler, 1989). The presence of graphite dust in a reactor is undesirable for a number of reasons.

Accumulation of dust particles in the heat exchanger and other equipment in the primary circuit of the reactor may disrupt regular maintenance and hinder proper function (Luo *et al*., 2004). Also, dust particles act as sites for the accumulation of radioactive fission products. Since these dust particles are mobile, it is a potential safety issue in the case of a de-pressurisation accident. Not only are these dust particles radioactive fission product carriers, but would burn when it reacts with the oxygen or water which ingress into the reactor. Furthermore, the decrease in moderator in the reactor core due to the graphite dust being carried away by the coolant is another reason why the formation of graphite dust is undesirable. The moderator to fuel ratio plays an important role in the criticality of the reactor. If the moderator is decreasing, the power output will fluctuate. Lastly, due to the severe wear of graphite pebbles it may be rejected by the fuel handling system and in turn prevent the fuel from being fully utilized (Slabber, 2006).

The Fuel Handling and Storage System (FHSS) performs all the required fuel manipulation. It is responsible for the initial loading of the reactor core with pebbles, replacing the graphite pebbles with a mixture of fuel and graphite pebbles during the initial start-up and loading fresh fuel pebbles to replace spent fuel. The circulation of the spheres are established by partly gravitational flow and pneumatic conveying processes using helium. The fuel spheres are re-circulated through the core for up to six times before they reach their maximum burn-up.

Thereafter the fuel spheres are discharged to the spent fuel storage tanks (Slabber, 2006). The FHSS occupies the following building spaces (Slabber, 2006):

- Beneath the Reactor Pressure Vessel (RPV) three reactor Core Unloading Devices (CUD) are located.
- A sloping floor above the RPV where the burn-up measurement and fuel management stations and helix are located.
- Pneumatic sphere lifting lines located in a vertical shaft.
- Above the helix the fuel and graphite replenishment equipment are situated.
- The spent and used fuel and graphite tanks are located next to the reactor cavity.

During reactor start-up the Core Loading Subsystem (CLS) loads the reactor core with graphite pebbles. The CLS also prevents the graphite spheres from being damaged by dropping them from an unacceptable height onto the core graphite structures. During the commissioning of the reactor, the RPV is open to the atmosphere. The start-up core consists of a mixture of graphite and fuel which is loaded under helium pressure on top of the graphite core while graphite spheres are removed from the bottom of the RPV on a one sphere to sphere basis. The CLS also makes provision for different fuel sphere to graphite sphere ratios which allows the reactor to have different enrichment levels. It is estimated that the helium pressure drop over the core will be approximately 3.2 bar. One of the reasons why helium is used as the primary coolant is due to the fact that it is inert which minimizes reactor component radioactive contamination (Slabber, 2006).

During normal operation the Sphere Circulation Subsystem (SCS) circulates the fuel and graphite spheres when it is in equilibrium mode. The three CUDs which acts as three chutes at the bottom of the RPV, also has the capability of separating damaged or undersized spheres from the reactor core. The spheres are transported from the CUDs to the top of the reactor pneumatically after it passed through the Activity Measurement System (AMS) to distinguish fuel from graphite and to measure the burn-up rate of each sphere. After the spheres have reached their maximum burn-up, it is transported to the spent fuel storage tanks. Other processes such as defueling and refuelling can occur during unplanned maintenance. During defueling the fuel spheres are removed from the core and replaced with graphite spheres. Refuelling is the reverse process whereby fuel spheres are placed inside the core (Slabber, 2006). Figure 2 illustrates the simplified fuel handling system and Table 1 shows the PBMR specifications. Due to refuelling the production of graphite dust during the operation of the PBMR is unavoidable and for this reason it is important to study the tribological behaviour of graphite.

Table 1: PBMR specifications (Slabber, 2006)

P_t	450 MWth
P_e	165 MWe
Coolant	Helium
Coolant Pressure	9 MPa
Coolant Pressure Drop over Core	3.2 bar
Helium Inlet Temperature	500ºC
Helium Outlet Temperature	900ºC
Hourly Circulation Rate	500-1100
Daily Operation Time	8-12h
Fuel Feeding Points	3
Fuel Defueling Points	3

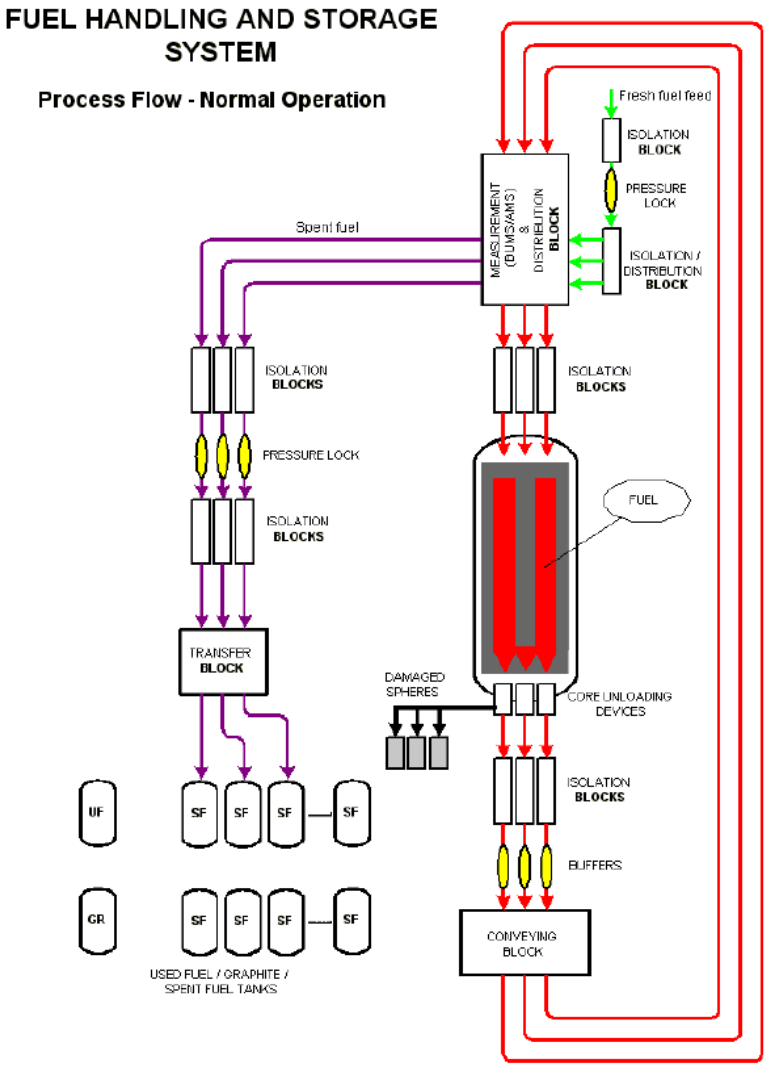

Figure 2: PBMR fuel handling and storage system layout (Slabber, 2006)

The first objective of this thesis is to identify the important aspects relating different tribological parameters to graphite wear through a literature study. Friction is influenced by the material and surface contact properties, which in turns influences the wear mechanisms and wear regimes. The results of a number of researchers are compared to determine the general trends in the literature. Wear is also affected by the effects of environmental conditions such as temperature, pressure, gas and gas impurities. Mechanical aspects such as load, speed, type of contact (rolling and sliding contacts) are also discussed. Radiation effects will not be considered in this thesis.

The second objective is to determine the necessary experimental requirements and specifications by means of a functional flow chart and House of Quality (also known as QFD). By means of a DEM simulation of an annular reactor filled with pebbles and Janssen's theory of pebble bed mechanics, the average load on a pebble will be specified. The contact velocity between pebbles during circulation will also be determined by the DEM simulation.

The third objective is to perform an experiment to obtain tribological data which will be used to perform a multi-linear regression analysis. From this analysis an empirical equation will be developed to capture effects of the tribological parameters on graphite wear. This equation will be incorporated into a DEM simulation.

The fourth objective is to create a DEM model which will simulate pebble motion and interaction during refuelling. This simulation will be used to predict the amount of graphite that is expected to accumulate in the reactor during a FPY.

2. LITERATURE STUDY

Friction and wear of different materials have been investigated extensively. Although much is known about these surface interaction phenomena, even today there is still uncertainty as to what the precise mechanism on a micro scale is to cause friction and wear. The relationship between these two quantities may also vary for different materials and reasons for this are unknown. What is known is that generally whenever one changes there is a change in the other. Contrary to belief, high friction can lead to a low wear rate (such as certain ceramics) or low friction may induce a high wear rate (certain solid lubricants and polymers) (Bhushan, 2000). Friction in general can be seen as the resistive force at the contact between two bodies due to the micro level surface effects such as adhesion and mechanical deformation by asperities (micro surface peaks and valleys) (Bayer, 1994). Wear of a material implies the physical detachment of a particle from a surface by means of fracturing and shearing. Due to the complexity of friction and wear of graphite, both will be addressed in different sections. These two quantities are both influenced by the material structure of graphite.

2.1 Graphite Structure

Graphite is a layered lattice material, typically as a hexagonal structure as shown in Figure 3. Large sheets of strongly bonded atoms form, in which the electrons are fairly mobile. The bonds between the layers are weaker than the bonds between the atoms in the sheets. The spacing between the sheets is also larger than between the atoms in the sheets. This structure results in an anisotropic material in which the shear strength is low in the a direction (parallel to the layers), and high in the c direction.

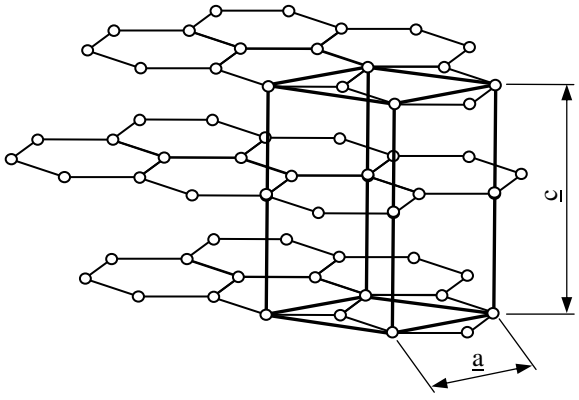

Figure 3: General graphite structure

The degree of isotropy can be influenced by the manufacturing process. During extrusion the graphite crystals will be aligned in the direction of extrusion. For another process the direction of the crystals may be in a different direction. If very small crystals with a random orientation are dominant, such as 'glassy' carbons, a fairly isotropic bulk material is obtained (Nightingale,1966). For extruded graphite Driesner and Wagner (1958) found that the anisotropy did not have a significant influence on the friction unless the size of the contact area was in the order of individual crystal size. As the areas of contact in PBMR applications are much larger than this, the bulk material can be treated as isotropic.

2.2 Friction

When two surfaces come into contact with one another, friction and wear are induced and therefore these quantities are essentially a study of the interaction between two mating surfaces. On a macro scale surfaces may appear to be smooth and continuous and therefore if two surfaces are brought into contact, the contact area is known as the apparent area. On a micro scale asperities and troughs occur and form localised points (or junctions) in the contact area. The real area of contact is the sum of all these junctions. Therefore the real area is only a part of the apparent area of contact and is much smaller. The real area of contact A_r can be determined as follows,

$$A_r \geq \frac{L}{H} \tag{2.1}$$

The indentation hardness H and the normal load L is sufficient to determine the real area of contact when ideally plastic deformation is assumed. Since hardness is in most cases constant for a given material, the real area of contact depends on the normal load and is independent of the apparent area. The real area of contact is also influenced by the distribution of asperities, material properties and contact geometry.

A simplified theory such as Coulomb friction assumes that only the normal and induced shear force S determines the friction coefficient μ. This equation is widely used but is only an approximate model (Bayer, 1994). It is given as,

$$S = \mu L \tag{2.2}$$

The shear force S is also determined by the average shear stress τ over the real area of contact,

$$S = \tau A_r \tag{2.3}$$

The average shear stress cannot exceed the bulk shear strength b. Therefore

$$S = bA_r \tag{2.4}$$

Combining equations (2.1), (2.2) and (2.4) leads to

$$\mu = \frac{b}{H} \tag{2.5}$$

Equation (2.5) shows how the friction coefficient could be dependent on the material properties. It is only an estimate since elastic deformation occurs at the junctions. The bulk shear strength can also be influenced by the solubility and cleanliness of the surface. In most cases the friction coefficient during sliding is lower than during static conditions. This is a result of junction growth which can occur under static conditions (Rabinowicz, 1995). In this thesis the kinetic coefficient of friction is implied unless otherwise stated.

2.3 Wear Mechanisms

The nature of junctions between the two surfaces and the manner in which they are formed and broken determines the type of wear that occurs. The main mechanisms of wear relating to this investigation are briefly described in this section.

2.3.1 Adhesive Wear

When two surfaces make contact at a junction, the attractive forces between the surface atoms create an adhesive bond at the junction. If some path through the bulk material exists which requires a smaller force to cause fracture than is required to break the adhesive bond at the junction, a fragment will be pulled away from one of the surfaces, as shown in Figure 4. This adhesive wear particle may then remain bonded to the new surface, or be broken off at a later stage to form a loose particle. The loose particle may re-bond to either surface at a different position or be lost from the system.

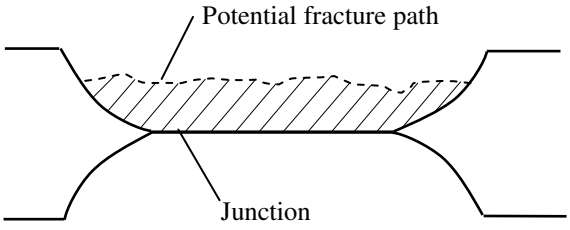

Figure 4: Adhesive Model

Considering the plastic deformation at an asperity contact, where the contact radius is R_c and the volume of the detached particle is assumed to be hemispherical in shape. The elemental normal force dL and volume dv is given by,

$$dL = \pi R_c^{\,2} H \tag{2.6}$$

$$dv = \frac{2}{3} \pi R_c^{\,3} \tag{2.7}$$

The elemental distance dx travelled to shear such a particle is given by,

$$dx = 2 R_c \tag{2.8}$$

Combining these equations gives,

$$\frac{dv}{dx} = \frac{1}{3}\frac{dL}{H} \tag{2.9}$$

Integrating equation (2.9), the volume of material removed during adhesive wear is given by Archard's equation (Rabinowicz, 1995),

$$V = \frac{k_{adh} L x}{H} \tag{2.10}$$

where k_{adh} is a constant representing 1/3 of the probability that an adhesive wear particle will be formed. The value of k_{adh} is influenced by several parameters including the compatibility of the materials in contact, the surface energy at the junction as well as the nature of the asperity contact and load distributions (Bayer, 1994). This value can vary by orders of magnitude as the normal load is increased and is usually determined from experimental wear data. Archard's equation is based on the assumption that there is a constant probability that an adhesive particle will be formed each time a junction is plastically deformed. In addition, all the fragment and junction diameters are the same and k_{adh} is independent of the junction size. The value of k_{adh} depends on the ratio of adhesive strength and cohesive strength of the junction (Rabinowicz,1995).

2.3.2 Abrasive Wear

Abrasive wear occurs when a hard material cuts into a softer surface and ploughs away a series of grooves. This type of wear is usually divided into *two-body* abrasion, where the asperities on a hard, rough surface cut into the softer surface (Figure 5), or *three-body* abrasion, where hard loose particles are present between two surfaces. These particles adhere to or become embedded into one of the surfaces and plough into the other.

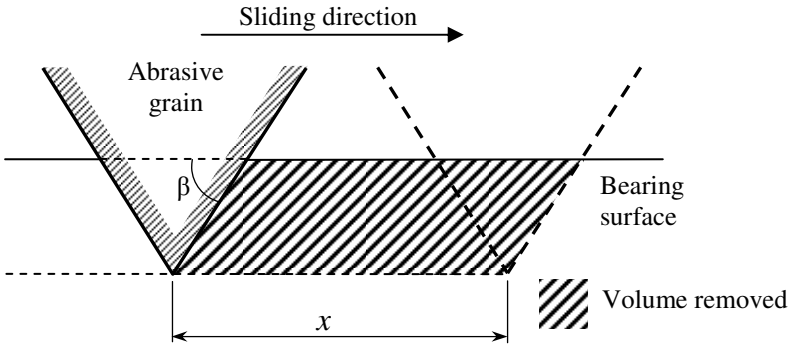

Figure 5: Two body abrasion model

Assuming the material yielded under the normal load (with of groove = 2 R_c for canonical asperity),

$$dL = \pi {R_c}^2 H \tag{2.11}$$

The volume displaced in a distance x at an angle β is,

$$dv = {R_c}^2 x \tan\beta \tag{2.12}$$

Combining equations (2.11) and (2.12) gives,

$$V = \frac{Lx\tan\beta}{\pi H} \tag{2.13}$$

This equation can also be written in the general form which is similar to Archard's equation (Bayer, 1994),

$$V = \frac{k_{abr} L x}{H} \tag{2.14}$$

In the above the constant k_{abr} is dependent on the physical average angle of the asperities in the harder surface β as well as material properties and the probability of wear. Again this must be determined experimentally.

2.3.3 Surface Fatigue Wear

Surface fatigue wear is takes place when two surfaces interact with each other during repeated cyclic loading. It is closely related to the general fatigue phenomenon in that there exists a direct correlation between the subsurface stresses developed during cyclic loading and the number of cycles to produce fracture. These subsurface stresses induce cracks which may propagate to the contact surface producing loose particles and resulting in fatigue wear. The subsurface stress is strongly dependent on the type of contact between two bodies. In general this contact can be one of two types namely a conforming or nonconforming contact and is illustrated in Figure 6.

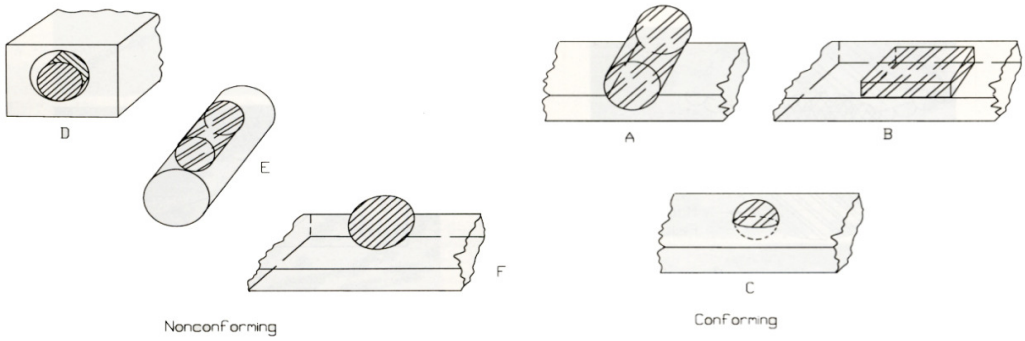

Figure 6: Conforming and nonconforming contacts (Bayer, 1994)

The maximum shear stress during a nonconforming contact is situated just below the surface and is located in the centre of the contact, as determined by the Hertz theory.

A nonconforming contact may become conforming during the wear process during which the location and distribution of subsurface stress and cracks may change as the apparent area is increasing (Bayer,1994).

2.4 Wear Regimes

Graphite is in general considered to be an excellent solid lubricant. It was found (Ramadanoff and Glass, 1944) however that under extreme sliding conditions or in very dry environments much higher friction was observed. This high friction was accompanied by a transition from the mild wear regime to a severe wear condition, called *dusting* wear due to its characteristic fine wear particles.

2.4.1 Mild Wear Regime

Graphite is widely used as a lubricant due to the fact that when operating in normal atmospheric conditions and at moderate sliding speeds it remains in the low friction/mild wear regime. This friction behaviour of graphite is governed by the bond structure of the crystal lattice. The bonds between atoms in the basal planes are strong, with relatively low interaction with adjacent surfaces. At the edges of the planes the atoms exhibit 'dangling' bonds, resulting in active edge sites. These increase the free surface energy and in turn the strength of adhesive interaction with the surface. The effects of these active edge sites can be reduced by mechanical actions which cause the alignment of the surface crystals parallel to the surface, making the edge sites less available for bonding. The free surface energy is also reduced by the presence of active gases such as water vapour or oxygen.

The reaction of the graphite surface to the presence of these active gases (oxygen, hydrogen and water vapour) is the foundation of the mild wear regime. Zaidi *et al.* (1990) explain this phenomenon by means of the 'reservoir' model. In this model two layers of active gas come into play (Figure 7). The first is a *chemisorbed* layer which consists of gas atoms (or molecules) chemically bonded to the active edge sites, passivating these sites and reducing the surface energy. The second layer is a loosely bonded and more mobile *physisorbed* layer. As the chemisorbed later is damaged or removed due to wear, the physisorbed layer acts as a 'reservoir' from which new gas atoms can move to quickly passivate the newly exposed edge sites. In this way the combination of the two layers maintains the low friction state.

Of the atmospheric gases, water vapour has the strongest affinity for passivation of the edge sites, and it is only in very dry conditions that it is not available in sufficient amounts to maintain the mild wear regime, provided the sliding speeds

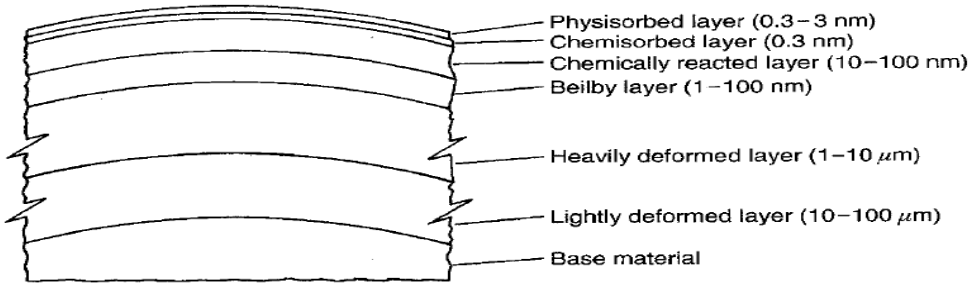

Figure 7: Graphite micro-surface layers (Bhushan, 2000)

remain moderate. Dry air, H_2, N_2 and inert gases are unable to prevent the transition to the *dusting* wear regime under atmospheric conditions. O_2 and CO_2 can prevent dusting, but only if they are present at partial pressures higher than those usually found in air (Lancaster and Pritchard, 1980). When the conditions that allow the passivation of a sufficient number of the active edge sites are no longer maintained, the mild wear regime ends and the severe wear regime is entered.

2.4.2 Dusting Wear Regime

The severe wear regime of graphite is known as *dusting* wear due to the roughening of the surface that occurs at the transition which results in the production of very finely divided wear particles. This is attributed to a change from elastic deformation of the asperities during mild wear to brittle fracture during dusting. The friction coefficient increases into the range of 0.5-1.0 and the wear rate to typically 10^2-10^3 times that observed in the mild wear regime (Lancaster and Pritchard, 1980). The transition is usually induced by an insufficient amount of active gas being present. At higher temperatures, higher partial pressures of active gas are needed to maintain mild wear, so an increase in sliding speed, which increases the surface temperature, can also cause the transition.

Lancaster and Pritchard (1980;1981) investigated the dusting wear regime of graphite in some detail. The transitions between mild and dusting wear with increasing and decreasing sliding speeds observed in their experiments are illustrated in Figure 8. As can be seen, the sudden transition to dusting at 7.8 m/s is indicated by the abrupt increase in the friction factor. It is interesting to note the large amount of hysteresis in the transition back to mild wear as the speed is decreased.

During the dusting wear regime an increase in the amount of active gas present (but still at a level below that required to prevent dusting) will cause an increase in the wear rate.

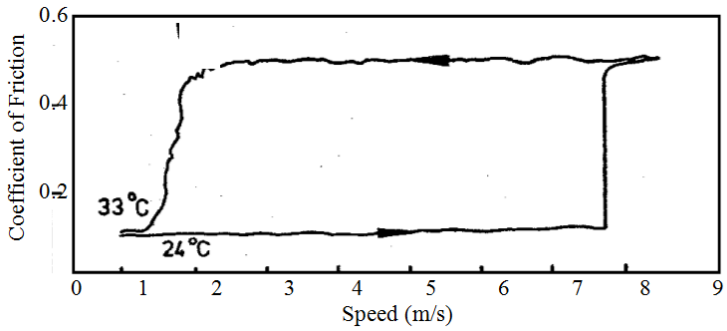

Figure 8: Hysteresis of friction coefficient during dusting regime (Lancaster and Pritchard, 1980)

It is postulated by Lancaster and Pritchard that this is due to the presence of these gases promoting micro-cracks in the bulk structure via a 'wedging' action as the gas molecules bond with the active sites inside existing surface cracks. The size and shape of particles formed at higher partial pressures of active gases (flake-like and of the order 1 μm in size as opposed to roughly spherical 0.1 μm particles usually associated with dusting wear), supports the above theory. In their work it was also found that wear increases with increasing chain length of hydrocarbon gases. Longer chain hydrocarbons have higher adsorption energies on graphite, which implies that the higher the adsorption energy of a gas, the more it will promote an increase in wear rate during dusting. When the extra energy required to propagate the crack further is balanced out by the reduction in surface energy due to passivation of the site, equilibrium is achieved. Thus the lowest rate of wear during the dusting wear regime is maintained in a vacuum or an inert gas.

From a number of experiments Lancaster and Pritchard came to the conclusion that the total contact temperature is the most influential parameter in the transition to dusting as it directly determines the amount of an active gas needed to prevent dusting. The total contact temperature is the combination of the ambient temperature and the heat generated by friction. In these experiments the frictional heat was dominant due to the high sliding speeds. This may not be the case at higher ambient temperatures and lower speeds.

2.5 Effect of Mechanical Conditions on Wear

The reaction of graphite to lower sliding speeds and/or higher environmental temperatures has been investigated by other researchers, and will now be discussed.

2.5.1 Normal Load

Driesner and Wagner (1958) evaluated the coefficient of friction for various types of graphite experimentally by measuring the frictional force generated for a given normal load. The normal load and area of contact were varied in order to investigate the effects of changing load and contact stress on the value of the coefficient of friction. It was determined that in the tested range of stress (around an average value of 1.7 MPa) neither of these parameter changes had any noticeable effect on the value of the friction coefficient (at room or elevated temperatures). This is in agreement with the basic wear theory.

Lancaster and Pritchard (1980) investigated the effect of changing the load while the dusting wear regime (Section 2.4.2) was maintained. They determined that the coefficient of friction showed a slight increase, but the wear rate remained essentially constant over the range 1- 60 N, as shown in Figure 9 below. Note that the wear rate is normalised with respect to load and sliding distance, so the constant wear rate indicates a wear volume proportional to L and x. This means that k is constant and equation (2.14) is valid for this range of loads.

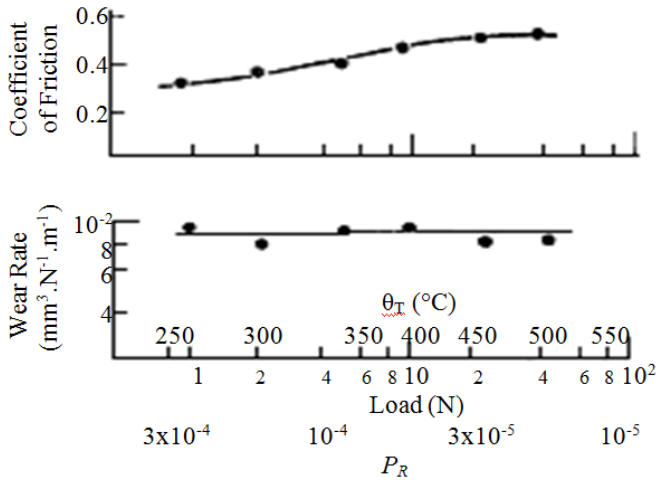

Figure 9: Effect of normal load on wear rate and friction coefficient (Lancaster and Pritchard, 1980)

Luo *et al*. (2004) investigated wear between two graphite specimens. Their experiments were performed at room temperature, in air, at speeds below 1 m/s and at a range of loads. The results are given in Figure 10 below. The upper and lower values indicate the wear for the upper (moving) and lower (stationary) test pieces. Initially the wear rate is high and after approximately 160 m steady state conditions are achieved.

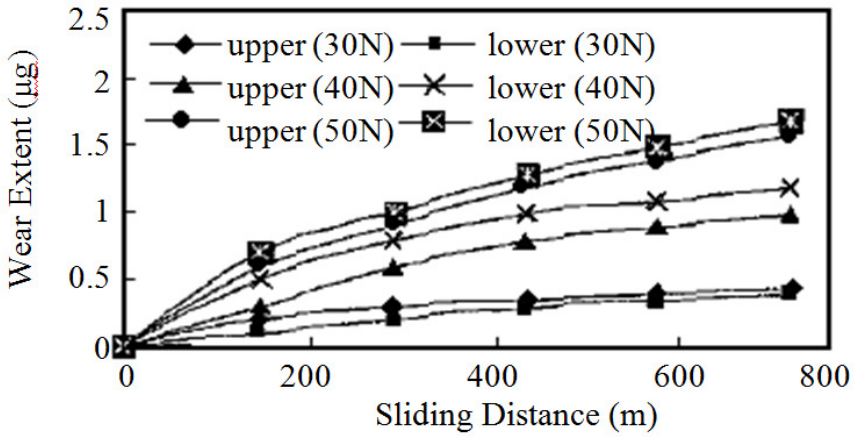

Figure 10: Effect of sliding distance on wear for different loads (Luo, *et al*., 2004)

Robert *et al*. (1995) performed experiments in which the wear properties of graphite in inert environments were investigated at a high load of 20 N and a low load of 4 N. It was found that in an inert gas environment, as the load decreased, the wear mechanism changed from abrasive (dusting) wear to a fatigue dominated regime. At the low load a reduction in both friction and wear rates occurred due to mechanical alignment of the surface basal plates of the graphite, even though no passivation processes occurred.

At the higher load abrasive wear occurs, but it was noted that the particles produced were large, which is not typical for the dusting wear observed in air or a vacuum. It may be that the helium promotes crack growth in a similar way to what Lancaster and Pritchard postulated water vapour does, by inserting into existing micro-cracks, producing larger wear particles.

2.5.2 Velocity

Lancaster and Pritchard (1980) investigated the effects of increasing the sliding speed to values of the order of 10 m/s, which induced the transition to dusting. At these speeds the heat generated by the friction becomes a very relevant factor to the friction and wear behaviour, as discussed in Section 2.4.2. As these higher speeds are not likely to occur inside the reactor, testing performed at lower velocities is more representative of the pebble movement.

2.5.3 Contact Type

In addition to speed and load, the manner in which contact is made has an influence on the friction and wear properties. Factors to be considered when discussing the type of contact include the shape(s) of the contacting surfaces, the type of movement between the surfaces and whether the contact is between like or unlike materials.

Driesner and Wagner (1958) found in their experiments that changing the area of contact between graphite specimens did not have any noticeable effect on the value of the friction coefficient (at room or elevated temperatures), unless the contact area was reduced until it approached the grain size of the graphite. If this occurred the anisotropy in the material began to influence the friction. This is in agreement with the simplified models of friction.

In experiments performed by Sheng *et al*. (2003) the effect of the shape of the contacting surfaces was investigated by comparing surface contact wear condition to a line contact condition. The surface contact was produced by means of the end surface of a cylinder rotating against a stationary surface. It was found that at a normal load of 31 N a wear rate of $2.27 \cdot 10^{-7}$ g/m was produced for surface contact, which was some 5 times smaller than for line contact at the same load. They attributed the difference to the lower contact pressure caused by the larger surface area at surface contact, as well as the fact that the sliding velocity was lower for the surface contact (0.54 m/s) than for the line contact (0.78 m/s).

Their findings thus indicate a wear rate dependent on area and/or velocity, which implies the simple models for wear do not hold under their experimental conditions. This trend does concur with the dependence of the coefficient of friction on velocity observed by Luo *et al*. (2004), as discussed in the previous section. The coefficients of friction for the work by Sheng *et al*. (2003) were not reported. The shape of wear particles indicated a combination of fatigue and abrasive wear as the dominant mechanisms. The particles produced were larger than the fine particles usually associated with dusting wear. From this and the fact

that sliding occurred in air it is expected that for these experiments the mild wear regime was maintained.

In addition to material and geometric effects, the type of motion will also influence the friction and wear. In the reactor both sliding and rolling contacts are expected. All the graphite research reviewed here deals with sliding contacts, as no work specifically referring to rolling between graphite surfaces was found. From the general theory, rolling contacts fall into the category of low friction contacts, with coefficients of friction usually < 0.1 (Bayer, 1994). This friction arises because even in pure rolling a small amount of sliding, on a micro-scale, occurs. This creates adhesive forces and results in a small amount of friction and wear.

A final consideration when dealing with the type of contact is the possibility of chemical reactions between the contacting surfaces. Semenov (2005) noted that the friction between graphite and some ceramics was observed to decrease dramatically due to chemical reactions at high temperatures. These reactions produced oxygen, thereby providing a means for the passivation of the active sites in the graphite. This reaction occurs between graphite and metals containing eutectic carbon. As the eutectic temperature is reached the graphite melts together with the metal to form an alloy of eutectic composition.

The reaction mentioned above occur at high temperatures, but are very specific to the type of material against which graphite slides. The general effects of the environment of the graphite itself will be considered next.

2.6 Effects of Environmental Conditions on Wear

2.6.1 Temperature

Early work relating to the temperature effects on graphite frictional behaviour was performed by Driesner and Wagner (1958), whose aim was to experimentally determine the static and kinetic coefficients of friction at elevated temperatures. The testing was performed in the test section of a furnace, using Graph-i-tite G type graphite and over a temperature range of 25 °C to 2450 °C. It was found that the kinetic friction coefficient increased from 0.2 at 25 °C to 0.4 at 2450 °C and that the static friction coefficient increased from 0.35 to 0.65. The experiments at room temperature were performed in air, while those at elevated temperatures were performed in flowing helium in order to prevent oxidation of the graphite.

Li and Sheehan (1981) investigated sliding friction and wear of graphite at temperatures from ambient to 850 °C in air, pure helium and HTGR helium (pure

helium with a controlled amount of impurities added to simulate reactor conditions). The steady state friction coefficient of the graphite was found to be high at room temperature in all environments, lowest at 450 °C in the two helium environments, with a slight increase from this value at 850 °C, with values at each indicated in Figure 11.

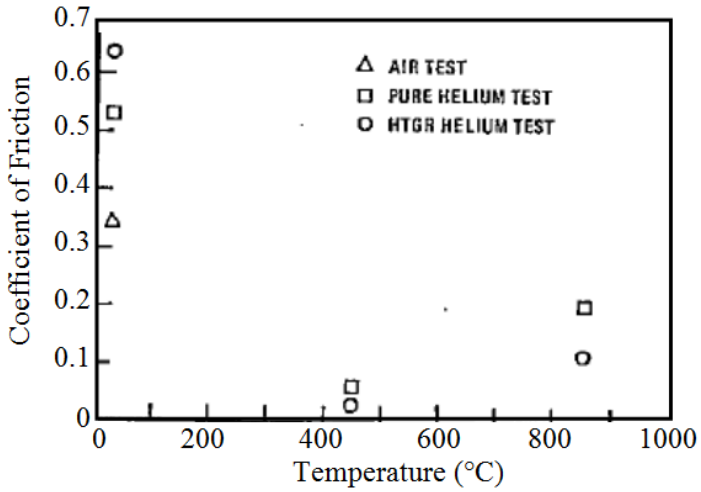

Figure 11: Effect of temperature on coefficient of friction (Li and Sheehan, 1981)

Cachon and Falcand (2008), performed tests using PCEA and NBG-17 graphite in helium with controlled impurities to represent the HTGR environment. Their results also exhibit a drop in frictional coefficient with an increase in temperature, as shown in Figure 12. In spite of the drop in friction, there is an increase in wear rates due to weakening of the surface bonds. This weakening may be caused by the temperature alone (as found by Semenov (1995)), or may be a result of interaction with the environmental gases. A more detailed investigation of the environmental gas effects is needed.

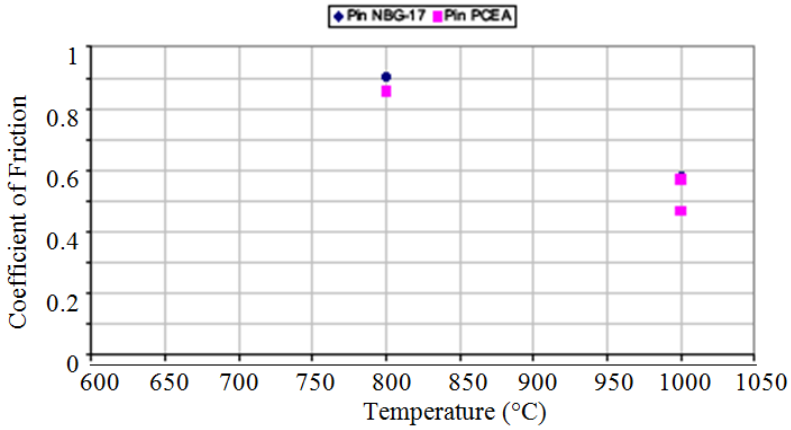

Figure 12: Effect of temperature on the coefficient of friction (Cachon and Falcand, 2008)

2.6.2 Environmental Gas

The friction and wear properties of graphite are influenced by the type of gas in which the wearing action is occurring, as well as by the overall pressure and the concentrations of any impurities present. As has been established, the mild friction and wear regime of graphite exists under atmospheric conditions, usually due to the presence of a sufficient amount of water vapour. Under these conditions a frictional coefficient of 0.2 is typical.

The severe dusting wear regime is observed in a vacuum with frictional coefficients in the range of 0.55 - 1.0 (Lancaster and Pritchard, 1980) at ambient temperatures. Both Lancaster and Pritchard (1980) and Semenov (1995) report no noticeable difference in friction between vacuum and inert gas environments under atmospheric conditions.

Kichuki *et al.* (1984) performed friction and wear testing on graphite PGX at 1000 °C and pressures of 2.0 MPa and 4.1 MPa, in helium. Various controlled amounts of impurities were added and the effects observed. The coefficient of friction varied between 0.3-0.7 in pure helium, before settling at 0.4, which is consistent with the friction expected in the dusting wear regime.

Li and Sheehan (1981), however, found that at higher temperatures the coefficient of friction for wear in pure helium and HTGR helium was lower than that expected for dusting wear in vacuum or even air. The frictional forces measured in pure and HTGR helium are compared in Figure 13 (at ambient, 450 °C and 850 °C). The steady state friction coefficient of the graphite was found to be high at room temperature and reached its lowest value, in the range of 0.03, at 450 °C in

both environments, with a slight increase from this value at 850 °C. The low friction at the mid-range temperatures is attributed to the graphite having a maximum affinity for chemisorbtion of impurities in this temperature range which reduces the surface energy of the graphite. At high temperatures the impurities are not as readily chemisorbed, but oxidation occurs which has a similar effect on the surface energy, resulting in the only slightly higher friction coefficients. This accounts for the slightly lower values measured in the HTGR helium compared to the pure helium. It does not fully explain the low results obtained at 450 °C in the pure helium test as this has neither oxygen nor impurities in significant amounts.

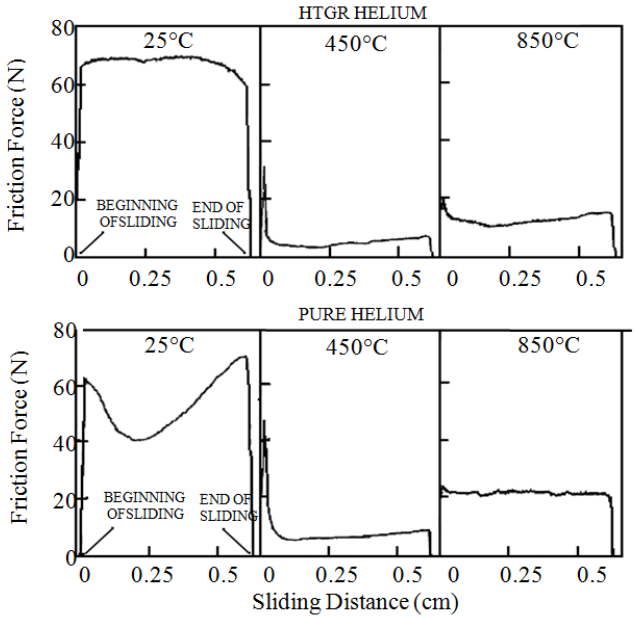

Figure 13: Steady state friction curves for pure and HTGR helium environments (Li and Sheehan, 1980)

Zaidi *et al.* (1995) observed a low friction condition in pure inert gas environments and suggested that although these gasses do not deactivate or oxidise the surface, a lubrication effect is achieved by the insertion of the gas atoms between crystallites which increase the crystallite mobility. This allows the basal planes to align parallel to the surface, reducing the number of exposed active sites and thus reducing the surface energy and frictional coefficient.

Now that all important tribological parameters have been identified, the specifications for the experimental design will be developed.

3. PRESSURE VESSEL DESIGN

3.1 Specification Development

The availability and cost of the latest tribological technology was researched and a conclusion was reached. Although current technology does exist to sufficiently test the wear behaviour of graphite at high temperature in helium, the cost of this technology is too high and therefore a system will have to be designed which will be much cheaper to design and manufacture and can still conform to specific design requirements.

The most common and preferred abrasion test is known as the pin-on-disk setup (Lancaster & Pritchard (1980), Zaidi *et al* (1990) and Robert *et al* (1995)). In this setup the pin and disk are made of the same material under investigation. For this system the force and speed at the contact can be easily controlled. Two ways to apply the load is by means of a hydraulic piston or a moment arm with weights attached to it. The concept of a moment arm was chosen since the PID control on the hydraulic valve could not yield the required force accuracy. The speed would be controlled accurately with a stepper motor.

The challenging part of this specific design is to perform the test in an environmental chamber such that the surrounding environmental gas is helium. The necessary mechanical seals will have to be used to at least minimize the helium leakage which is to be expected since helium is a low density gas. It must also be possible to vary the temperature at the point of contact in between tests and during tests the high ambient temperature must be kept constant. In the pin-on-disk setup one graphite specimen will be fixed. A thermocouple will be inserted into this specimen to measure the graphite surface temperature. A PID controller together with all the necessary hardware will be used to adjust the graphite specimen temperature as required. The environmental chamber will also have to be insulated to minimize heat loss. Figure 14 illustrates the simplified design concept with the component descriptions given in Table 2.

From Figure 14 it is clear that when the lateral position of the weights is adjusted, so does the amount of force applied to the axial shaft due to the change in torque. The axial shaft pushes the axial graphite specimen against the rotating graphite specimen. The rotating graphite specimen in turn is supported by high temperature bearings and a mechanical seal will minimize helium leakage between the rotating shaft and chamber wall. A torque transducer will be used to measure the resulting torque on the rotating shaft. This torque measurement can be used to calculate the resultant shear force at the contact between two graphite specimens and hence the friction coefficient can then be calculated. The rotation will be established by the timing belt driven pulley. It is connected to a smaller pulley (not shown in Figure 14) which is in turn connected to a stepper motor of which the rotational speed can be controlled very accurately (up to 0.1 rev/s).

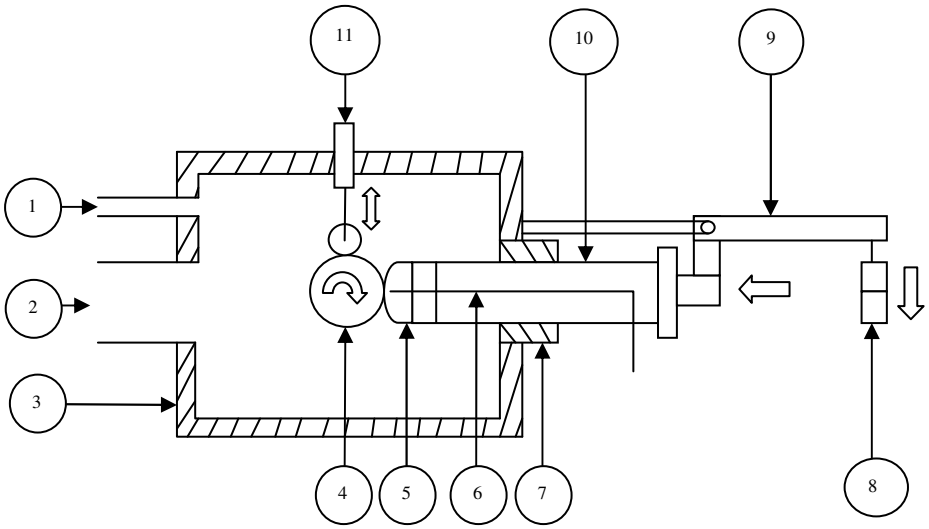

(a) - Side view of pressure vessel concept (full section)

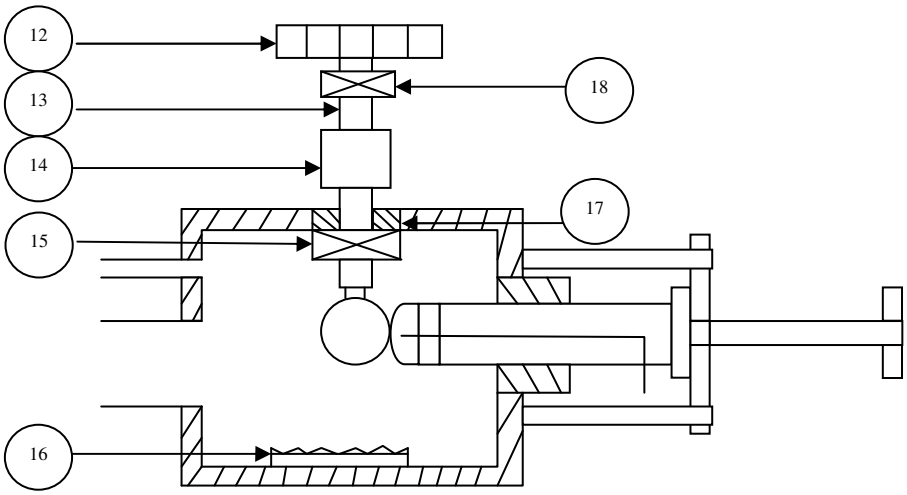

(b) - Top view of pressure vessel concept (full section)

Figure 14: Pressure vessel concept

Table 2: Concept components

1	Helium Inlet.	10	Axial shaft.
2	Chamber inlet.	11	High temperature displacement transducer.
3	Chamber insulated wall.	12	Timing belt pulley.
4	Rotational graphite specimen.	13	Rotational shaft.
5	Axial graphite specimen.	14	Torque transducer.
6	Thermocouple.	15	High temperature bearing.
7	Axial graphite packing seal.	16	Heating element.
8	Weights.	17	Shaft mechanical seal.
9	Moment arm.	18	High temperature bearing.

A high temperature displacement transducer will be connected to a high temperature bearing which is located on the surface of the rotating graphite surface. As the surface is worn away, the bearing will follow this surface and the displacement will be measured by the displacement transducer. From this displacement the amount of worn graphite mass can be determined. The rotating graphite specimen must also be weighed to ensure dust mass accuracy. Table 2 gives the description for various concept components. The general requirements which must be considered during the design process are given in Table 3 below.

Table 3: Design requirements

1	The system must be able to rotate the graphite disk and the graphite pin must be fixed to simulate simultaneous sliding and rolling at contact.
2	The centre line of the disk (or rotational graphite specimen) and pin (or axial graphite specimen) must be as close as possible in order to ensure minimal misalignment.
3	The mating face of the pin must be spherical to account for any misalignment.
4	The disk and pin must be in a horizontal position such that the formation of dust does not influence any one more than the other.
5	It must be possible to remove the graphite disk and pin in between tests.
6	It should be relatively easy to remove the disk and pin.
7	During removal, the loss of graphite must be minimal to ensure the correct weight is measured.
8	The time it takes to change or re-insert the graphite specimens must be kept to a minimum by minimizing the amount of parts to be removed.
9	The speed of rotation at the contact must be kept constant during each test and variable in between tests.
10	The temperature at the contact must be kept constant during each test and variable in between tests.

Table 3: Design requirements (continued)

11	The environmental chamber temperature must not exceed the specified maximum operating temperature and must be monitored continuously during all tests.
12	The chamber must be cooled by means of natural convection such that it is safe for any human being to touch the chamber outer surface.
13	All metal equipment entering the chamber must be cool enough for measuring devices such as torque transducers and load cells to be attached. This is possible by adding insulation to all metal surfaces.
14	The load at the contact must be kept constant by making use of weights.
15	The position of the weights must be adjustable to increase or decrease the load at the contact.
16	The load must be measured by making use of a load cell.
17	The torque needed to rotate the graphite disk must be measured with a torque transducer to indirectly measure the friction force.
18	The environmental chamber must be designed in such a manner that helium leaks are minimised.
19	Vibrations during tests must be minimal.
20	The individual parts of the system should be relatively easy to manufacture.
21	The number of parts to be removed, when the graphite must be weighed, must be minimal.
22	Safety for personnel should be a priority when the system is operational by incorporating safety features into the design.

From this set of requirements it is obvious that the load to be applied during the experiment must be specified, as well as the rotating velocity. In the PBMR there are different normal loads and rotational velocities at the contact of every pebble. In the following sections the average load on a pebble will be calculated. Also a histogram will be used to look at the velocity distribution when the pebbles are in motion during refuelling.

3.2 Load

Load and velocity was specified by developing a DEM program for an annular reactor of an arbitrary height and diameter and to fill it with pebbles. The average normal load for each pebble at the bottom of the reactor will be higher due to the mass of the pebble bed and therefore the load will be dependent on the height of the reactor. Due to the friction at the side walls of the reactor the average load will be less than the total weight of the pebble bed. To capture this effect, Janssen's equation for annular cylindrical geometries (equation (3.1)) could predict the vertical pressure as a function of reactor height (z) given the variation of horizontal pressure with the height of the reactor (Sperl, 2005). Once the vertical pressure (P_V) is known, the average normal load could be calculated assuming the pebbles are as tightly packed as possible. Janssen's formula is given as,

$$P_V = \frac{\rho_{Bed} g D}{4\mu k}\left(1 - e^{-\frac{4\mu k z}{D}}\right) + P_{V_0}\left(e^{-\frac{4\mu k z}{D}}\right) \tag{3.1}$$

The appropriate density (ρ_{Bed}) must be determined to include the effect of helium pressure drop over the core. In Section 6.1.2 the density for the PBMR pebbles is determined. Other constants is the gravitational acceleration (g), the wall friction coefficient (μ), and the ratio between the horizontal and vertical pressure drop (k). The effective reactor diameter (D) also affects the vertical pressure profile. If no additional weight is placed on top of the pebble bed (as in this case), the resultant initial pressure (P_{V_0}) is zero. Refer to Appendix B for the derivation of equation (3.1).

Since only a maximum of roughly 100 000 pebbles can be modelled on a single computer, the full scale PBMR reactor cannot be simulated. Instead, an annular reactor of inner diameter of 0.25 m and outer diameter of 1.2 m with a height of 18.5 m was filled with 65700 pebbles of equal diameter 60 mm (Figure 15).

The variation of horizontal pressure with height was determined from the DEM simulation by dividing the outer reactor wall into equal cylindrical segments. The resultant horizontal force for each of these segments was determined from the DEM simulation once the pebbles settled under gravitational loading. When the resultant force on each segment was known, the horizontal pressure for each segment could be determined by dividing each segment's force by its outer area. An exponential data fit was used to determine the average horizontal pressure through the height of the reactor. Once this pressure distribution was known, the vertical pressure distribution was obtained from the following assumption,

$$P_v = \frac{P_H}{k} \tag{3.2}$$

This pressure distribution was compared to that of the predicted distribution by equation (3.1). The value of k in Janssen's formula could be changed such that the two pressure distributions were in agreement. The correct PBMR reactor dimensions (height = 11 m, D_i = 2 m and D_o = 3.7 m) could be used in equation (3.1) to determine the PBMR vertical pressure profile. The last step was to determine the average normal load on a pebbles in the vertical direction. Since the PBMR vertical pressure profile was calculated, all that was necessary to determine the average normal load on a pebble is the reactor annular area and the number of pebbles that can fit into the annular area. That was 2460 pebbles, under the ideal assumption that all pebbles are packed as closely as possible. By dividing the vertical pressure profile by the reactor annular area and the number of pebbles, the average normal load on a pebble through the vertical height of the reactor was obtained.

The derivation of Janssen's formula and the description of the DEM program can be found in Appendix B & C. Figure 15 shows the annular reactor in which pebbles were created and allowed to settle under gravity loading. Also, Figure 16 to Figure 19 show the DEM results. In Figure 16, each data point represents the pressure on each of the cylindrical segments on the outer wall of the reactor from top to bottom.

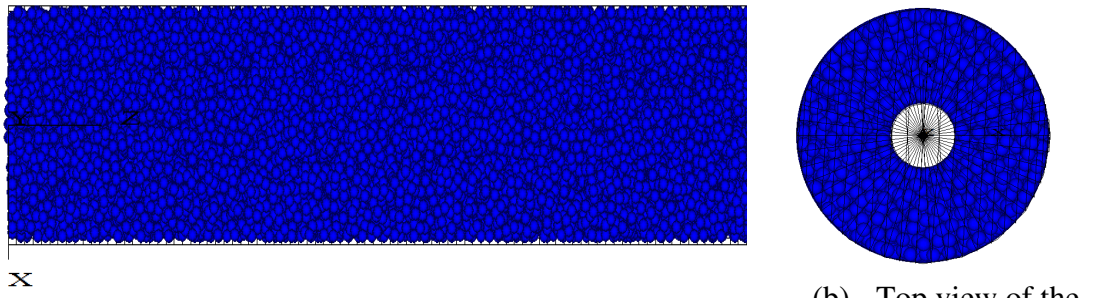

(a) - Side view of the annular reactor geometry

(b) - Top view of the annular reactor geometry

Figure 15: Annular reactor with D_i = 0.5 m and D_o = 1.2 m and 18.5 m high

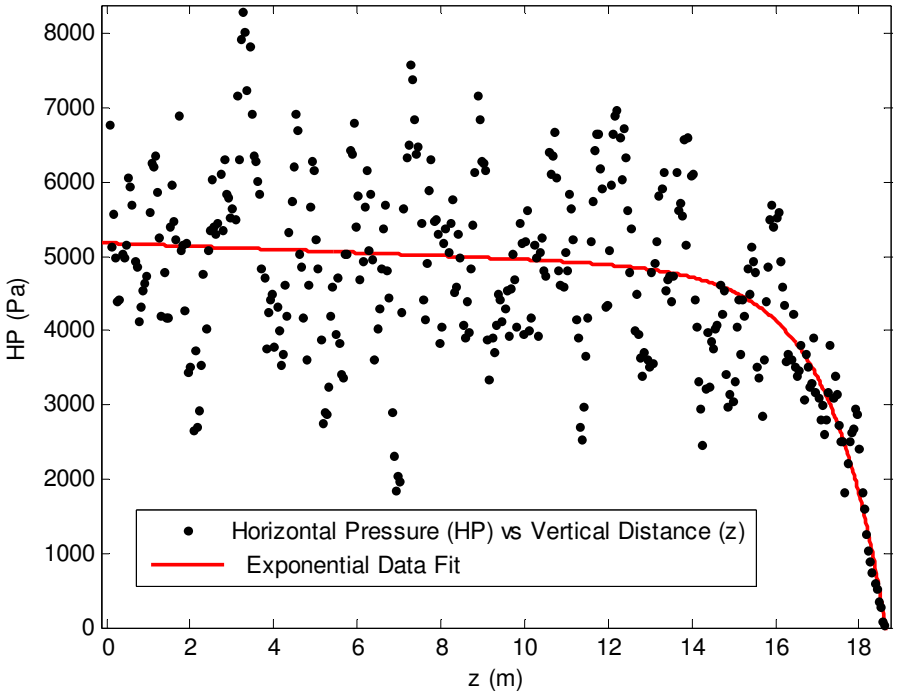

Figure 16: Horizontal pressure (HP) vs vertical height (z) profile on outer wall of annular reactor

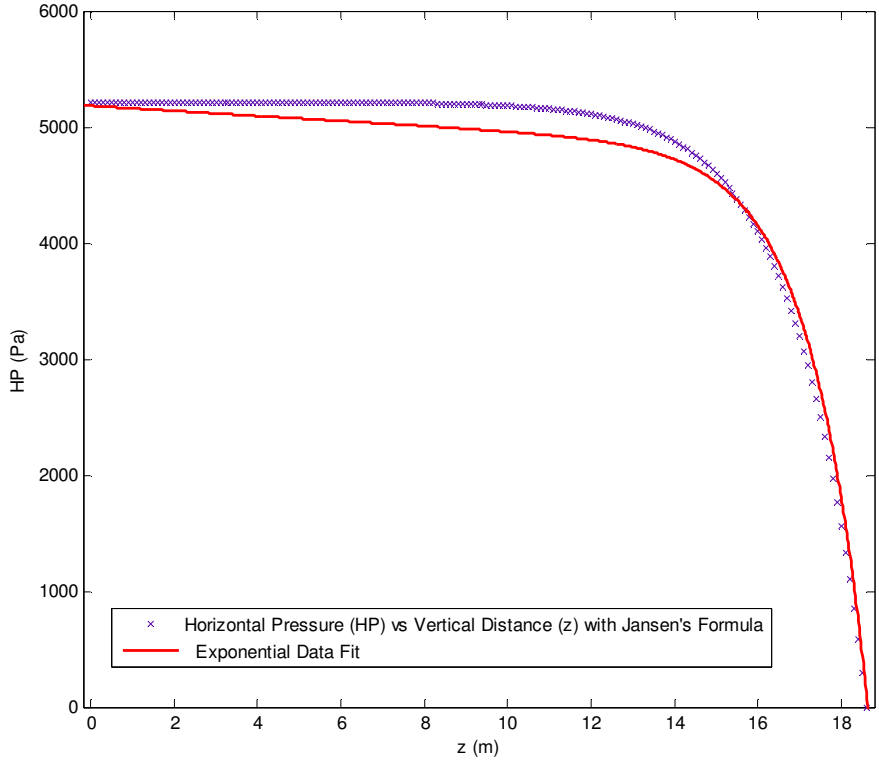

Figure 17: Approximation of horizontal pressure (HP) vs vertical height (z) profile using Janssen's equation with μ = 0.7, k = 0.047, c = 20, D = 0.2217

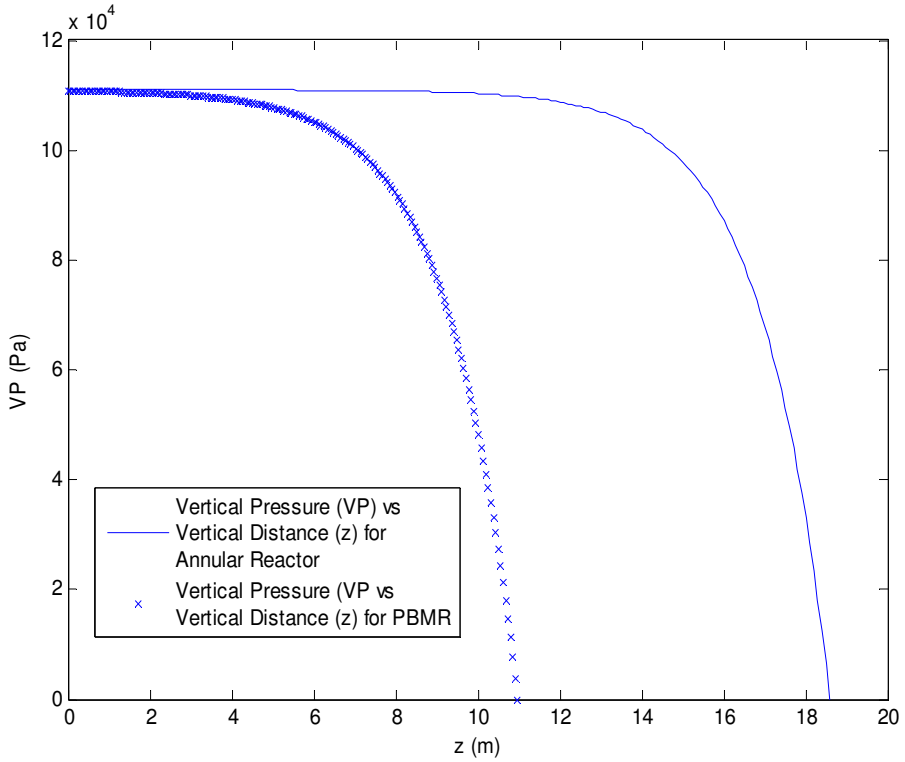

Figure 18: Estimation of PBMR vertical pressure (VP) profile vs vertical height (z)

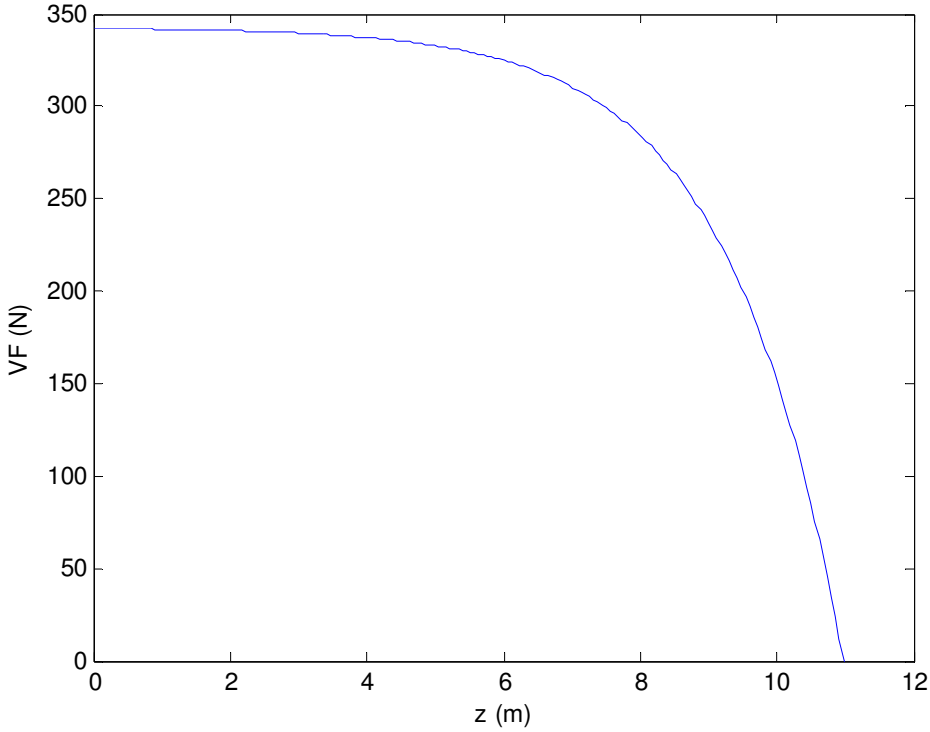

Figure 19: Estimation of the average vertical force (VF) on a pebble as a function of the PBMR vertical height (z)

From the horizontal and vertical pressure profile (Figure 16 and Figure 17) the influence of the friction at the contact between the pebbles and the reflectors can be seen. If no friction existed between them, there would be a linear increase in pressure from top to bottom and the total pressure at the bottom would be the pressure due to the weight of all the pebbles ($11.55 \cdot 10^4$ Pa*) plus the total helium pressure drop over the pebble bed (P_D = $32.42 \cdot 10^4$ Pa (Slabber,2006)), that is $43.97 \cdot 10^4$ Pa. But since the friction does influence the vertical pressure distribution, it is reduced to approximately $11 \cdot 10^4$ Pa which is nearly 75% reduction in vertical pressure which is significant. Also, from Figure 18 it can be seen the bottom pressure of the annular reactor geometry and the PBMR is the same since the ratio of inner and outer reflectors are also the same. If it is assumed the vertical pressure is evenly distributed among the pebbles, then Figure 19 predicts the average force experienced by pebbles from top to bottom. From this it can be concluded that the estimated average force at the bottom of the reactor is 350 N.

3.3 Velocity

The velocity distribution when the pebbles are recycled, can be obtained from the main DEM simulation. Refer to Section 6.1.3 which shows how the relative velocity is calculated and Appendix C for the DEM code. After 0.1 seconds of removing the pebbles from the three bottom chutes, the relative velocity for each pebble contact is calculated as the pebbles are settling under gravitational loading. The scale factor for the reactor geometry is 0.2 which makes the simulated reactor a 0.2 scale of the full scale PBMR dimensions. A histogram (see Table 4) is used to show the overall contact velocity distribution. The result shows that only 152 pebble contacts with a relative velocity less than 0.001 rpm exists and on the other end only 2 contacts exits with a relative velocity of more than 50 rpm. The majority of the pebbles have a relative velocity between 0.001 rpm and 0.5 rpm. The conclusion to be made is that pure rolling occurs only at a small number of contacts and most contacts experience a combination of rolling and sliding.

3.4 Pressure and Temperature

The pebble centre temperature is approximately 1100 ºC in helium at 90 bar pressure (Slabber, 2006). These specifications will not be considered in this study due to the design complexity of a pressure vessel in which wear can be tested at such high temperature and pressure. For a first time study it will also be too

* In Section 6.1.2 the pebble bed mass is calculated. Dividing the weight (m_{Bed}*g) by the annular reactor area (A_{Bed}), results in the pressure at the bottom of the reactor due to the pebble bed mass.

expensive to meet these specifications. To minimize fabrication costs and time, the manufacturing of the pressure vessel/environmental chamber must not require any expert welding, but it must still be safe to operate at elevated temperatures which is part of the requirements. According to pressure vessel regulations (SABS,2010), in order to determine how statutory regulations will apply to specific pressure equipment, the equipment will be divided into five hazard categories. The first and most relevant class to this design is category 0. In this category sound engineering practice (SEP) applies to equipment that is not subjected to conformity assessment, but shall be designed and manufactured in accordance with SEP in order to ensure safe use, where an applicable code is available it shall be used.

Table 4: Histogram of sample relative velocity during reactor defueling

Relative Rotational Velocity (RPM)	*Frequency*
0.001	152
0.5	2313
1	252
2	106
3	32
4	15
5	14
6	11
7	7
8	7
9	4
10	4
20	43
30	8
40	3
50	2

For an operating temperature of 400 ^{o}C (673 K) in helium the pressure would be

$$P = \frac{R_G T}{v_s} = \frac{2077 \cdot 673}{6.037} = 231.54\ kPa = 2.26\ \text{bar} \tag{3.3}$$

R_G is the Individual Gas Constant and v_s the specific volume for helium. From Figure 20, in order to conform to the maximum pressure of 2.26 bar, the chamber volume cannot exceed 10 to 12 litres in order to be classified as category 0.

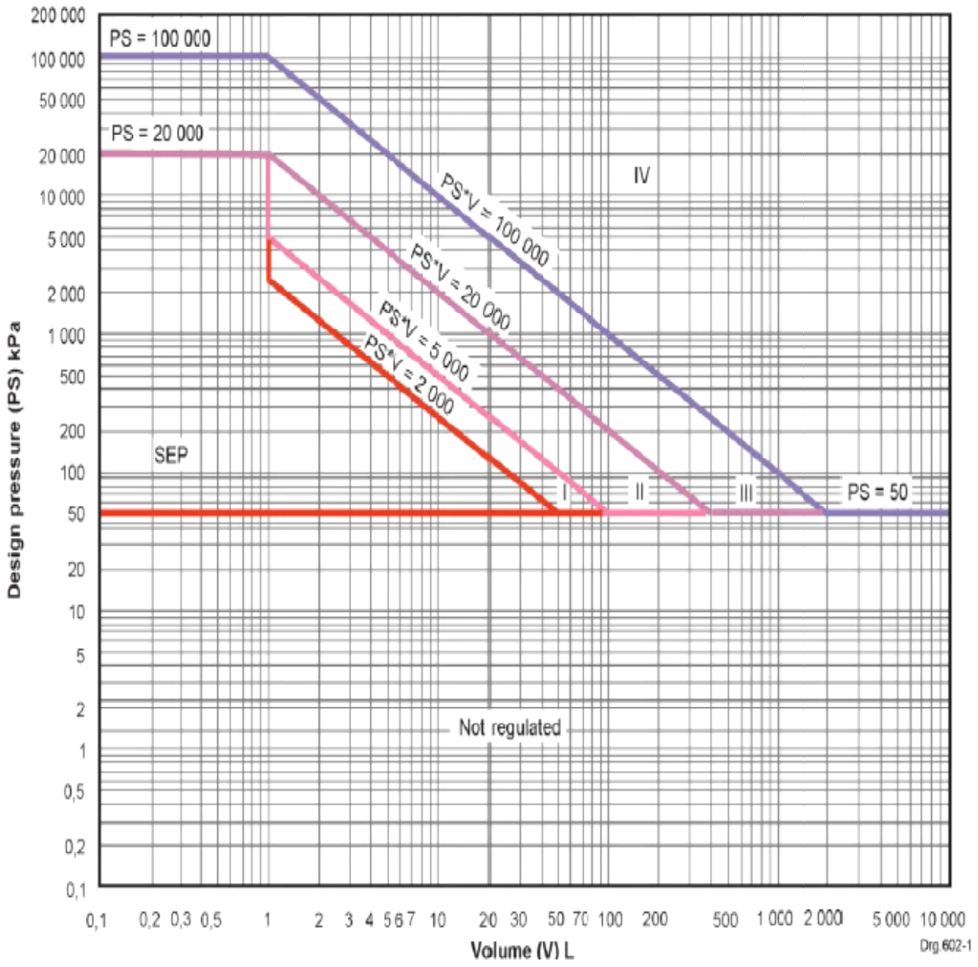

Figure 20: Pressure vessel design chart (SABS, 2010)

3.5 Functional Flow Chart

To ensure that all necessary requirements are incorporated as functional requirements, a functional flow chart will established. Following the flow chart will be the quality functional deployment (QFD). With QFD the functional requirements are translated into engineering specifications (Ullman, 2003). Refer to Figure 21 for the functional flow chart.

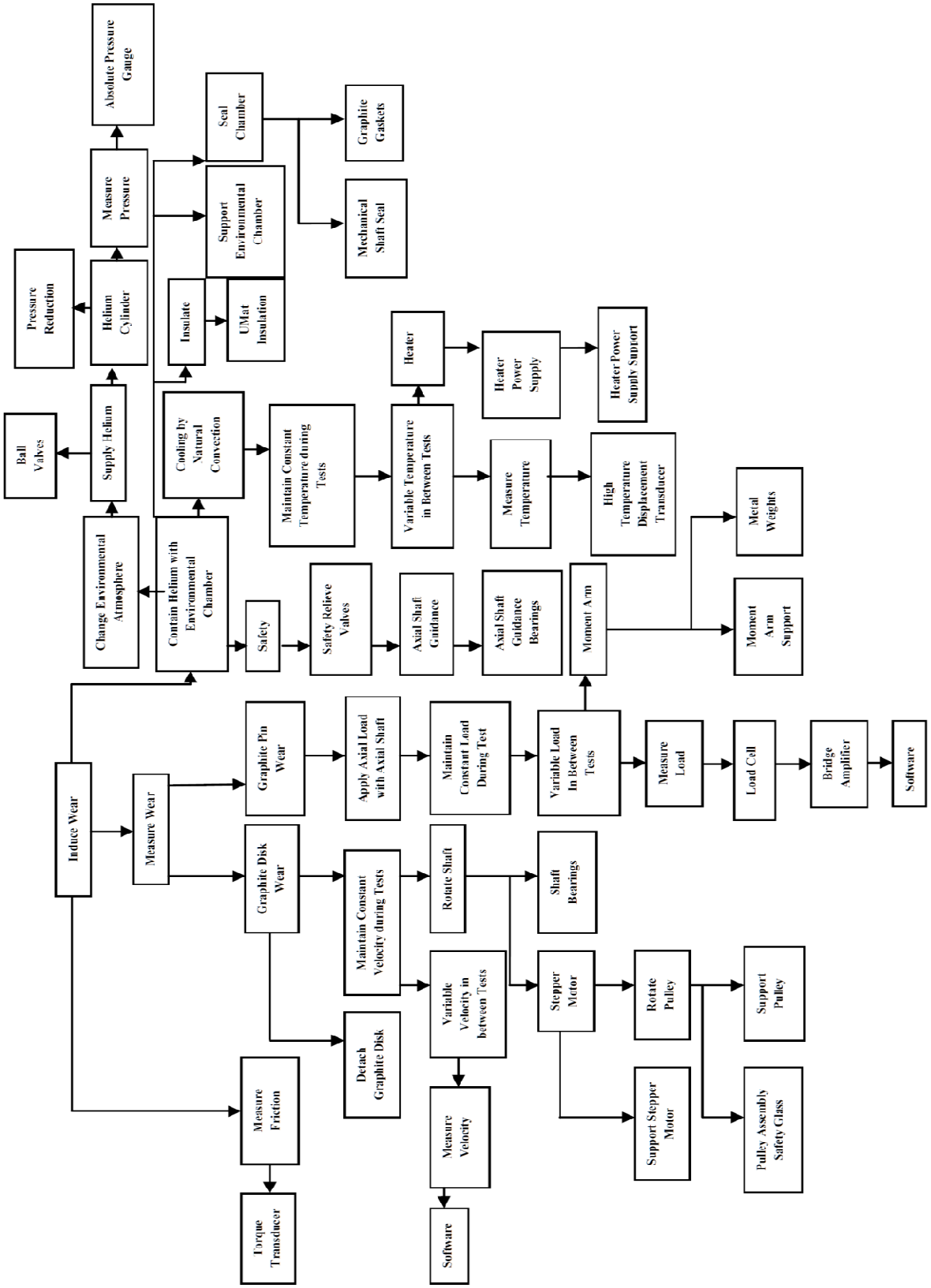

Figure 21: Functional flow chart

3.6 Quality Functional Deployment

The relations between requirements will be identified with the help of quality functional deployment as illustrated in Figure 22. Refer to Table 3. The general requirements from Table 3 are listed on the left, with the engineering specifications at the top. The different markers identify the relation between the two sets of requirements/specifications. The target value for each engineering requirement is listed in the bottom row.

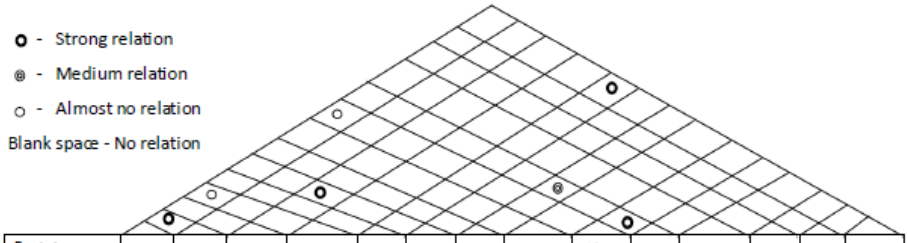

Prototype	Range of Force	Change in magnitude	Speed Accuracy	Force Accuracy	Temperature Accuracy	Rotation Speed	Weight Accuracy	Torque accuracy	Parts changing time	No. of parts removed	Graphite specimens misalignment	Pressure accuracy	Temperature accuracy	Range of Temperature
Units	N	N	m/s	N	°C	rpm	g	Nm	min	#	mm	kpa	°C	°C
Vary the load for different tests	O	○					O	◎						
Constant load during a specific test	◎	O					◎	O						
Speed of rotation accurately measured		◎	O			◎								
Load accurately measured	◎			O				◎						
Temperature accurately measured					O									O
Measuring Helium Pressure									◎			O		
Helium Leakage Minimal												◎		
Vibrations minimal	○	◎				◎		O						
Measure torque accurately			○		○							○		
Change time minimum									O					
Easy to replace pebble									◎	O	◎			
Measure graphite wear							O							
Safe operation												O		
Maximum Temperature													○	◎
Different rotation speeds											◎			O
Target	0 - 250	20	0.05	1	10	100	10^{-4}	10	2	5	0.1	10	70	Room - 400

Figure 22: House of quality

3.7 Detail Design

All the engineering specifications needed for design has been specified in Figure 22. The following section will show how the specifications were implemented into the design. The graphite specimens that were used in the experiment is UCAR type ATJ. The isomolding process for this product is similar to that of the graphite used in the PBMR. The process starts with raw delayed coke being calcined in rotary kilns and then crushed to a fine powder (flour) with the average particle size less than 210 µm. The hot flour and coal tar binder pitch is cooled and milled into molding powder. During isostatic molding, the powder is loaded into a rubber bag and shaped at elevated pressure in an isostatic press. The mold is baked at 700 ºC to 900 ºC and impregnated with a liquid pitch. Rebaking occurs to obtain the desired carbon properties. From this point on ATJ graphite is formed by baking the carbon between 2600 ºC and 3300 ºC. The result is a fine-grain isomolded graphite with the average particle size less than 12 µm (UCAR, 2001).

3.7.1 Graphite Specimen and Shaft Design

To form the graphite pin and disk, a number of pieces were cut from the ATJ cylindrical rods of diameter 60 mm. The final pieces were manufactured with a CNC machine. The final product can be seen in Figure 23. All dimensions are in mm. The curved axial graphite specimen (or pin) and rotational graphite specimen (or disk) had a spherical diameter of 60 mm which represented the contact between two pebbles. The spherical diameter also minimize any misalignment.

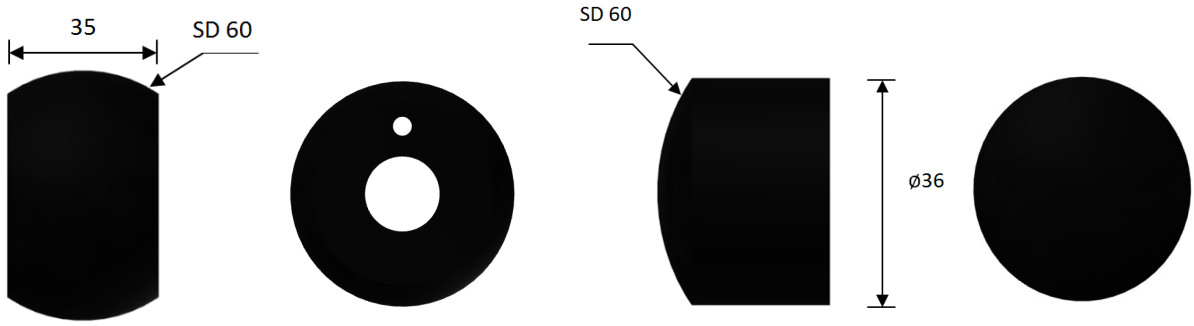

(a) - Rotational graphite specimen with hole diameters 20 mm and 5 mm

(b) - Axial graphite specimen

Figure 23: Graphite specimens dimensions

The disk had to be rotated whilst in contact with the pin. Also, the pin applied an axial load to the disk during rotation. This would induce wear between the two surfaces whose relative rotational velocity was the same as the tangential velocity of the disk. From this setup, the velocity could be controlled very precisely. In order to be rotated, the disk had to be fixed to a rotating shaft. Another functional requirement is for the disk to be easily removed from the shaft. The part which performed these functions, is called the rotational disk fixture pin (RDFP). Refer to Figure 24 which shows how the pin fitted inside the small hole. The pin was fixed during rotation. It would also be required that it is easy to remove after each test. Figure 24 also shows how the axial and rotational graphite specimens fitted onto the fixtures.

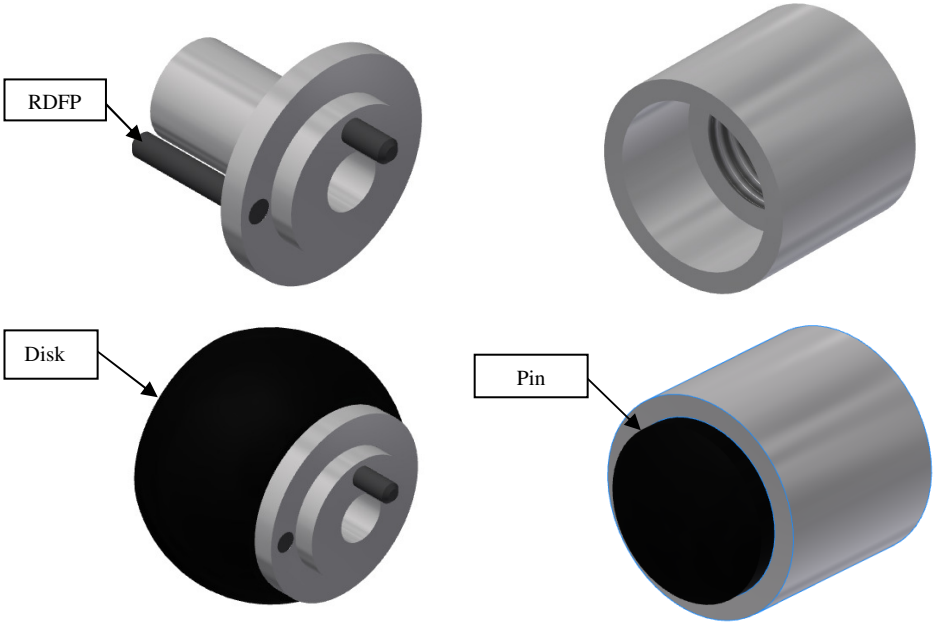

Figure 24: Different views of rotational and axial graphite fixtures

When the disk needed to be removed, the RDFP could be taken off the rotational shaft and the disk could slide off the RDFP and also from the pin. The pin fixture had thread on it to attach to the axial shaft. The fixture would be removed from the axial shaft by unscrewing it. The pin could be easily removed from the fixture. Another requirement is to measure the temperature at the contact surface. A thermocouple (for calibration see Appendix B) was inserted into the pin through the axial shaft. Refer to Figure 25 (a).

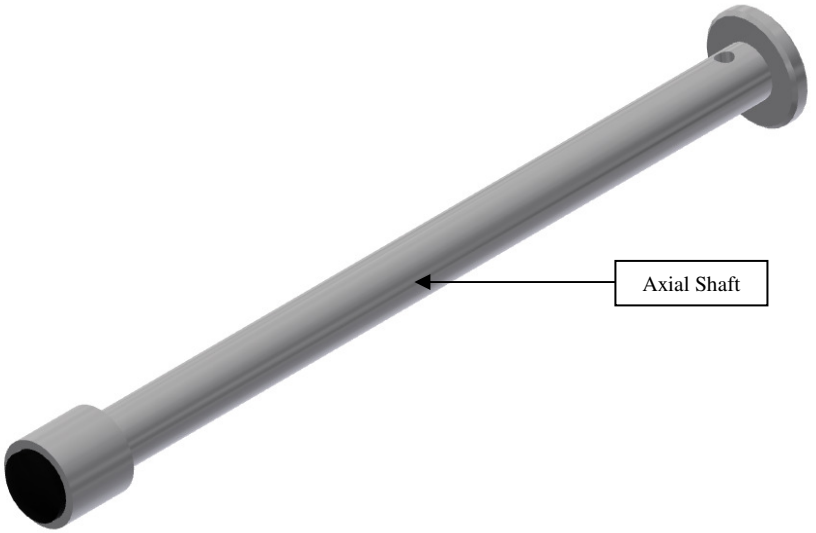

(a) - Axial shaft with graphite specimen

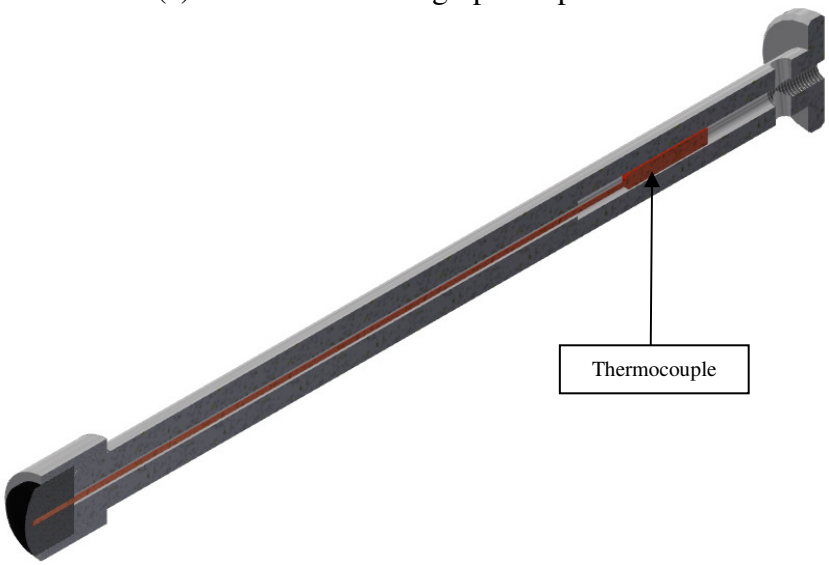

(b) - Sectional view of axial shaft and thermocouple

Figure 25: Axial shaft with graphite specimen and thermocouple

Figure 25 (b) shows the thermocouple. It extended up to 5 mm from the pin surface. The thermocouple measured the temperature at the surface contact. This temperature was used as input to a PID heating system which controlled the temperature. The PID heating system consisted of a k-type thermocouple, PID controller, a 2.3 kW transformer and a 110 V heating element which was located inside the pressure vessel.

The axial shaft was guided in such a way to apply a constant load as the graphite surface wore. Since there existed a lateral force at the point of contact, the axial shafts horizontal movement had be independent of this force. To guide the shaft during the test, two axial shaft guidance bearing assemblies (Figure 26) would be used. Two bearing assemblies were needed to prevent shaft misalignment as it

moved horizontally. Since a contact force between the graphite specimens were to be induced during rotation, another function of the guidance bearing assemblies was to prevent any additional normal friction forces to move the axial shaft as the graphite specimens were worn.

Three high temperature SKF® bearings (part nr. 6201-2Z/VA201) spaced 120º apart, were used in each guidance assembly. The rotational shaft (Figure 27) was also supported by two high temperature bearings (part nr. 6006-2Z/VA208). These roller bearings can support a load of 3000 N at a maximum operating temperature of 350 ºC below 100 rpm. The shaft temperature was too high for standard linear bearings to be used.

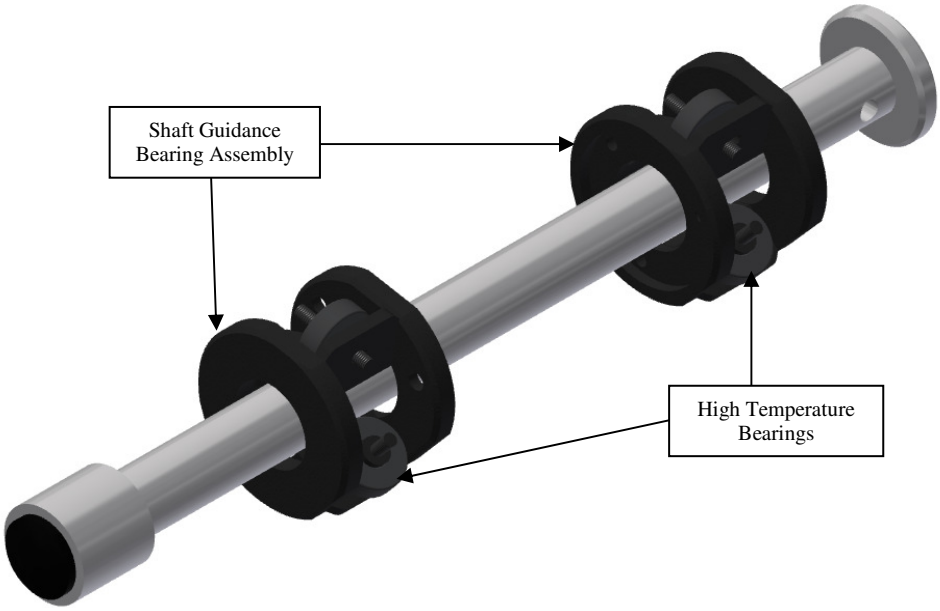

Figure 26: Axial shaft support

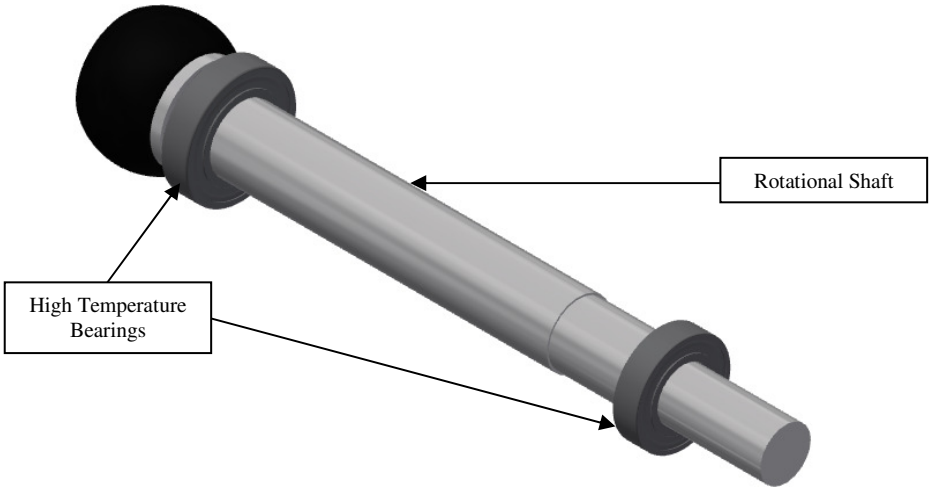

Figure 27: Rotational shaft support

3.7.2 Chamber Design

In order to support the axial - and rotational shafts, a chamber was developed. The chamber consisted of an inner stainless steel box and two other mild steel boxes. Stainless steel 304 is the preferred material for the inner chamber since this material is dimensionally very stable at temperatures in excess of 400 ºC. Each of the boxes were connected to each other by means of steel webs. Since the temperature will be the highest inside the most inner chamber, the stainless steel webs would direct the heat towards the most outer chamber. This was done to ensure the safety of the personnel operating the oven. Since the surface temperature of the middle and outer boxes were reasonably lower than the inner stainless steel box, it was manufactured from mild steel. The third and largest chamber had a surface area which was large enough to be cooled through natural convection. Refer to Appendix B for a FEM model that simulated the outer surface temperature of the outer chamber. The maximum measured outside temperature was 110 ºC.

Refer to Figure 28 to see how the inner chamber was manufactured. The webs were welded onto the inner chamber and screwed onto the middle chamber since welding between the two chambers walls will be difficult. The chamber front face had twelve M6 holes for a front plate to be bolted. This was done to ensure that if necessary, any item such as the heating element can be removed from the inner chamber.

Between the two plates were a graphite gasket which was compressed when the two plates were bolted. The back plate of the inner wall was welded to the back face since it would not be necessary to remove this plate. This ensured that helium did not escape between the two plates.

On top of the inner chamber there were two pieces welded to the chamber. Figure 28 illustrates a stainless steel piece which housed a thermocouple. Another stainless steel piece located the high temperature displacement transducer.

The thermocouple was fixed during all tests which measured the chamber wall temperature. On each of the side walls there was also the same configuration for two more thermocouples. Together these three thermocouples gave an indication of the average inner chamber wall temperature.

In Figure 28 it can be seen that one of the side walls is not present. This is due to the fact that three of the chamber walls were cut and bent out of one piece of stainless steel sheet. The missing side wall for each of the chambers were welded in place after the three chambers were welded and bolted into place.

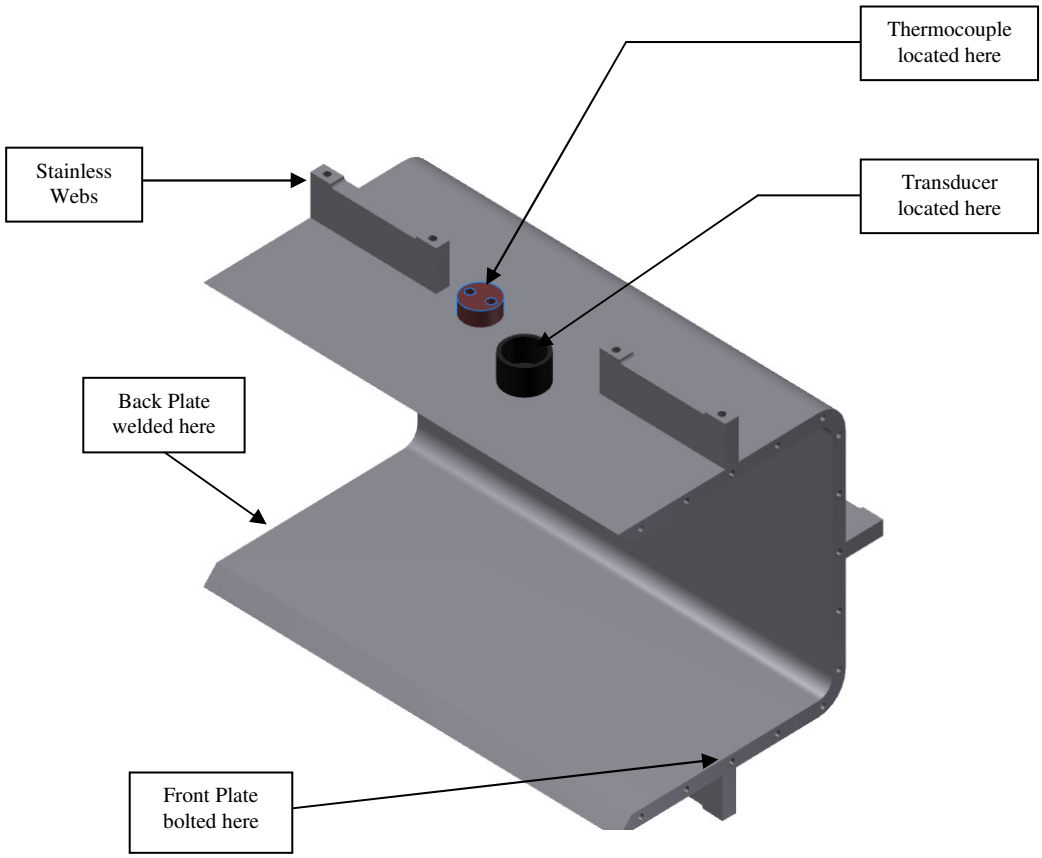

Figure 28: Inner stainless steel chamber

Between the steel walls of each box an insulating material called UMat 8 was placed. This material could withstand temperatures in excess of 600 ºC. The insulating material ensured minimal thermal radiation between the box walls. If the insulator were not present, the wall temperature of each box would be significantly higher. Figure 29 illustrates how the chamber looked when all three boxes were welded together with no side walls. The reason the side walls were welded only after the three boxes were welded together, was that the axial and rotation support/guidance pieces would not fit for welding after the side walls had been welded.

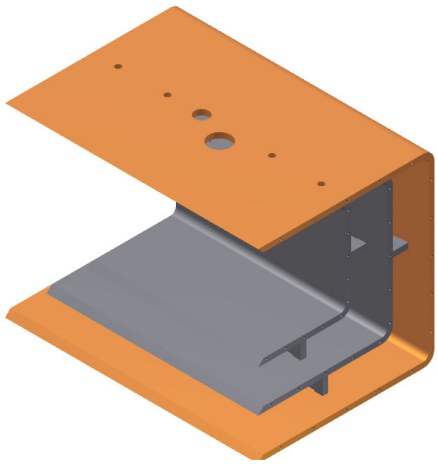

Figure 29: Chamber with insulation space

3.7.3 Axial and Rotation Pipe Design

Figure 30 illustrates a full section view from the top view which shows the axial pipe and rotation pipe. The rotation pipe was firstly welded to the side wall of the inner stainless steel box and then the side wall plate was welded to the inner box. Once the inner wall side plate was welded, the rest of the side plates could be welded. After the side walls had been welded, the back plates for each box were also welded, with the axial pipe welded to the inner chamber back plate.

Figure 31 shows the subassembly of the axial pipe. The main purpose of this subassembly was to locate the front and back axial shaft guidance assembly in such a way to be concentric and therefore misalignment between the axial graphite specimen and the rotation graphite specimen was minimal. Another function of this subassembly was to seal the chamber from the moving axial shaft by means of graphite packing which could withstand temperatures as high as 400 ºC. The graphite packing was located inside the packing housing and pushed against the axial shaft and the wall of the packing housing. This packing was chosen due to its good lubricating properties when the axial shaft was moving but still provided a seal between the shaft and the housing. From top to bottom was the axial stuffing seat which bolted onto the housing. As the seat was bolted to the housing, it pushed against the graphite packing, thereby compacting the graphite against the axial shaft and the housing. Following the seat was four graphite packing rings and then the mild steel packing housing. The housing slid over the axial pipe and was welded into place.

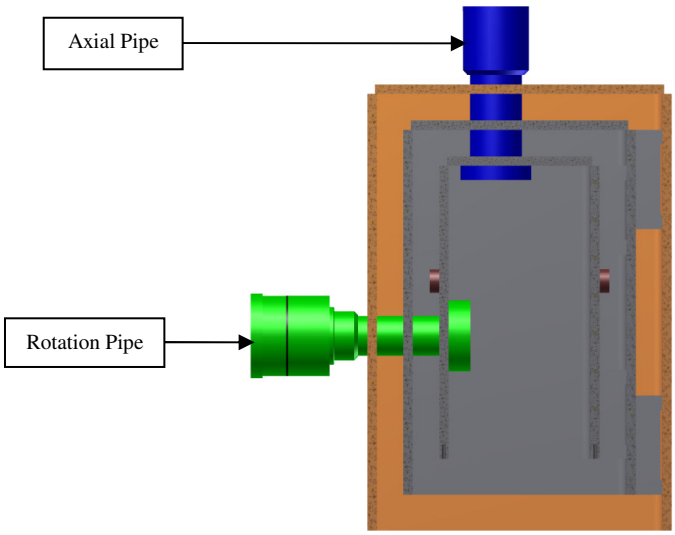

Figure 30: Top view of chamber with axial and rotation pipes

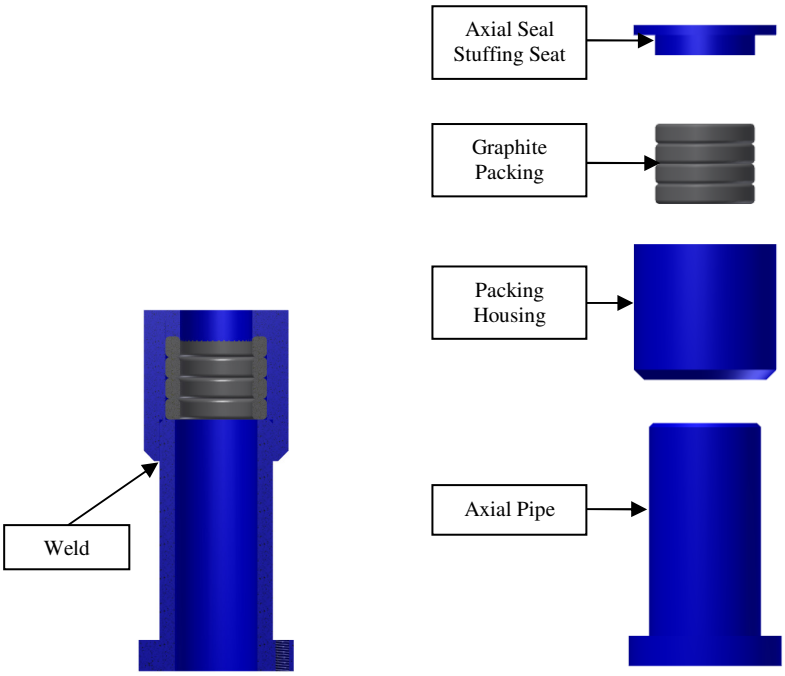

(a) - Full section view of axial pipe (b) - Exploded view of axial pipe

Figure 31: View of axial pipe subassembly

Figure 32 (a) shows a full section view of the rotation pipe subassembly. The main function of this subassembly was also to guide the rotation shaft from the inner stainless steel box to the outer mild steel box. It also supported the high temperature bearings which was located on the shaft and housed a part of the rotational seal. The seal consisted of two parts of which the one part is the shaft seal which rotated with the shaft and the other part was the titanium-nickel alloy stationary seal which is located in the rotation seal stuffing. The seal face of the stationary seal pushed against the face of graphite rotational seal face.

Figure 32 (b) illustrates the rotation pipe assembly. A high temperature 25 mm SKF® roller bearing (part nr 6005_2Z_VA20) supported the shaft. Following the bearing is the stationary seal stuffing which housed the stationary seal. It also supported and located the bearing. A graphite packing ring sealed the space between the stationary seal and the seal stuffing. The shoulder of the stationary seal (John Crane part nr. 87021455) pressed against the graphite packing and in turn the packing was compressed against the mild steel seal stuffing.

The rotary seal (John Crane part nr. 89296380) mounted onto the shaft and was compressed against the face of the stationary seal. When the seal stuffing and seal housing bolted together, the 3 mm thick graphite gasket sealed the space between the seal housing and seal stuffing. Following the graphite gasket is the seal housing. This part was welded onto the rotation pipe and ensured a concentric geometric tolerance between the graphite bearing inside the inner box and the outer bearing which was located inside the seal stuffing.

Below the rotation pipe is the bearing housing which bolted onto the rotation pipe and supported the inner bearing. The inner bearing was also a 30 mm high temperature SKF® bearing. All these components except for the seal was manufactured from mild steel.

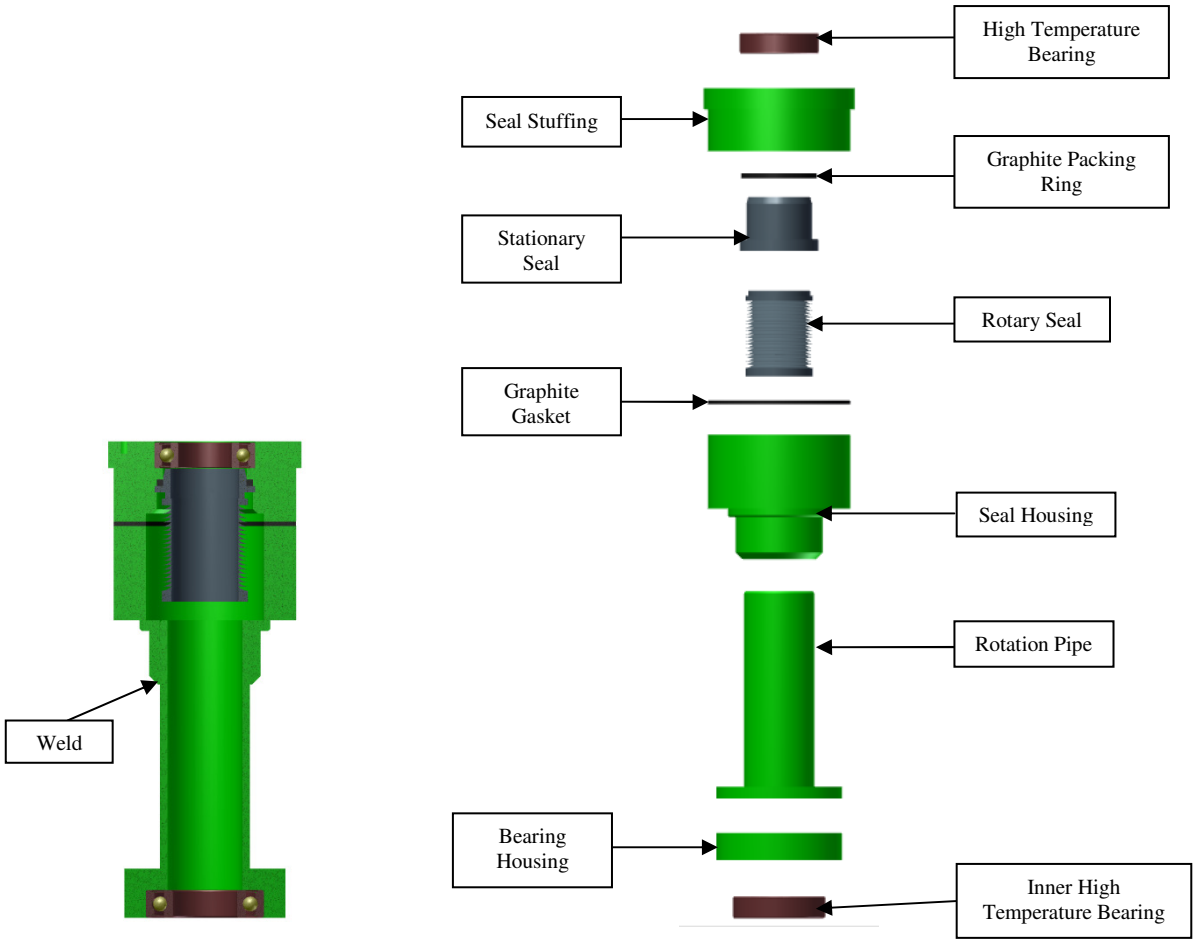

(a) - Sectional view of rotation pipe assembly

(b) - Rotation pipe assembly exploded view

Figure 32: Subassembly of rotation pipe

Figure 33 shows how the axial and rotation subassemblies are located and supported by the chamber. A normal force was applied to the axial shaft, which in turn moved and pressed the axial graphite specimen against the rotation graphite specimen. This layout ensured the graphite specimens were not misaligned and that the applied normal force as well as the rotation speed between the surface of the specimens could be controlled.

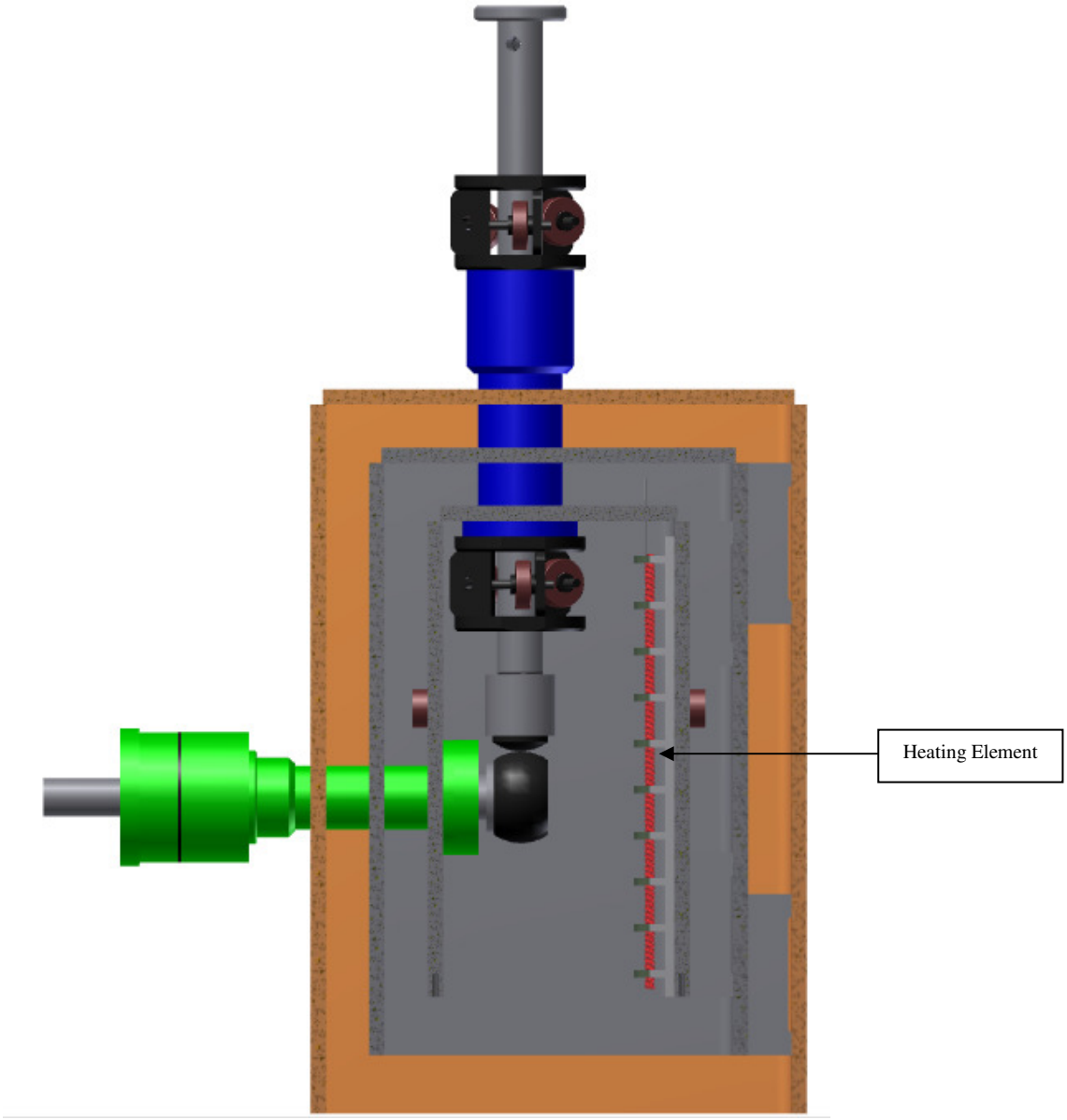

Figure 33: Top sectional view of pressure vessel

3.7.4 Heating Element and Electrical Feedthrough

On the right hand side of Figure 33 is the heating element which increased the inner chamber temperature. A 110 V voltage was applied between the terminals of the heating element. This was achieved by a 220 V to 110 V transformer which in turn was connected to a PID controller. During each test, after the temperature have been set to a specific value, the PID controller would keep the temperature

between the surfaces of the graphite specimens as constant as possible (±5 ºC). During start-up of the experiment, the temperature was set to a value. The thermocouple measured the graphite temperature and used this value during the "soft" start mode of the controller to correct for the power necessary to achieve a certain temperature.

Figure 34 (a) shows the electrical feedthrough (Spectite part nr. PF-1/2 "NPT-0.375"-L-A) and how it was located inside the chamber. From this sectional view of the pressure vessel only one outlet pipe can be seen, when in fact there were two pipes beneath each other. The heater outlet pipe was welded onto the back plate during the chamber assembly. This pipe acted as a feedthrough for the heating elements two terminals. The wire of the heating element terminals was covered with ceramic insulation. It prevented any electrical contact between the feedthrough pipe and the terminals. Figure 34 (b) shows the sectional view of the feedthrough assembly. The feedthrough assembly also acted as a gas seal.

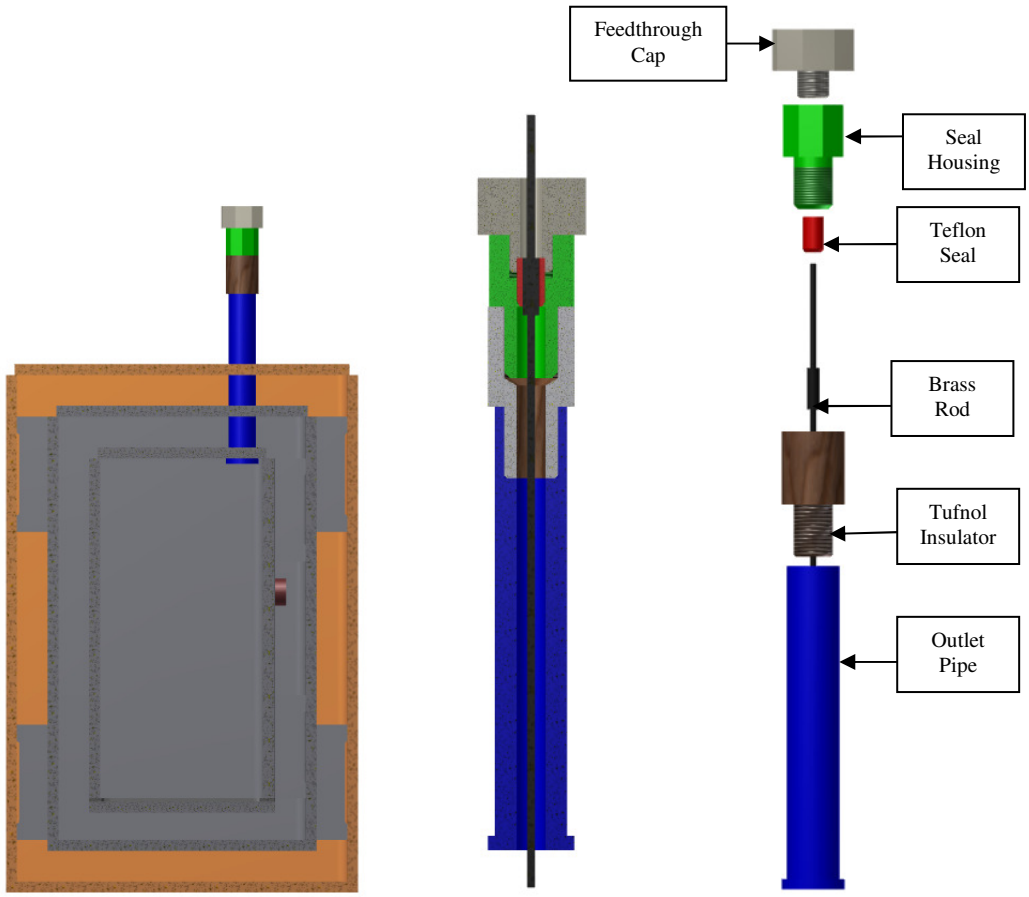

(a) - Sectional view of pressure vessel and feedthrough

(b) - Feedthrough sectional view

(c) - Feedthrough exploded view

Figure 34: Chamber and feedthrough

Figure 34 (c) shows the exploded view of all the parts that made up the subassembly. From top to bottom is a cap of the feedthrough which pushed the seal against another part of the feedthrough. As the cap was screwed onto the bottom part, the was compressed and pushed against the inner wall of the bottom part, as well as the brass rod. The formed a gas seal between these parts. Each of the brass rods were connected to separate heating element terminals.

During the assembly of the heating element and the inner chamber, the brass rods were soldered onto the heating element terminals. The Tufnol, which acted as a electrical and temperature insulator, separated the feedthrough from the outlet pipe.

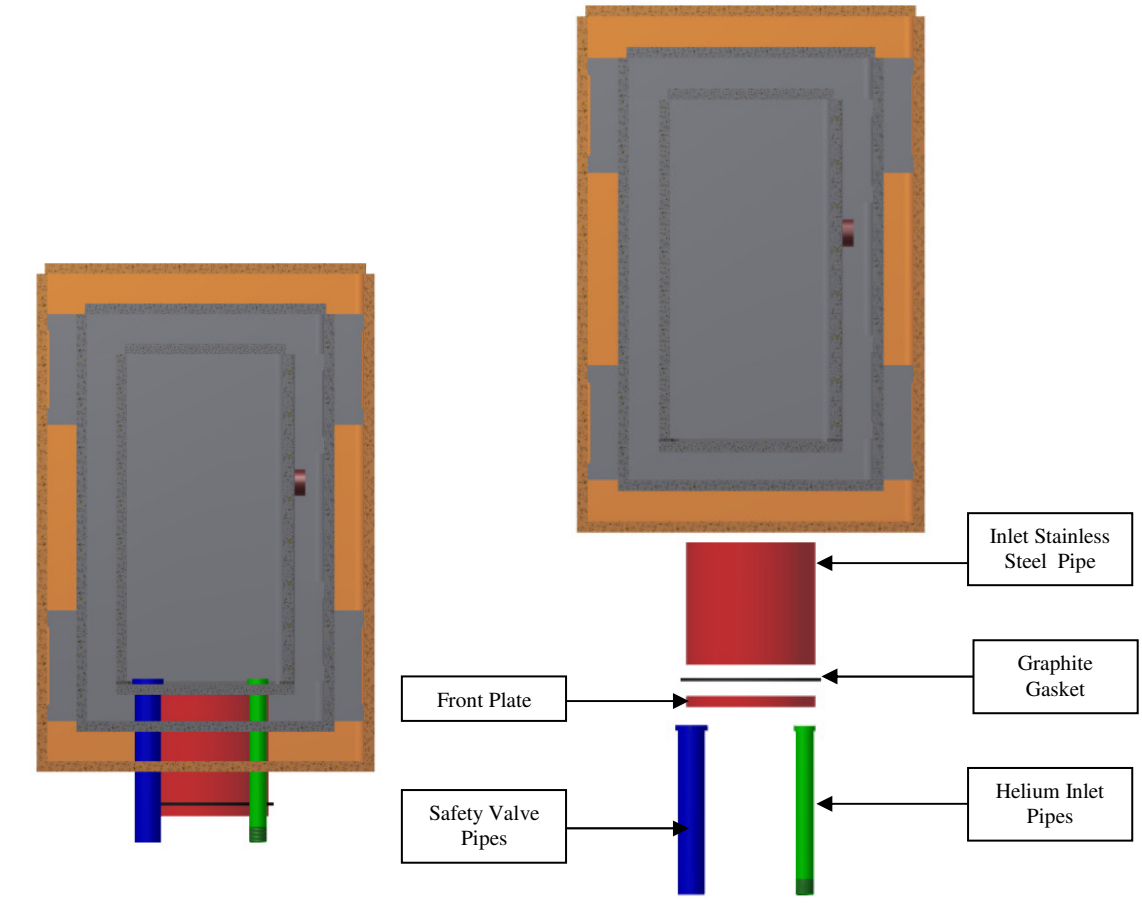

(a) - Sectional view of the pressure vessel and inlet pipes

(b) - Exploded view of the pressure vessel and inlet pipes

Figure 35: Chamber and inlet pipes

Figure 35 shows where the helium inlet pipes and safety valve pipes were located. The helium inlet pipes were welded onto the front plate and served as an inlet for the helium. Figure 35 (a) shows the top sectional view of the pressure vessel, two helium inlet pipes and two safety valve pipes which were present but cannot be seen from this view. The one helium pipe was used to purge the inner chamber. Helium flowed into the inner chamber by means of opening a ball valve, since initially the chamber was filled with regular air. Since helium is lighter than air, it pushed the heavier air to the bottom of the inner chamber. As the air was pushed to the bottom, the other helium pipe was used to purge the compressed air out of the inner chamber. This process was repeated a few times and ensured the whole chamber was filled with pure helium. A pressure gauge was also connected to one of the helium pipes to measure the helium pressure.

The brass safety valves were connected to the safety valve pipes by means of a Tufnol part which insulated the safety valves thermally since the maximum temperature for these valves is 150 ºC. The two brass safety valves were set to 2 bar. The inlet stainless steel pipe was welded to the inner stainless steel chamber and lends access to remove or insert the graphite specimens. It had a 120 mm diameter and was sealed by a graphite gasket. A front plate was bolted onto the inlet pipe and compressed the graphite gasket until a good seal was achieved.

3.7.5 Wear Measurement

Different methods exist for measuring wear. The first method is known as an optical method. A small micro-hardness indentation is made in the surface of the specimen and during sliding the indentation is reduced. The reduction in size is measured optically. The resolution of this method is typically 10^{-4} cm. The second method is known as the mechanical gaging method in which a micrometer is used to measure the track depth of the wear scar. The resolution is typically 10^{-3} cm for a track surface area of 10^{-2} cm^2. Another variation of this method is to use a profile meter to track the profile of the track and from this information the amount of material worn away can be estimated (Rabinowicz, 1995).

A third method is to measure the worn track on the graphite surface by means of a displacement transducer. A gage or bearing can be used to follow the worn track and in turn is connected to the displacement transducer. The fourth method is the weighing method, since it is the simplest way of measuring wear and typical resolution is 10^{-4} g (Rabinowicz, 1995). The third and fourth method was implemented into the design. The third method offers the advantage of in-time measurement of the track depth on the surface of the graphite without removing the specimen from the chamber. This decreased the experimental time which means more experimental tests could be performed.

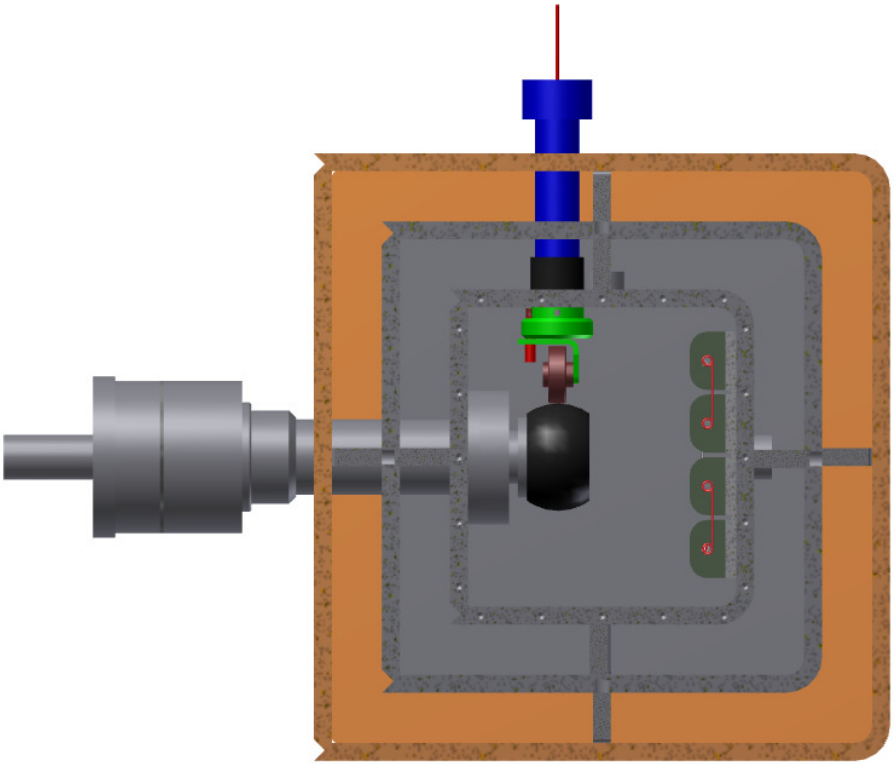

(a) - Sectional view of pressure vessel and HTDT

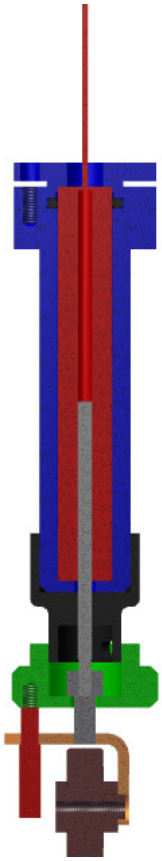

(b) - Full sectional view of HTDT

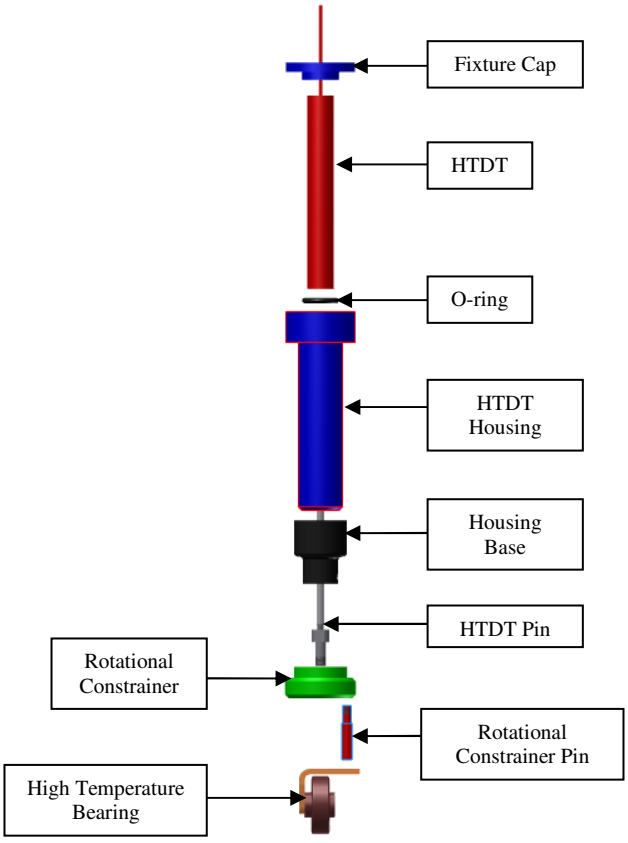

(c) - Exploded view of HTDT assembly

Figure 36: Pressure vessel and HTDT

Figure 36 (a) shows the front full sectional view of the chamber and where the High Temperature Displacement Transducer (HTDT) (RDP Group Part nr. LIN56) is located in the chamber. A high temperature bearing was positioned on the surface of the rotation graphite specimen. As the graphite rotated and was worn away, the bearing stayed on the graphite surface and measured the distance worn away. When a unworn graphite specimen was put into place, the position of the bearing was zeroed electronically. As the bearing followed the worn surface vertically, the position of the bearing with respect to its original position was shown on the HTDT display. From the displayed distance, the amount of worn graphite could be calculated. In Figure 36 (b) the sectional view of the HTDT assembly can be seen. In Figure 36 (c) from top to bottom is the fixture cap which was bolted on. An o-ring fitted around the HTDT which sealed the gap between the transducer and the housing. After the o-ring is the HTDT housing which was press fitted into the black base. This base was welded to the inner stainless steel box. The HTDT pin was connected to the bearing. This pin was free to move in the vertical direction. Part of the pin entered the HTDT and as the pin moved, it changed the flux in the HTDT which was converted to an electrical signal. This signal was then transferred to the display. The rotational constrainer kept the bearing from rotating while a test was done. It also kept the bearing and pin from falling out when the graphite rotation specimen was removed from the inner chamber.

3.7.6 Final Assembly

Figure 37 and Figure 38 shows the final design. A frame was constructed to support the weight of the chamber as well as the motor assembly. The rotation shaft was connected to a piece of Tufnol which insulated the rest of the system thermally. A coupling was connected to the Tufnol, as well as a torque transducer (HBM Part nr. T22/100Nm).

The torque transducer was used to measure the torque required to rotate the graphite specimen with a predetermined rotational velocity. Refer to Appendix B for the torque transducer calibration curve. Two parameters are necessary to calculate the friction between the graphite surfaces. One is the measured torque and the other is the diameter of the graphite specimen. Since it was expected that the diameter of the graphite specimen would not change significantly during the test, it was taken as a constant diameter of 60 mm. From these parameters the frictional force could be calculated and once the magnitude of this force was known, the friction coefficient could be calculated since magnitude of the applied normal force was always known during the experiment. The torque transducer was connected to a flexible coupling on each side to account for any misalignment between the connecting shafts as well as minimize damage to the transducer due to any misalignment. The transducer was free floating and only supported by the two couplings. The other coupling of the transducer was connected to a pulley

shaft which was supported by a precision bearing. The bearing was supported by a mild steel frame which in turn was connected to the main support frame.

The pulley assembly consisted of a bigger and smaller pulley and was connected with a timing belt. The speed reduction of rotation was three to one. This served two functions namely an increase in torque and a decrease in speed. This reduction allowed the stepper motor to operate with minimal torque at a appropriate speed. As the motor speed increased, so did its torque. If the pulley system were not in place, the stepper motor would stall. The motor was connected to an electrical drive which in turn was connected to the computer. X-ware was the software which was used to control the stepper motor. Refer to Appendix B for some experimental setup photos. The pulley belt could transmit a maximum torque of up to 30 Nm. The pulley assembly, torque transducer and couplings were surrounded by plexiglass which ensured the safety of the personnel operating the prototype.

The moment arm was used to transmit the weight to the axial shaft. Weights were stacked onto each other to increase the weight. Alternatively the position of the weights could be adjusted along the length of the moment arm to adjust the applied force. The moment arm was the preferred choice for this function since it was easy to use and the applied force could be controlled very accurately. Other alternatives such as PID control of a hydraulic piston had been considered to apply the normal force since vibrations of the chamber could possibly be eliminated. Alternatively, when the moment arm is used and rotational speeds are below 80 rpm, the vibrations would not interfere with the experiment. Between the moment arm and the axial shaft was two components namely the load cell (HBM 2 kN load cell) to measure applied normal force as well as the Tufnol which acted as a thermal insulator.

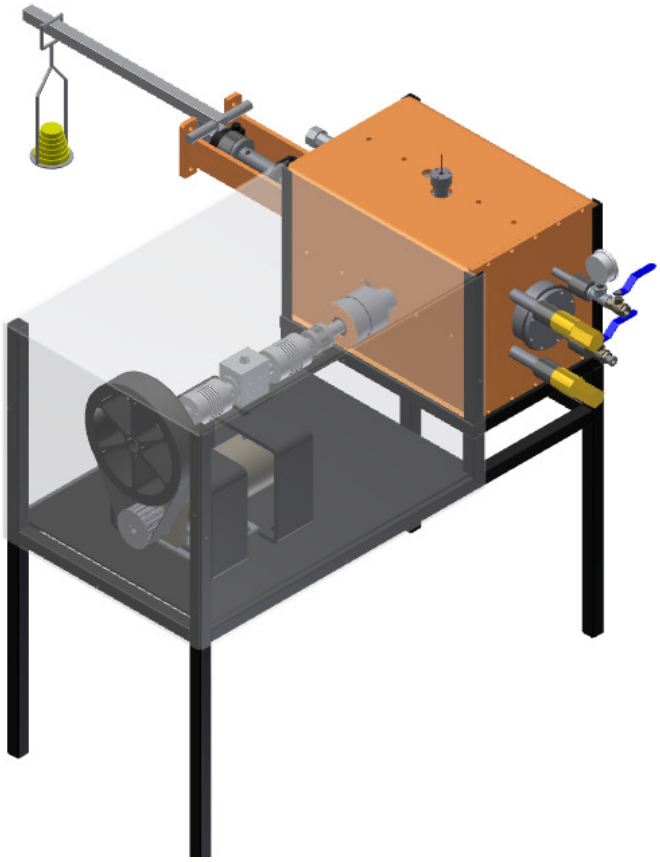

Figure 37: Right view of experimental setup

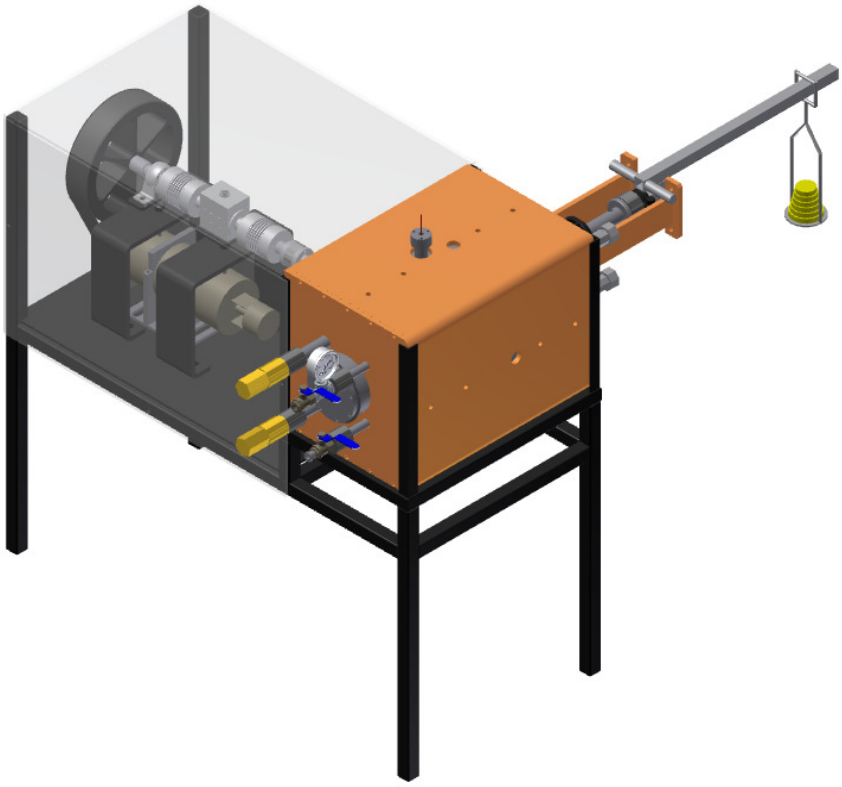

Figure 38: Left view of experimental setup

4. EXPERIMENTAL SETUP

4.1 Experimental Procedure

Initially the stepper motor was not rotating and the moment arm was removed from the support such that no load was applied. Each test began by inserting the axial graphite specimen into its fixture which in turn was screwed onto the axial shaft. When the fixture was screwed on, the thermocouple was 5 mm from the contact surface. When the temperature was measured, it was assumed that the thermocouple measured the surface temperature. This assumption is reasonable since graphite has a high thermal conductivity of up to 200 W/mK (UCAR, 2001). Next, the rotating graphite specimen was placed into its fixture and fixed to the rotation shaft. Once the specimen was in place, a bolt was screwed through this fixture into the shaft.

Once the graphite specimens were into position, the inlet pipe cap together with the graphite gasket was bolted in place and tightly secured. The temperature inside the chamber was controlled by means of a PID controller which was connected to the heating element. When it was required for the temperature to be increased above ambient temperature, the controller was set to the specified temperature point and the temperature steadily increased. In less than a hour the inner chamber temperature reached 400 ºC. The graphite surface temperature also increased when it rotated due to frictional heat which was generated between the two contacting surfaces. The temperature could be controlled within ±5 ºC.

To evacuate the atmosphere inside the chamber, the helium regulator was opened as well as the helium inlet ball valve. The helium was displaced from the high pressure helium container into the chamber. As the helium was flowing into the chamber, the pressure in the chamber increased to 1 bar absolute pressure which was measured with a pressure gauge. Once the pressure level reached 1 bar, the outlet ball valve was opened to purge the chamber. Lighter helium pushed the heavier air out of the chamber. The process was repeated two to three times once the pressure decreased to atmospheric pressure. This ensured that the chamber atmosphere was mostly filled with helium (Helium baseline 5 with 99.999 % purity).

Next, the stepper motor was set to rotate at the required speed. The torque required to rotate the graphite specimen was recorded and this value was subtracted from the measured torque during the experiment. The torque measured during no load was due to the friction between the two contacting surfaces of the seal. The no load torque was measured for a few minutes since the friction increased between the two seal surfaces as it heated. The bearings also had a rolling friction component to overcome. Once the torque stabilised, the value was zeroed and from this point on only the torque between the two graphite surfaces was measured.

The required normal applied force to the axial shaft was measured with a load cell. The bearings that guided the axial shaft as well as the graphite packing had a frictional component that had to be taken into account. The no-load force was measured by making repeated measurements. Once the no-load force was accounted for, it could be subtracted when the normal force was measured. The weights were attached to the weight holder and this in turn was attached to the moment arm. The weights position was adjusted by moving it up or down the moment arm. The load cell output was displayed on the screen and the correct required force could be obtained. Once the graphite surfaces came into contact, the test time was started and measured by means of a stopwatch. When the required test time had elapsed, the test was stopped by stopping the stepper motor.

The helium regulator was closed as well as the helium inlet ball valve. The weights were removed and if the chamber temperature was too high, it had to cool off which took two hours. After each test the graphite specimen was weighed and then the next test was started.

The whole experiment consisted of three sets of data, each with unique default values for sliding distance, velocity, normal force and temperature. The default values for each set are given in Table 5. Each set in Table 5 consisted of twenty tests during which each parameter was varied. For instance, during the first set, the first five tests were performed to obtain the correlation between the wear mass and sliding distances at 226 m, 452 m, 678 m, 904 m and 1130 m. For each of these five tests all the other parameters were kept constant at their default values. During the next five tests the velocity (0.0314 m/s, 0.0628 m/s, 0.0942 m/s, 0.1256 m/s, 0.157 m/s) was allowed to vary and all other parameters were kept constant at their default values. These velocities correspond to 20 rpm, 40 rpm, 60 rpm, 80 rpm and 100 rpm. The next five tests followed in the same manner where the normal force (50 N, 100 N, 150 N, 200 N, 250 N) was varied and also for the last five tests where the temperature (36 ºC, 100 ºC, 200 ºC and 300 ºC) was varied.

Table 5: Default values for each data set

Data Set	Sliding Distance, x (m)	Sliding Velocity, v (m/s)	Normal Force, L (N)	Temperature, T (ºC)	Wear Extent (g)
Experimental Uncertainty	0.2	0.0063	1	10	0.0001
1	226	0.1256	100	36	-
2	226	0.0628	150	36	-
3	226	0.0942	50	36	-

For the next set of data, the default values for each parameter were reset as indicated in Table 5, after which the next twenty tests were performed in the same manner as described in the previous paragraph. By following this procedure, all three data sets were obtained.

4.2 Regression Analysis

From the literature review it follows that in some cases Archard's wear equation can represent the experimental wear data reasonably well. In this case it will be assumed that graphite wear extent is given as some form of a power series where normal load L, velocity v, sliding distance x and temperature T are the variables.

The equation may be given as:

$$W(L, v, x, T) = a\, L^b\, v^c\, x^d\, T^e \tag{4.1}$$

Taking the natural logarithm on each side of equation (4.1), leads to the following,

$$\ln(W) = \ln(a) + b \ln(L) + c \ln(v) + d \ln(x) + e \ln(T) \tag{4.2}$$

By keeping all parameters but one constant at a time, equation (4.2) is a linear function for which each individual constant, $ln(a)$,b,c,d and e must be solved. The first two sets was used to obtain the necessary data to solve each constant by means of a regression analysis. The third set of data was used to compare the behaviour of the predicted theoretical wear to the experimental data. The results for the experiment are illustrated graphically in the following section.

5. EXPERIMENTAL RESULTS

5.1 Data Regression Analysis Results

From the multi-linear regression analysis the constants from equation (4.2) are as follows:

$$lnW = -19.78671 + 1.96813lnL - 0.34676lnv + 0.74923lnx - 0.12884lnT \quad (5.1)$$

with a correlation factor $R^2 = 0.946$ and standard deviation $\sigma = 0.1951$. Assuming a Gaussian normal distribution in the measured results, approximately 95% of repeated measurements will lie within $\pm 2\sigma$ (or 0.3902 g).

In the original form it can be written as:

$$W(L, v, x, T) = 2.55117.10^{-9}\, L^{1.96813} v^{-0.34676} x^{0.74923} T^{-0.12884} \quad (5.2)$$

The distance can be expressed as a function of time:

$$x = v\, t \quad (5.3)$$

Substituting this into equation (5.2), the wear is given by:

$$W(L, v, T, t) = 2.55117.10^{-9} L^{1.96813} v^{40247} T^{-0.12884} t^{0.74923} \quad (5.4)$$

In the following subsection the worn mass as predicted by equation (5.2) is compared to the three sets of subsequent data acquired during the experiment. The results are discussed in Section 5.4.

5.2 Comparison between Empirical Equation and Experimental Data

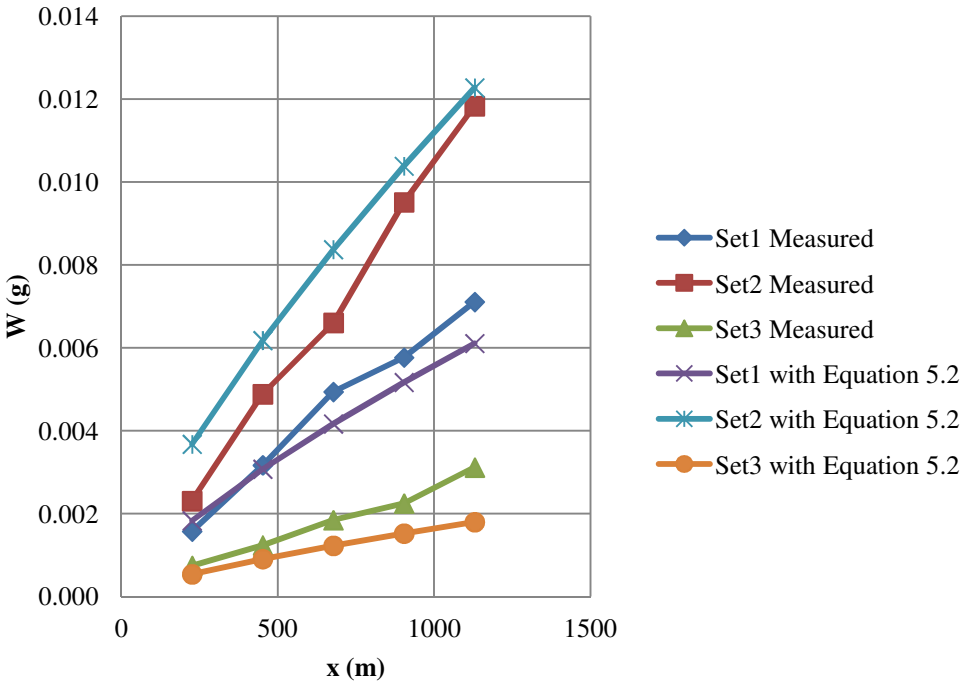

Figure 39: Wear extent (W) and sliding distance (x) for all data sets and empirical equation

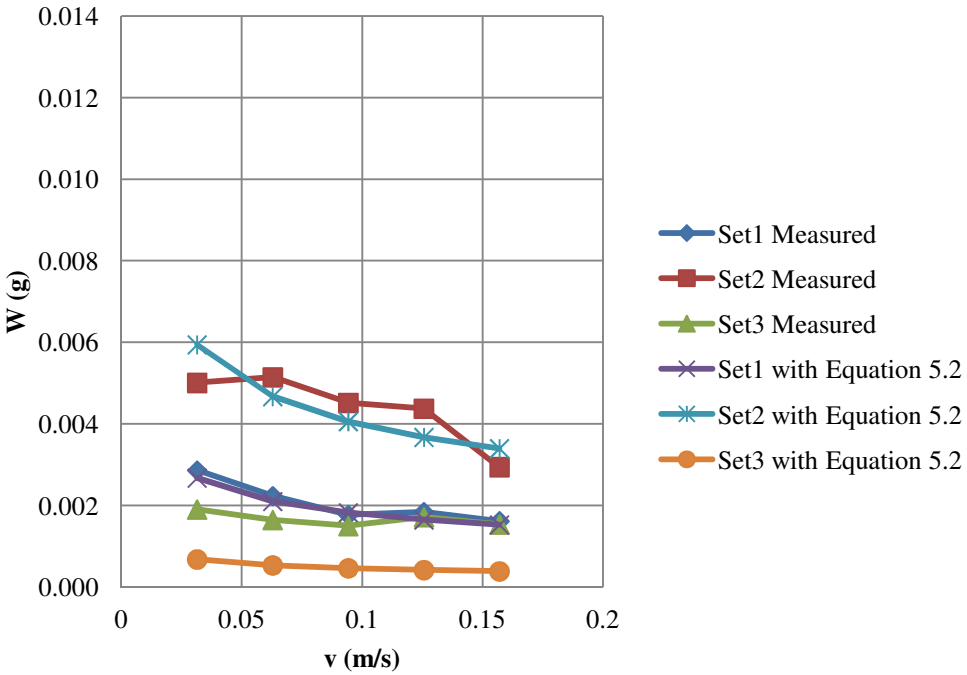

Figure 40: Wear extent (W) and velocity (v) for all data sets and empirical equation

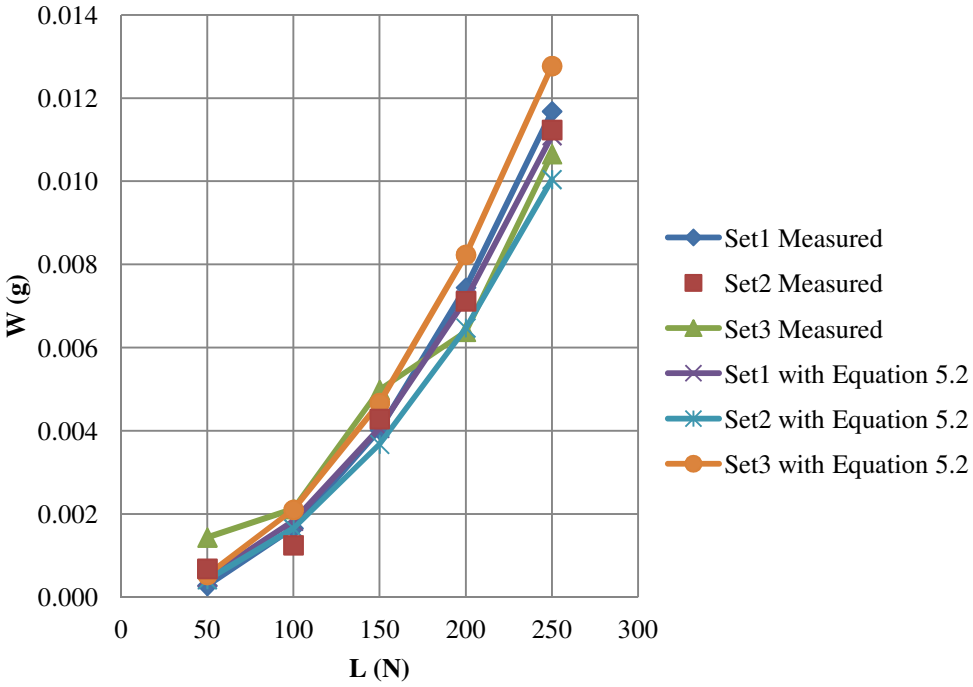

Figure 41: Wear extent (W) and normal force (L) for all data sets and empirical equation

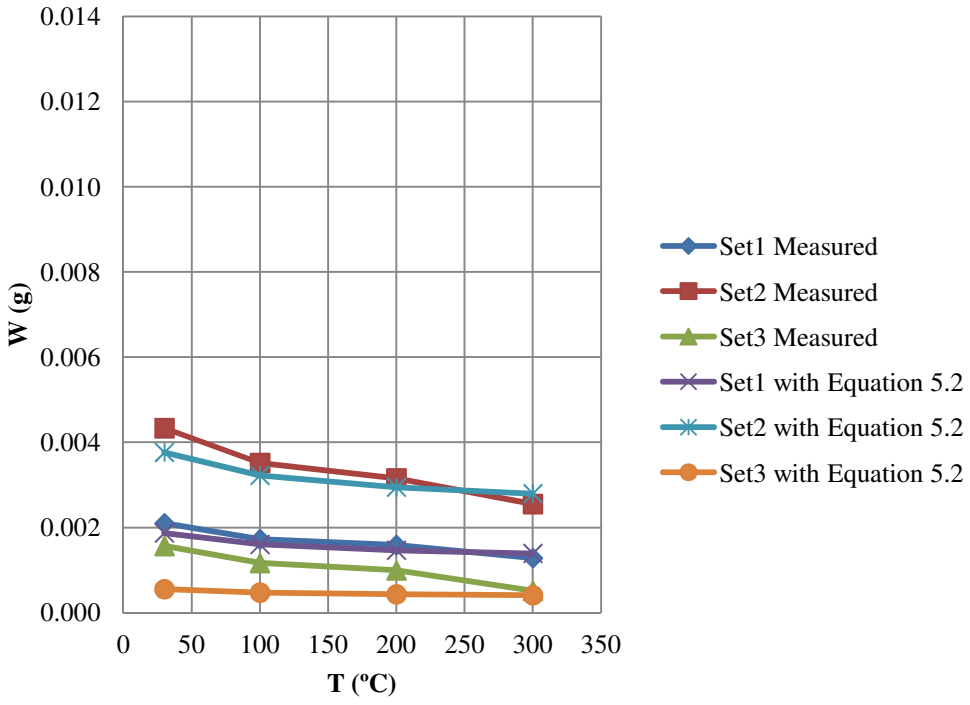

Figure 42: Wear extent (W) and temperature (T) for all data sets and empirical equation

5.3 Photographs of Worn Graphite Specimens

In Figure 43 (a) the rotational graphite specimen is shown inside the chamber. In Figure 43 (b) the smooth worn surface is shown. Small cracks and pits can be observed on the worn surface. In Figure 43 (c) the axial graphite worn specimen is illustrated.

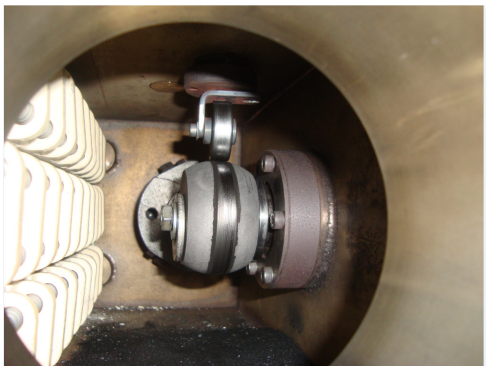

(a) - Graphite specimens inside the pressure vessel

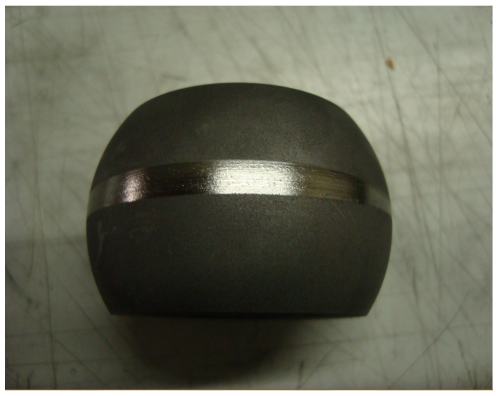

(b) - The rotational graphite specimen with a worn surface

(c) - The axial graphite with the worn contact area

Figure 43: Samples of worn graphite specimens

5.4 Discussion of Experimental Results

In Section 5.2 the experimental data has been compared to the semi-empirical model. Figure 39 shows the comparison between increasing sliding distance and wear for all three sets of data as well as the model prediction based on the multi-linear regression analysis. The wear is proportional to the sliding distance, but the wear rate is dependent on the other tribological parameters since the slope for each set is different in Figure 39. Set 3 has the lowest wear rate, followed by set 1 and 2. From the experimental data it seems that the wear rate is most sensitive to the normal force, as seen in Figure 41. An explanation for this is the Hertz contact stresses that develops beneath the surface in the graphite at the contact. The Hertz theory (Johnson, 1985) can be used to approximate the force distribution beneath the surface of the pebble during static compression with another pebble. Assuming the contact area (due to an applied load L) between both pebbles is circular in shape, it has a radius a. This radius is given by

$$a = \left(\frac{3LR^*}{4E^*}\right)^{\frac{1}{3}} \tag{7.1}$$

The effective curvature and modulus for the two pebbles (each referred to with subscripts 1 and 2) are given as,

$$\frac{1}{R^*} = \frac{1}{R_1} + \frac{1}{R_2} \tag{7.2}$$

$$\frac{1}{E^*} = \frac{1 - \upsilon_1}{E_1} + \frac{1 - \upsilon_2}{E_2} \tag{7.3}$$

E^* is expressed in term of the Poisson ratio, υ. The pressure distribution on the surface (as a function of the contact circle radius r) with the maximum pressure (p_0) at the contact centre is given by

$$p = p_0\left(1 - \left(\frac{r}{a}\right)^2\right)^{\frac{1}{2}} \tag{7.4}$$

where

$$p_0 = \frac{3L}{2\pi a^2} \tag{7.5}$$

The subsurface principal stresses in the direction perpendicular to the contact surface (z - direction) are given by

$$\sigma_x = \sigma_y = -p_0(1+\nu)\left[1-\left(\frac{z}{a}\right)tan^{-1}\left(\frac{a}{z}\right)\right]+\frac{1}{2}\left(1+\frac{z^2}{a^2}\right)^{-1} \tag{7.6}$$

$$\sigma_z = -p_0\left(1+\frac{z^2}{a^2}\right)^{-1} \tag{7.7}$$

$$\tau_{max} = \frac{\sigma_x - \sigma_z}{2} \tag{7.8}$$

These stresses are illustrated in Figure 44. The maximum shear stress beneath the surface may induce fracture near the surface by means of induced cracks at the position of maximum shear (z = 0.48a). This may contribute to fatigue wear.

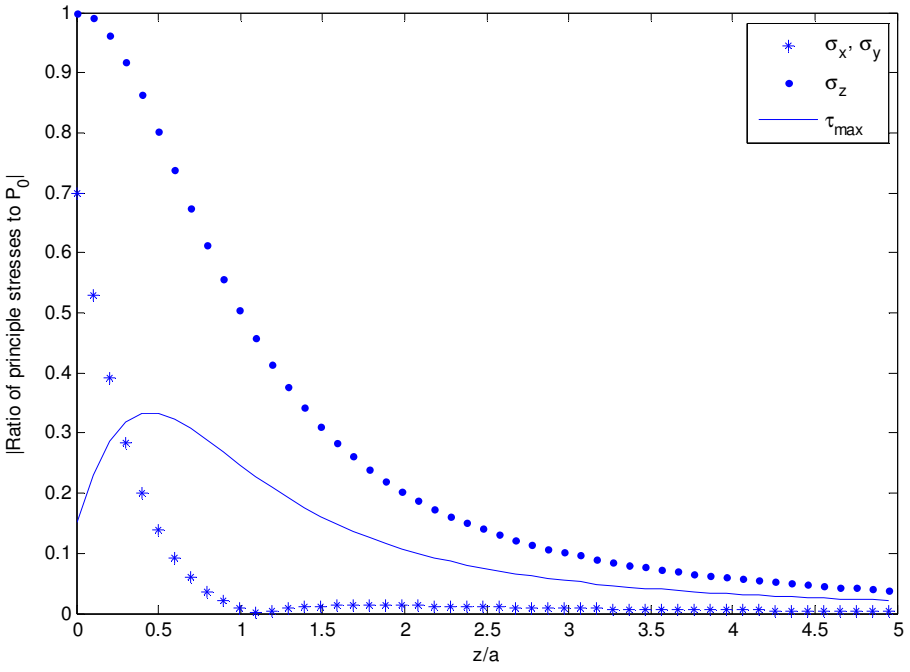

Figure 44: Hertz subsurface stresses along the z-axis (centreline of pebble)

It is possible to incorporate a yield criterion such as the Drucker-Prager to predict the failure load of quasi-brittle materials such as graphite. Becker (2011) has

shown that this model may be valid for certain graphite materials. Such an analysis is however outside the scope of this thesis since additional experimental data have to be acquired specifically for type ATJ to be applied to the yield criterion.

From Figure 40 and Figure 42 the wear is inversely proportional to the velocity and temperature. It yields higher values for a decrease in velocity at higher loads than a change in temperature at the same loads. The drop in wear with increasing temperature is favourable during reactor operation, although it is expected that the relative velocity will be lower as seen in Section 3.2. The decrease in the wear extent with higher temperatures has also been observed by Stansfield (1969). He used two pieces of graphite which slid against each other with a linear stroke. He measured the wear extent at 25 ºC, 400 ºC and 800 ºC. The wear values were about an order of magnitude higher at the lowest temperature compared to the other temperatures.

During the experiment mainly dusting wear has been observed due to the high friction, fine produced dust particles and helium atmosphere which also promotes crack growth as mentioned in the literature review.

6. SIMULATION OF PBMR PEBBLES CIRCULATION

6.1 DEM Simulation

6.1.1 Reactor Geometry

The DEM simulation for in-core pebble movement will be based on the specifications in Table 1. The power output will determine the surface temperature of the pebbles. Although the temperature profile of the RPV will not be constant with its height, it will be assumed that the temperature for all pebbles will be the same, as specified in Section 3.3.

As already mentioned, the movement of all these pebbles cannot be simulated with PFC^{3D} since the software is limited to simulating roughly 100 000 spheres. Due to this limitation, the height and diameter of the reactor geometry was scaled using a geometric scale factor. Initially, the scale factor was 0.15 and multiplied by the reactor height and diameters to obtain a 0.15 scale of the full scale PBMR geometry. With the scaled down version of the reactor, only a few thousand pebbles would be necessary to fill the reactor. During different simulations the scale factor was increased to a maximum of 0.6. When the scale factor was increased any further, the limit for the maximum number of fuel spheres was reached. For each scale factor a number of simulations regarding the circulation rate was performed. By using different scale factors with different circulation rates, the results could be extrapolated to the full scale scenario as an approximation to the dust production of the PBMR during normal operation.

The reactor geometry is an annulus with three outlet chutes spaced out at a 120º angle. The helix which act as a outlet path for the graphite spheres inside the real reactor was not included in the simulation. Furthermore, the simulated reactor was not filled by dropping pebbles into the core. Only the equilibrium mode of the reactor was simulated during which all the fuel spheres were already packed together as tightly as possible. The refuelling mode, transport and handling of pebbles outside the core were also not simulated.

6.1.2 Pebble Properties

It is important to establish the correct contact model for the simulation. The DEM contact model was based on physical contact data which in turn was determined from experimental data. Parameters such as friction, material density and stiffness were assigned to the reactor wall and pebble properties. Two different contact

models were used in the simulation namely the linear contact model which was assigned to all the reactor walls and the Hertz contact model, assigned to all the pebbles. The linear contact model assumes a linear relationship between the contact overlap and the contact force. It was assumed the reactor walls were rigid and therefore the stiffness assigned to these walls were in the order of $1 \cdot 10^8$ N/m.

To validate contact data of all DEM simulations, an experiment was performed during which a pebble was compressed between two plates. One plate was fixed whilst another was compressing the pebble at constant velocity during which the normal force was recorded. The correct material properties such as Young's Modulus and Poison's Ratio were obtained by developing a DEM program which simulated this experiment. Finally, validation of material properties were obtained by means of a comparison between the experimental and DEM results.

In the Hertz contact model the applied force between the pebbles themselves or the reactor wall is proportional to $\delta^{1/3}$, where δ is the deformation (overlap) distance of each pebble (Itasca Consulting Group, 2003). The relation between force and deformation for a graphite pebble was found experimentally by compressing a graphite pebble between two mild steel plates as described earlier. If the two mild steel plates are compressed with constant velocity and the force as well as deformation distance is measured, the relationship between these two parameters could be obtained. Once the result is known, it can be compared to a DEM simulation of the exact experiment. In the simulation a ball with the same properties (radius, density, etc.) as the experimental graphite pebble is created. The upper wall is given a constant downward (-z direction) velocity whilst the lower wall is fixed. The pebble is compressed between the walls. The shear modulus of the pebble can then be adjusted to obtain different force versus displacement graphs. Once the force/displacement graph for the DEM simulation corresponds to that of the experimental results, the main DEM simulation is based on the correct physical quantities and therefore validated. Figure 45 illustrates the DEM representation of the experimental setup and refer to Appendix C for the code.

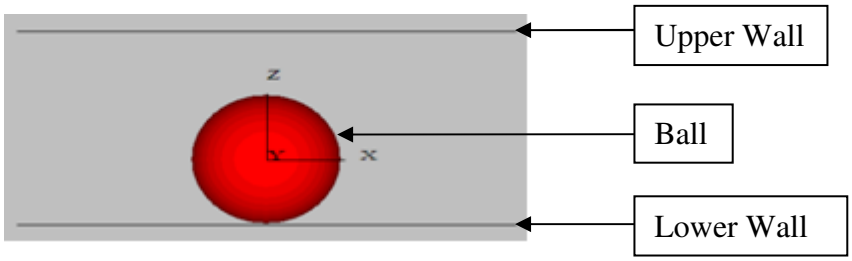

Figure 45: DEM simulation of pebble deformation experiment

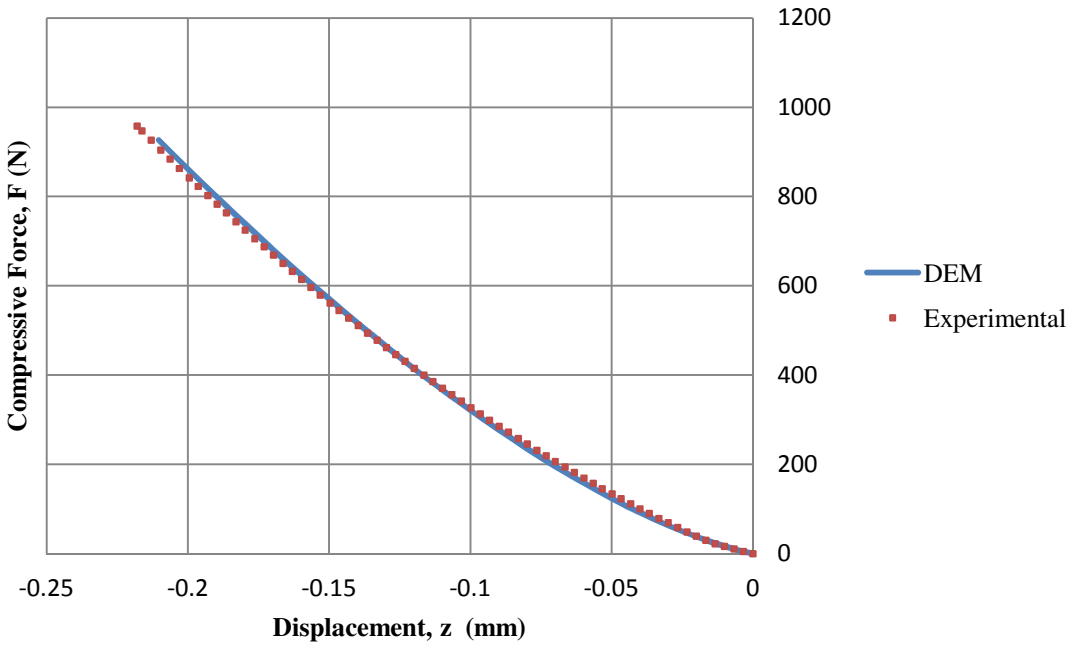

Figure 46: Comparison between DEM results and experimental results when a pebble is compressed between two mild steel plates

As can be seen from Figure 46, the DEM and experimental results are in agreement and therefore the deformation of the graphite pebbles are adequately described by the Hertz contact theory. The DEM simulation has the right contact model when the value of the shear modulus is 1.4 GPa (compared to 3.93 GPa as indicated by UCAR (2001)) and the Poisson ratio is equal to 0.2. Now that the correct contact model is incorporated into the DEM, other properties such as graphite friction must be specified.

The friction in all the DEM simulations is specified as 0.7 since this is the average value obtained from all the data sets combined. Refer to Appendix A for the friction coefficients measured during all tests. This friction value is reasonably high for a material that is considered to be a solid lubricant. This may be due to the fact that the contact pressure is much higher for spherical shaped materials during abrasion than flat graphite bars which is mostly used in other experiments. Also, the contact temperature does increase the surface friction. The friction coefficient for the pebbles and walls are the same since all parts of the reactor core is assumed to be graphite.

The density must also be specified in the DEM simulation. As already mentioned, the graphite has a density of 1760 kg/m^3 (UCAR, 2001). The pressure drop over

the pebble bed also adds to the total weight of the bed itself. The pressure drop was incorporated into the simulation by assuming the pressure drop over the pebble bed was linear (Mitchell and Polson, 2006). The resultant force due to the pressure drop was calculated and converted to mass which was then added to the pebble bed's own mass. Knowing the total pebble bed volume, a density could be calculated which included the effect of the pressure drop over the bed. The inner and outer diameters of the annulus are respectively 3.7 m and 2.0 m. The pebble bed area is given by

$$A_{Bed} = \frac{\pi({D_o}^2 - {D_i}^2)}{4} = 7.607 \text{ m}^2 \tag{6.1}$$

The total pebble mass can be calculated by knowing the weight of each pebble (m_P) as well as the number of pebbles which is 450 000.

$$m_P = \frac{4\,\pi\,\rho_P\,{R_P}^3}{3} = 0.19895 \text{ kg} \tag{6.2}$$

The pebble bed mass is

$$m_{Bed} = 450000\,m_P = 89\,528 \text{ kg} \tag{6.3}$$

The resultant force due to the pressure drop (P_D = 324.16 kPa) is

$$F_{Pressure} = P_D\,A_{Bed} = 2\,465\,772 \text{ N} \tag{6.4}$$

This pressure drop can be converted to mass which is

$$m_{Pressure} = \frac{F_{Pressure}}{g} = 251\,352 \text{ kg} \tag{6.5}$$

The total mass is then the sum of the pebble bed mass and the pressure drop component,

$$m_{total} = m_{Bed} + m_{Pressure} = 340\,880 \text{ kg} \tag{6.6}$$

The total pebble bed volume is

$$V_{Bed} = \frac{m_{Bed}}{\rho_P} = 50.87 \text{ m}^3 \tag{6.7}$$

From this information the density can be calculated

$$\rho_{Bed} = \frac{m_{total}}{V_{Bed}} = 6701 \text{ kg/m}^3 \tag{6.8}$$

Now all the correct properties are assigned to the walls and pebbles (also known as balls in PFC^{3D}). Next the reactor geometry was created. Besides the inner, outer diameter and height of the reactor, the three outlet diameters were also scaled. At full scale the diameters were all 0.5 m and was located at a height of 0.5 m below the origin. The geometry connecting the outlet and the annulus was triangular walls. The mouth of the outlets was closed to keep the balls from falling out the bottom of the reactor when they were created and settled. This was also done by creating triangular walls in a circular motion. All wall points were created in a clockwise direction such that the active side of the side walls were known, otherwise the balls would fall through the wall of the reactor. The top of the reactor was also closed. Figure 47 shows the reactor geometry in perspective view.

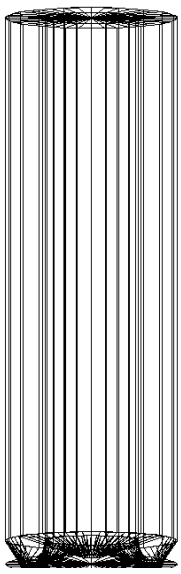

(a) - Side view of PBMR geometry

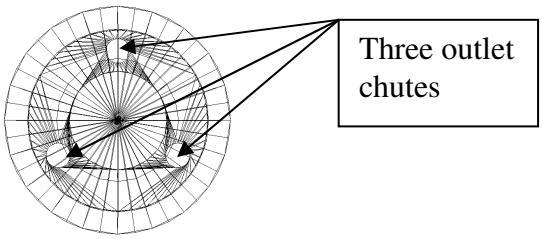

(b) - Top view of reactor geometry

Figure 47: PBMR scaled reactor geometry

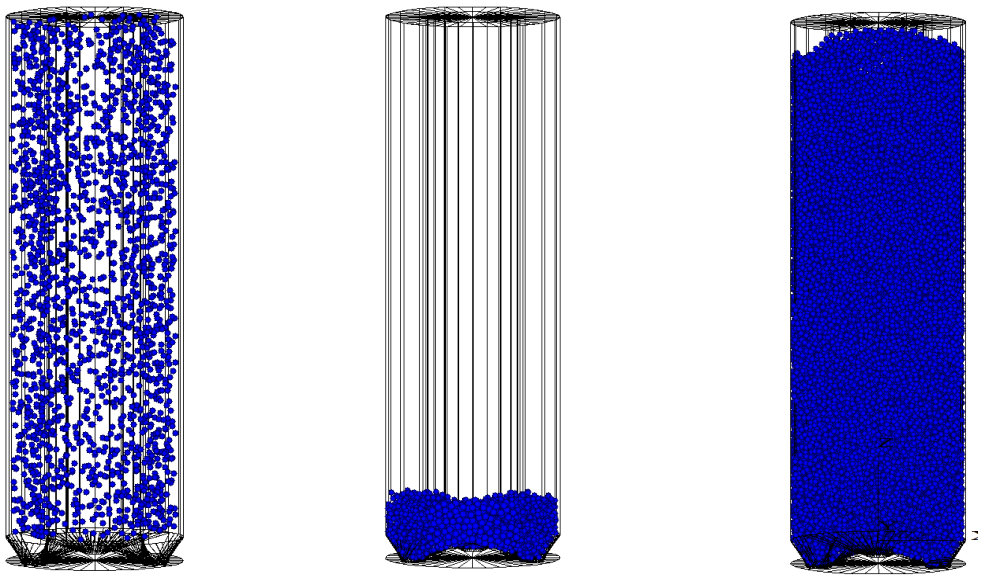

(a) - Initial creation of balls in reactor

(b) - Balls settled

(c) - Alls balls settled after multiple positions were copied

Figure 48: Creation of balls inside scaled PBMR

Initially balls were generated at random positions as shown in Figure 48 (a). Once these balls have settled (Figure 48 (b)), all the positions of balls with a height greater than zero were copied and a few levels of these compacted balls were created to fill the full height of the scaled reactor. The advantage of creating balls in the reactor in this manner is that the balls are already closely packed before settling starts. This method of packing shortens the total simulation time. Initially the unbalanced forces between the balls were significant, but since the reactor was closed at the bottom and top, the balls could not escape the reactor geometry and therefore settled until the settling criteria were met. After all the balls settled, the top part of the reactor still had space for balls which was filled by randomly generating balls in the annulus and allowed to settle for a third time. At this point the reactor was filled with balls as shown in Figure 48 (c).

6.1.3 Modelling Pebble Circulation

The geometric scale factor was chosen arbitrarily as 0.2 up to 0.6 in increments of 0.1. For a scale factor smaller than 0.2 the reactor geometry was too small in comparison to the balls since the diameters of the balls were not scaled. For a

scale factor greater than 0.6 the number of balls required to fill the reactor were too great due to the fact that only 100 000 balls can be modelled. For each scale simulation the circulation rate was doubled starting from 1500 balls/hour, 3000 balls/hour, 6000 balls/hour and lastly 12000 balls/hour. Although these circulation rates are high compared to the PBMR specifications, it was chosen as such to decrease the total simulation time. With each simulation the total graphite wear mass was computed and logged. By varying the scale factor as well as the circulation rate for each scale factor, the effect of scaling and circulation could be accounted for to calculate the wear mass for the full scale reactor.

Each simulation started with a ball being removed from each of the defueling points and was repeated at specific time intervals corresponding to the particular circulation rate. Once the balls had been removed from all three defueling points, the balls in the annulus settled. As the balls settled, data was recorded and stored in time stepping intervals of 0.1 s. At the contact between each ball and its neighbour the wear mass was computed using equation (5.4). The wear mass for all the contacts were summed together and this was repeated for each time increment until the total simulation time was reached. The total simulation time was 7.2 s. The two most important quantities which were calculated in the simulation was the normal force and relative velocity at the contact between two balls. During each time step the normal force could be calculated and stored, but the relative velocity was not so readily available. To determine it, the velocity for each ball had to be calculated. The velocity ($\bar{v}$) at the contact point of each ball has two components, the translational velocity ($\bar{v}_{tl}$) and a rotational component as shown in equation (6.9) below.

$$\bar{v} = \bar{v}_{tl} + \bar{\omega} \times \bar{r} \tag{6.9}$$

The Cartesian components for the velocity and translational velocity are

$$\bar{v} = v_x \underline{i} + v_y \underline{j} + v_z \underline{k} \tag{6.10}$$

and

$$\bar{v}_{tl} = v_{tlx} \underline{i} + v_{tly} \underline{j} + v_{tlz} \underline{k} \tag{6.11}$$

The radial vector ($\bar{r}$) is from the origin of each ball to the point of contact (Figure 49). The components for the velocity are given as,

$$v_x = v_{tx} + \omega_y r_z - \omega_z r_y \tag{6.12}$$

$$v_y = v_{ty} - (\omega_x r_z - \omega_z r_x) \tag{6.13}$$

$$v_z = v_{tz} + \omega_x r_y - \omega_y r_x \tag{6.14}$$

At the point of contact between two balls the global contact position vector ($\bar{c}$) is known as well as the global position ($\bar{b}$) of the ball centre. From these two vectors $\bar{r}$ (Figure 49) can be calculated.

$$\bar{c} = c_x \underline{i} + c_y \underline{j} + c_z \underline{k} \tag{6.15}$$

$$\bar{b} = b_x \underline{i} + b_y \underline{j} + b_z \underline{k} \tag{6.16}$$

$$\bar{r} = r_x \underline{i} + r_y \underline{j} + r_z \underline{k} \tag{6.17}$$

$$\therefore \bar{r} = (c_x - b_x)\underline{i} + (c_y - b_y)\underline{j} + (c_z - b_z)\underline{k} \tag{6.18}$$

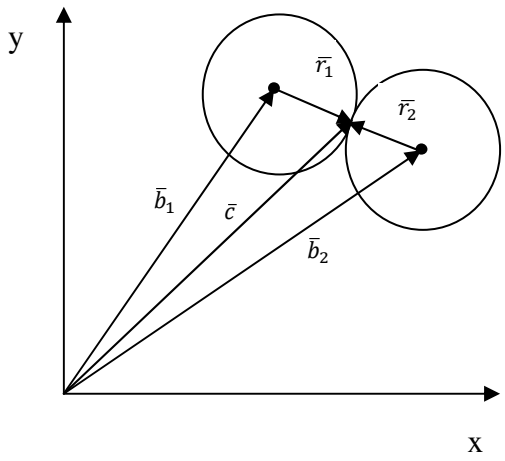

Figure 49: Radial vector representation for each pebble

Now that the velocity of each ball at the contact can be determined, the tangential component of the relative velocity ($\|\bar{v}_{rt}\|$) can be calculated and substituted into equation (5.4). Since the unit normal vector ($\bar{c}_n$) at the contact point of both

pebbles is known, the normal component of the velocity ($\bar{v}_n$) for each pebble can be determined by the dot product between $\bar{v}$ and $\bar{c}_n$ (Figure 50),

$$\bar{v}_n = (\bar{v} \cdot \bar{c}_n)\bar{c}_n \tag{6.19}$$

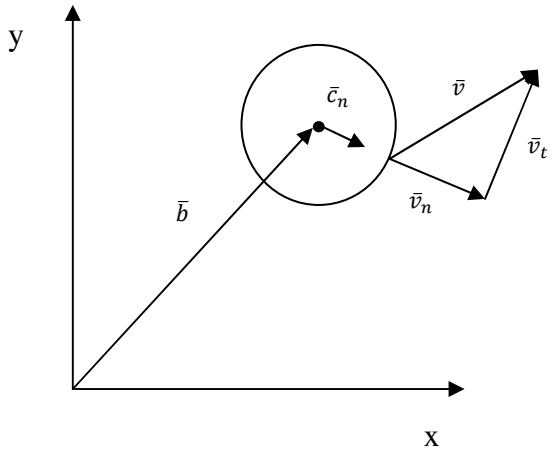

Figure 50: Velocity vector representation for each pebble

The tangential component ($\bar{v}_t$) is the difference between the ball velocity at the contact and the normal component:

$$\bar{v}_t = \bar{v} - \bar{v}_n \tag{6.20}$$

Both pebbles have a different tangential velocity in the same plane. Therefore the absolute relative velocity ($\|\bar{v}_{rt}\|$) is the difference between these two vectors:

$$\|\bar{v}_{rt}\| = \|\bar{v}_{t1} - \bar{v}_{t2}\| \tag{6.21}$$

This is true when two balls are in contact. A ball can also be in contact with the wall of the reactor. If this is the case and since the wall of the reactor has no velocity, the relative velocity between the ball and wall can be determined by calculating the normal velocity component of the ball and subtracting this from the contact velocity. The resulting tangential velocity component is parallel to the reactor wall and therefore is the correct relative velocity. The DEM results follows in the following section.

6.2 DEM Results

Table 6: DEM results for accumulated wear extent (g) in 7.2 seconds

Scale Factor (SF)	Circulation Rate (CR) (Pebbles/hour)			
	1500	3000	6000	12000
0.2	4.854e-003	7.856e-003	1.929e-002	3.675e-002
0.3	3.429e-002	3.932e-002	4.624e-002	4.705e-002
0.4	6.849e-002	1.384e-001	2.245e-001	2.956e-001
0.5	1.751e-002	1.032e-001	2.345e-001	4.871e-001
0.6	1.139e-002	6.127e-002	2.884e-001	1.306

Using the same multi-linear regression technique as in the experimental results, the following relationship exists between the wear extent W, scale factor SF and circulation rate CR,

$$W = 4.32489E-5(SF^{2.2207}CR^{1.14048}) \tag{6.22}$$

with a correlation factor, $R^2 = 0.7584$ and standard deviation, $\sigma = 0.7555$.

From equation (6.22) the wear rate $\dot{W}$ (g/s) can be given as,

$$\dot{W} = 6.00679E-6(SF^{2.2207}CR^{1.14048}) \tag{6.23}$$

For a full scale reactor geometry (SF = 1) with CR = 500, the amount of graphite mass is 0.051772 g in 7.2 seconds or 0.00719056 g/s. The annual amount of graphite dust which was calculated, assuming a FPY, is 217.4 kg/year.

6.3 Discussion of DEM Results

In Table 6 the wear extent increases with the increasing scale factor and circulation rate, which is to be expected since the number of contacts increases with increasing scale factor and higher contact velocities with increasing circulation rate. The DEM results of approximately 217 kg per annum dust production seems high when compared to the annual dust production of 3 kg for the AVR and 6 kg for the THTR-300. One of two reasons why it may be so high,

is the fact that the PBMR has much more pebbles (as much as four times) in the core compared to the other two reactors. This allows for much more multiple contacts between the pebbles which increases the potential surface area to produce dust particles. The second reason may be due to the high circulation rate of 1100 pebbles per hour, compared to the average circulation rate of 300-500 pebbles per day for both the AVR and THTR-300.

7. CONCLUSION AND RECOMMENDATIONS

In a literature review the effects of normal load, velocity, sliding distance and temperature on graphite wear in a helium atmosphere have been investigated. All these tribological parameters influence the friction at the contact which in turn may influence the wear mechanism (abrasive and adhesive) and the regime (mild or dusting). For both mechanisms, Archard's wear equation is valid, given a moderate normal force, sliding velocity and temperature. Assuming Archard's general wear equation to be valid for graphite in helium at elevated temperatures, the influence of load, velocity, sliding distance and temperature have been investigated experimentally. All the necessary requirements and specifications have been identified to design and implement a prototype pressure vessel to test the wear of graphite pebbles. An experimental method was used to acquire tribological data in such a way to determine the coefficients of the general Archard's equation. The empirical equation has been implemented into a DEM program, which simulates the gravitational flow of pebbles in the PBMR core, to estimate the annual in-core dust production. From this study it can be concluded that the amount of in-core dust production is much more when compared to earlier pebble reactor technologies such as the AVR and THTR-300. Therefore, the appropriate dust filters must be able to filter out hundreds of kilograms of annual accumulated graphite dust in order for the PBMR to function safely and effectively.

In order to continue to develop and improve the accuracy of the model, a few recommendations will be made. Firstly, more experimental data must be acquired for different grades of graphite materials. A rough grade graphite with the average particle size more than 100 µm may behave different tribological behaviour when compared to a fine grade graphite such as ATJ.

Also, the wear must be tested at temperatures in excess of 1000 ºC to simulate more realistic in-core conditions. The temperature inside the reactor is not constant. The change in temperature along the vertical position of the reactor must also be taken into account since helium entering the core is cooler at the inlet compared to the outlet and thereby affecting the distribution of pebble surface temperatures. Lower temperature increases the wear and therefore the annual estimation may even be higher. The influence of a high pressure helium environment (90 bar in PBMR) on graphite wear is also unknown.

From a DEM perspective, a small scale experimental setup must be designed and implemented in order to validate the DEM results. Alternatively, the DEM code can be altered to simulate the dust production of other pebble reactors given all necessary operational specifications such as primary coolant pressure drop and core temperature are known.

Only the dust production in the core has been simulated. In the rest of the fuel handling and storage system such as the pneumatic pebble lifting lines and loading devices graphite dust may also be produced. The pebble wear in these components may possibly also be severe due to the handling. This graphite dust may possibly also be transported back to the reactor core with a further detrimental effect on the operation of the reactor.

APPENDIX A: LITERATURE REVIEW

Experimental results for the wear extent are given in Appendix A.1. In Appendix A.2 an experimental work review is given from different authors as summarized by Hayworth (2009).

A.1 Experimental Results

Table 7: Data Set 1 with default values: x = 226 m, L = 100 N, v = 0.0942 m/s, T = 36 ºC

W	x	L	v	T	lnW	lnx	lnF	lnv	lnT	μ
0.0023	226	150	0.1256	36	-6.07485	5.420535	5.010635	-2.07465	3.583519	0.30864
0.0049	452	150	0.1256	36	-5.31852	6.113682	5.010635	-2.07465	3.583519	0.286492
0.0066	678	150	0.1256	36	-5.02069	6.519147	5.010635	-2.07465	3.583519	0.30864
0.0095	904	150	0.1256	36	-4.65646	6.806829	5.010635	-2.07465	3.583519	0.313069
0.0118	1130	150	0.1256	36	-4.43966	7.029973	5.010635	-2.07465	3.583519	0.295351
0.0050	226	150	0.0314	36	-5.29832	5.420535	5.010635	-3.46095	3.583519	0.30864
0.0051	226	150	0.0628	36	-5.27851	5.420535	5.010635	-2.7678	3.583519	0.257701
0.0045	226	150	0.0942	36	-5.40368	5.420535	5.010635	-2.36234	3.583519	0.330787
0.0044	226	150	0.1256	36	-5.42615	5.420535	5.010635	-2.07465	3.583519	0.317498
0.0029	226	150	0.157	36	-5.84304	5.420535	5.010635	-1.85151	3.583519	0.30421
0.0007	226	50	0.1256	36	-7.26443	5.420535	3.912023	-2.07465	3.583519	0.357364
0.0013	226	100	0.1256	36	-6.64539	5.420535	4.60517	-2.07465	3.583519	0.352934
0.0043	226	150	0.1256	36	-5.44914	5.420535	5.010635	-2.07465	3.583519	0.366223
0.0071	226	200	0.1256	36	-4.94766	5.420535	5.298317	-2.07465	3.583519	0.330787
0.0112	226	250	0.1256	36	-4.49184	5.420535	5.521461	-2.07465	3.583519	0.361793
0.0043	226	150	0.1256	36	-5.44914	5.420535	5.010635	-2.07465	3.401197	0.30864
0.0035	226	150	0.1256	100	-5.65499	5.420535	5.010635	-2.07465	4.60517	0.397229
0.0032	226	150	0.1256	200	-5.7446	5.420535	5.010635	-2.07465	5.298317	0.662997
0.0026	226	150	0.1256	300	-5.95224	5.420535	5.010635	-2.07465	5.703782	0.574408

Table 8: Data Set 2 with default values: x = 226 m, L = 150 N, v = 0.1256 m/s, T = 36 ºC

W	x	L	v	T	lnW	lnx	lnF	lnv	lnT	μ
0.0007	226	50	0.0628	36	-7.26443	5.420535	3.912023	-2.7678	3.583519	0.939207
0.0012	452	50	0.0628	36	-6.72543	6.113682	3.912023	-2.7678	3.583519	0.992361
0.0018	678	50	0.0628	36	-6.31997	6.519147	3.912023	-2.7678	3.583519	1.005649
0.0022	904	50	0.0628	36	-6.1193	6.806829	3.912023	-2.7678	3.583519	1.018937
0.0031	1130	50	0.0628	36	-5.77635	7.029973	3.912023	-2.7678	3.583519	0.91263
0.0019	226	50	0.0314	36	-6.2659	5.420535	3.912023	-3.46095	3.583519	0.859477
0.0017	226	50	0.0628	36	-6.37713	5.420535	3.912023	-2.7678	3.583519	0.886053
0.0015	226	50	0.0942	36	-6.50229	5.420535	3.912023	-2.36234	3.583519	0.806323
0.0017	226	50	0.1256	36	-6.37713	5.420535	3.912023	-2.07465	3.583519	0.779746
0.0015	226	50	0.157	36	-6.50229	5.420535	3.912023	-1.85151	3.583519	0.753169
0.0014	226	50	0.0628	36	-6.57128	5.420535	3.912023	-2.7678	3.583519	0.819611
0.0021	226	100	0.0628	36	-6.16582	5.420535	4.60517	-2.7678	3.583519	0.965784
0.0050	226	150	0.0628	36	-5.29832	5.420535	5.010635	-2.7678	3.583519	1.523897
0.0064	226	200	0.0628	36	-5.05146	5.420535	5.298317	-2.7678	3.583519	0.78639
0.0107	226	250	0.0628	36	-4.53751	5.420535	5.521461	-2.7678	3.583519	1.457455
0.0016	226	50	0.0628	30	-6.43775	5.420535	3.912023	-2.7678	3.401197	0.859477
0.0012	226	50	0.0628	100	-6.72543	5.420535	3.912023	-2.7678	4.60517	0.992361
0.0010	226	50	0.0628	200	-6.90776	5.420535	3.912023	-2.7678	5.298317	1.085379
0.0005	226	50	0.0628	300	-7.6009	5.420535	3.912023	-2.7678	5.703782	1.616915

Table 9: Data Set 3 with default values: x = 226 m, L = 50 N, v = 0.0628 m/s, T = 36 ºC

W	x	L	v	T	lnW	lnx	lnF	lnv	lnT	μ
0.0016	226	100	0.0942	36	-6.43775	5.420535	4.60517	-2.36234	3.583519	0.47751
0.0032	452	100	0.0942	36	-5.7446	6.113682	4.60517	-2.36234	3.583519	0.629064
0.0049	678	100	0.0942	36	-5.31852	6.519147	4.60517	-2.36234	3.583519	0.540696
0.0058	904	100	0.0942	36	-5.1499	6.806829	4.60517	-2.36234	3.583519	0.522757
0.0071	1130	100	0.0942	36	-4.94766	7.029973	4.60517	-2.36234	3.583519	0.533587
0.0029	226	100	0.0314	36	-5.84304	5.420535	4.60517	-3.46095	3.583519	0.476248
0.0022	226	100	0.0628	36	-6.1193	5.420535	4.60517	-2.7678	3.583519	0.552855
0.0018	226	100	0.0942	36	-6.31997	5.420535	4.60517	-2.36234	3.583519	0.552855
0.0017	226	100	0.1256	36	-6.37713	5.420535	4.60517	-2.07465	3.583519	0.509867
0.0016	226	100	0.157	36	-6.43775	5.420535	4.60517	-1.85151	3.583519	0.832443
0.0003	226	50	0.0942	36	-8.11173	5.420535	3.912023	-2.36234	3.583519	0.409806
0.0017	226	100	0.0942	36	-6.37713	5.420535	4.60517	-2.36234	3.583519	0.443027
0.0040	226	150	0.0942	36	-5.52146	5.420535	5.010635	-2.36234	3.583519	0.489536
0.0074	226	200	0.0942	36	-4.90628	5.420535	5.298317	-2.36234	3.583519	0.462959
0.0117	226	250	0.0942	36	-4.44817	5.420535	5.521461	-2.36234	3.583519	0.49618
0.0021	226	100	0.0942	36	-6.16582	5.420535	4.60517	-2.36234	3.401197	0.49618
0.0017	226	100	0.0942	100	-6.37713	5.420535	4.60517	-2.36234	4.60517	0.829321
0.0016	226	100	0.0942	200	-6.43775	5.420535	4.60517	-2.36234	5.298317	1.006455
0.0013	226	100	0.0942	300	-6.64539	5.420535	4.60517	-2.36234	5.703782	1.585829

The average friction coefficient for all the tests is approximately 0.7.

A.2 Summary of Experimental and Theoretical Results from Literature (Hayworth, 2009)

Table 10: Summary of literature review

Reference	Type of Contact	Load	Speed	P	Type of gas	T (°C)	Coeffcient of friction	Wear	Comments:
Driesner and Wagner (1958)	Graph-i-tite G Homogeneous button on ring	7.1Mpa	1mm/s	1atm	air	room	0.35 (s) 0.25 (k)		
					helium	2450	0.65 (s) 0.4 (k)		
Lancaster and Pritchard (1980)	Electrographite pin on non-graphitic carbon ring	22N	8m/s	1atm	air	room to 260	0.5	0.0085 $mm^3N^{-1}m^{-1}$	Dusting wear was maintained at all times during these experiments.
		1 to 60N	8m/s	1atm	air	200	0.3-0.5	0.0085 $mm^3N^{-1}m^{-1}$	The total surface temperature was higher than the ambient temperature due to the sliding speeds, and ranged from 200 to 600°C. The decrease in wear rate at the high sliding speeds for 22N load occurred at a surface temperature above 500°C and a relative partial pressure of water vapour below 10^{-5} relative partial pressure of water
		22N	2 to 10m/s	1atm	air	200	0.4-0.5	0.0085 $mm^3N^{-1}m^{-1}$	
			10 to 20m/s	1atm	air	200	0.5	0.0085 to 0.003 $mm^3N^{-1}m^{-1}$	
Li and Sheehan (1981)	POCO AXF-5Q graphite Homogeneous button on plate	3.45MPa	0.0071mm/s (Linear motion 6.4mm stroke)	1.68 atm	air	room	0.35	3.5 x 10^{-4} g/m	-
					Helium (pure 5ppm O_2 2ppm H_2O)	room	0.52		
						450	0.05		
						850	0.2		
					HTGR Helium (pure 5ppm O_2 2ppm H_2O 12ppm CH_4 12ppm H_2 6ppm CO)	room	0.63		
						450	0.02		
						850	0.12		

Table 10: Summary of literature review (continued)

Reference	Type of Contact	Load	Speed	P	Type of gas	T (°C)	Coeffcient of friction	Wear	Comments:
Kichuki *et al.* (1984)	PGX Graphite Plate: against PGX graphite hemisphere	9.8N	5Hz 5mm stroke		Helium (pure)	1000	0.3-0.7	In order of $0.5x10^{-6}$ g/m for most impurity variations, but $55.2x10^{-6}$ g/m for high O_2 concentration ($553x10^3$ ppm)	Friction was lowest (0.1) at the $553x10^3$ ppm O_2, but this amout of O_2 causes oxidative burn off producing the very high wear rate observed.
					Helium (variable impurities)	1000	0.1-0.4		
	against Hastelloy XR hemisphere	9.8N	5Hz 5mm stroke	0.2MPa	Helium (variable impurities)	1000	0.2-0.5	Not specified	No strong dependence on the impurities was observed
	against calorized Hastelloy XR hemisphere	9.8N	5Hz 5mm stroke	0.2Mpa	Helium (variable impurities)	1000	0.1-0.2		No strong dependence on the impurities was observed Reduction in friction attributed to properties of calorized layer
	Against Cr-Mo steel hemisphere	9.8N	5Hz 5mm stroke	0.2Mpa	Helium (variable impurities)	500	0.6-1.1		Friction increases from pure helium to high O_2 content due to formation of iron oxide layer
Zaidi *et al.* (1990)	Pin of unspecified material against high purity soft graphite.	10N	$3x10^{-4}$ to 3m/s	10 to 10^5 Pa	Vacuum with H_2O, O_2 or H_2 added	-	0.3-0.6	Not specified	The experiments were performed in order to determine the wear transitions induced by each of the active gases over the range of pressures.
Robert *et al.* (1995)	Pin of unspecified material against Electrographite EG 319 P and Morganite MY3 A	4N	0.03m/s	10^{-4}Pa	vacuum	-	0.45-0.6		
				10^{-4} to $1.6x10^5$ Pa	Argon/ Helium	-	0.45 -0.02 (with time)		
		20N	0.03m/s						

Table 10: Summary of literature review (continued)

Reference	Type of Contact	Load	Speed	P	Type of gas	T (°C)	Coefficient of friction	Wear	Comments:
Zaidi *et al.* (1995)	Pin of unspecified material on graphite disc	-	-	-	vacuum	-	0.55	-	The friction in the air/argon environment decreases with both increasing argon partial pressure and time. The low friction in inert gas environments is attributed to the insertion of the gas molecules into the lattice, promoting alignment of the basal plates
					O_2	-	0.25		
					air	-	0.2		
					Water vapour	-	0.12		
					Inert gas	-	0.02		
		4N	0.03m/s	$1.5x10^5$ Pa	Air/argon	-	0.45-0.02		
Semenov (1995)	АГ-1500, АГ-600 and ЭЭR graphite (tube on sphere)	-	-	10^{-5} torr	vacuum	room	0.7-0.75	-	No difference in friction was observed between sliding in vacuum and inert gas environments
						1500	0.1-0.15		
				-	air	-	0.08		
Sheng *et al.* (2003)	KG11 graphite (surface contact)	31N	0.54m/s	latm	air	room	-	$2.27x10^{-7}$g/m	Examination of worn surfaces and debris showed no clear difference in wear mechanism from one case to another. Overall fatigue wear seemed dominant and dusting wear was not observed
	KG11 graphite (line contact)	31N	0.78m/s	latm	air	room	-	$1.02x10^{-6}$g/m	
		62N	0.78m/s	latm	air	room	-	$1.99x10^{-6}$g/m	
Luo *et al.* (2004)	IG-11 graphite (Homogenous cylinder on disc)	20N	10Hz	latm	air	room	-	$1.4\text{-}0.3x10^{-6}$g/m	The wear rates decrease steadily from the break-in condition initially to the equilibrium wear rate.
		30N	10Hz	latm	air	room	-	$2.1\text{-}0.7x10^{-6}$g/m	
		40N	10Hz	latm	air	room	-	$4.2\text{-}1.4x10^{-6}$g/m	

Table 10: Summary of literature review (continued)

Reference	Type of Contact	Load	Speed	P	Type of gas	T (°C)	Coeffcient of friction	Wear	Comments:
Luo *et al.* (2004) (Cont.)	IG-11 graphite cylinder on stainless steel disc	30N	10Hz	1atm	air	room	-	7.6-2.8x10^{-6}g/m	Wear rate decreases from break in to equilibrium but unlike homogeneous contact, formation of a third body film results in equilibrium wear rate being independent of load (for this range)
		40N	10Hz	1atm	air	room	-	8.3-2.8x10^{-6}g/m	
		50N	10Hz	1atm	air	room	-	10.4-2.8x10^{-6}g/m	
Sheng and Yu (2004)	Theoretical model using previously obtained experimental results	31N (and 38.5kPa)	0.54m/s	-	-	-	0.4	2.27x10^{-10}kg/m resulting in a 48mm wear depth over 10 years	The theoretical model assumes wear volume proportional to friction and velocity. The origin of the value used for their proportionality factor is unclear. Also unclear is what surface area the stated depth of wear will cover. Overall their conclusion, that 80% of the volume of the pebbles will be worn away, seems excessive compared to other research.
Luo *et al.* (2005)	IG-11 graphite homogeneous rounded cylinder on disc	30N	10Hz (2mm stroke)	1atm	helium	room	-	8.3-2.1x10^{-6}g/m	Wear decreases from break-in to equilibrium. No clear pattern of wear with temperature is observed, other than the wear rate is lowest at room temperature and highest at 400°C. The equilibrium wear rates for sliding against both graphite and stainless steel settle at 2.1x10^{-6}g/m, except at the highest temperatures, when an increase is seen. The break in wear rates are much higher for sliding against stainless steel
						100	-	7.6-2.1x10^{-6}g/m	
						200	-	5.5-2.1x10^{-6}g/m	
						300	-	11.1-2.1x10^{-6}g/m	
						400	-	13.2-3.5x10^{-6}g/m	
	IG-11 graphite rounded cylinder on stainless steel disc	30N	10Hz (2mm stroke)	1atm	helium	room	-	17.4-2.1x10^{-6}g/m	
						100	-	42.7-2.1x10^{-6}g/m	
						200	-	40.2-2.1x10^{-6}g/m	
						300	-	47.2-9.0x10^{-6}g/m	
						400	-	52.8-9.7x10^{-6}g/m	
Luo *et al.* (2006)	IG-11 graphite homogeneous flat cylinder on disc	30N	≈0	1atm	air	room	0.05	-	These coefficient of friction values are not equilibrium values. The surfaces were prepared to a given set of roughness values in order to determine the effect of roughness. In general the rougher surfaces had lower friction coefficients than the smoother ones.
					helium	room	0.02	-	
			0.005-0.08m/s	1atm	air	room	0.19-0.3	-	
					helium	room	0.16-0.44	-	

Table 10: Summary of literature review (continued)

Reference	Type of Contact	Load	Speed	P	Type of gas	T (°C)	Coefficient of friction	Wear	Comments:
Cachon and Falcand (2008)	CEA tribometer Homogeneous PCEA graphite pin on rail	5MPa	0.01m/s 18mm stroke	2.5atm	Helium with impurities	800	0.18	0.01mm/200m	The wear values are given as depth worn per total sliding distance. The difference in friction observed between the two test setups is attributed to the larger surface area of the CEA test pin, which allows more debris to be trapped and a more significant third body film to form. It is also noted that the impurity levels are higher in the CEA apparatus, leading to possible protection of metal surfaces by oxidation.
		10MPa	0.01m/s 18mm stroke	2.5atm	Helium with impurities	1000	0.22	0.02mm/200m	
	CEA tribometer PCEA graphite pin on 800H steel rail	10MPa	0.01m/s 25mm stroke	2.5atm	Helium with impurities	500	0.04	0.05mm/200m	
						850	0.04	0.03mm/200m	
	ANP tribometer homogeneous PCEA graphite pin on disc	10MPa	0.01m/s Stroke -	1.1atm	Helium with impurities	800	0.85	0.02mm/200m	
						1000	0.47	0.02mm/200m	
		20MPa	0.01m/s Stroke -	1.1atm	Helium with impurities	1000	0.56	0.02mm/200m	
	ANP tribometer NBG-17 graphite homogeneous pin on disc	10MPa	0.01m/s Stroke -	1.1atm	Helium with impurities	800	0.90	0.02mm/200m	
						1000	0.58	0.06mm/200m	
Siemens (-)	-	-	-	-	helium	100	0.65	-	Experimental methods used to determine these values are not specified.
						600	0.5		
						1000	0.3		
Cogliati and Ougouag (2008)	DEM computer simulation of graphite dust production in the PBMR	Varies in model	Varies in model	-	-	-	0.4 (k) 0.65 (s)	3.290×10^{-8} g/(Nm) results in 4.0g dust per year	The result is 3 orders of magnitude less than the dust produced by the AVR. Values for friction and wear coefficients that are more applicable to the actual environment in the reactor are needed to improve result.

APPENDIX B: EXPERIMENTAL SETUP AND DESIGN

B.1 Pressure Vessel Finite Element Method Design

The Inventor Algor FEM analysis for the steady-state temperature distribution of the outer chamber surface is shown in Figure 51. The minimum outside temperature is 51.7 ºC and the maximum inside temperature is just above 400 ºC. The 3D model was created with Inventor Professional 2011 and exported to Algor. In this analysis the solid mesh type is bricks and tetrahedras. Also, an automatic geometry-based mesh size function is used to create the mesh. A value of 0.05 is used for as a fraction of the surface mesh size.

A surface heat flux of 3000 W/m^2 was specified for one of the side walls of the stainless steel chamber. Furthermore, a surface convection load was specified for the outside chamber with a convection coefficient of 15 W/ºC m^2. This value was assumed since it is a typical value for a heat transfer analysis for a object at room temperature.

The surface heat flux was increased until the inside temperature of the chamber was just above 400 ºC which is the maximum design temperature for the pressure vessel. Once the maximum temperature was reached, the simulated outside temperature of the pressure vessel was obtained. The maximum measured outside temperature during the experiment was approximately 60 ºC.

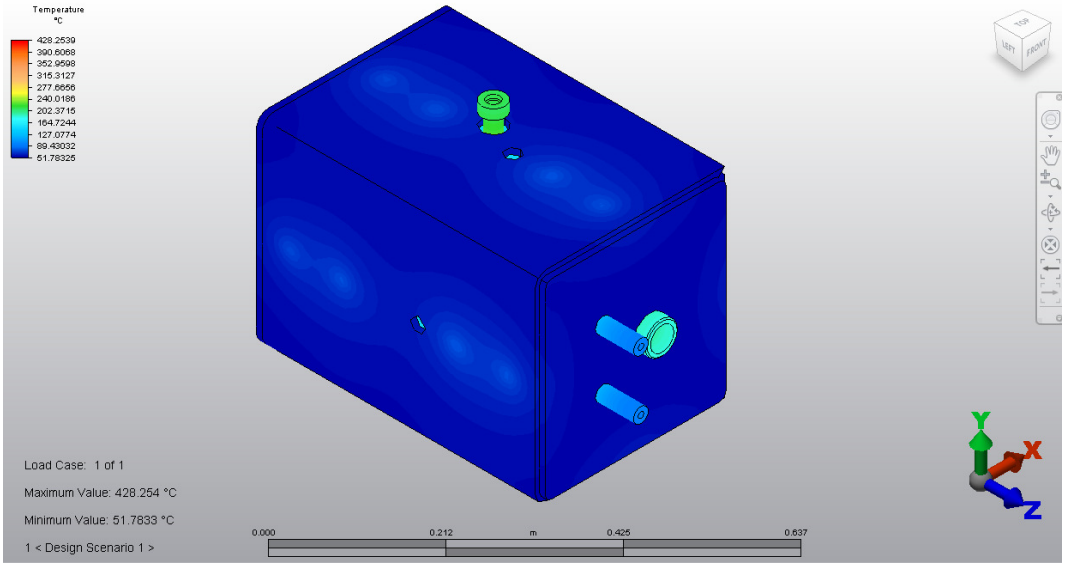

Figure 51: Pressure vessel steady-state surface temperature

B.2 Pebble Bed Mechanics

B.2.1 Derivation of the Modified Janssen's Theory for Flow of Granular Material in an Annular Geometry

The vertical and horizontal pressure on a cylinder due to the mass of granular material are affected by the friction between the material and cylinder. The effect of this phenomenon is that the pressure at the bottom of the cylinder are less if compared to the pressure when the cylinder walls are frictionless. See Figure 52 for the resultant forces on a section of an annular cylinder filled with granular material. The following assumptions apply (Sperl, 2005),

1. P_v = constant in a horizontal plane.
2. The relation $k = P_h/P_v$ is constant and independent of depth x.
3. The density, ρ , is independent on the depth x.
4. The material is on the verge of moving down.
5. The friction coefficient is constant.

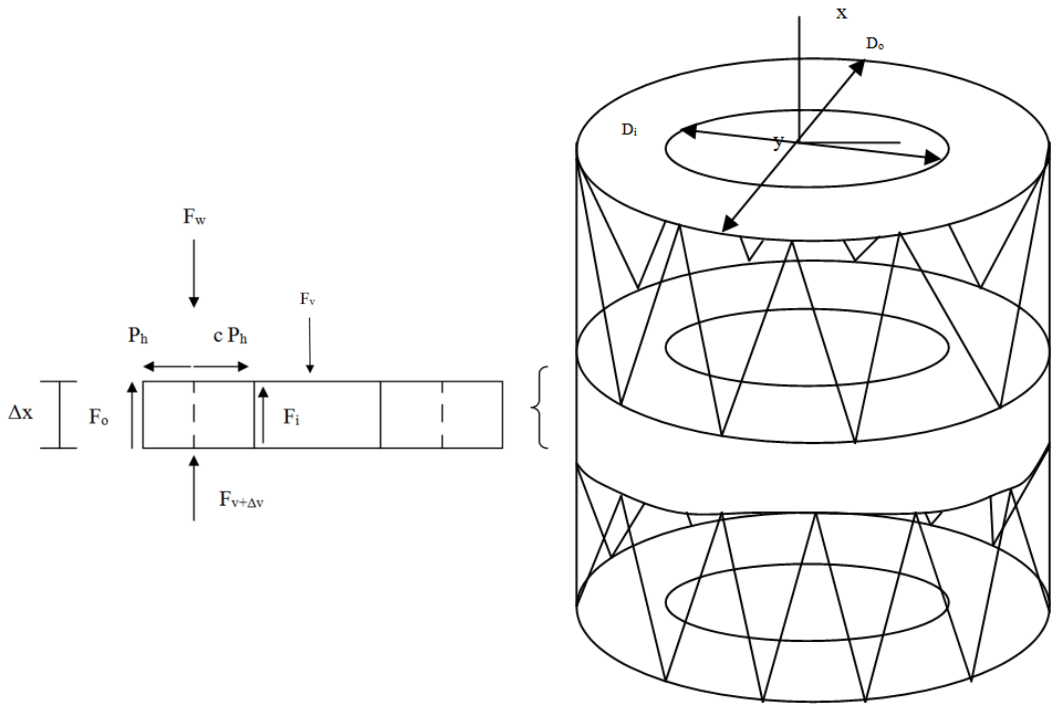

Figure 52: Elemental disk section from an annular reactor geometry

The resultant forces of the elemental disk Δx is,

$$F_V = \frac{\pi}{4}\left({D_o}^2 - {D_i}^2\right)P_V \tag{B.1}$$

$$F_{V+\Delta V} = \frac{\pi}{4}\left({D_o}^2 - {D_i}^2\right)(P_V - \Delta P_V) \tag{B.2}$$

$$F_i = \pi D_i \Delta x \mu c P_H \tag{B.3}$$

$$F_o = \pi D_o \Delta x \mu P_H \tag{B.4}$$

$$F_w = \frac{\pi}{4}\left({D_o}^2 - {D_i}^2\right)\Delta x \rho g \tag{B.5}$$

If the disk is on the verge of moving downwards:

$$F_{V+\Delta V} + F_i + F_o = F_V + F_w \tag{B.6}$$

Substituting $P_H = kP_V$ into the equation, the following is obtained:

$$\frac{\Delta P_V}{\Delta x} + \frac{4k\mu(D_o + cD_i)P_v}{{D_o}^2 - {D_i}^2} = \rho g \Delta x \tag{B.7}$$

Letting $\Delta x \to 0$ and $D = \frac{{D_o}^2 - {D_i}^2}{D_o + cD_i}$, solving the equation:

$$P_V = \frac{\rho g D}{4\mu k}\left(1 - e^{-\frac{4\mu k x}{D}}\right) + P_{V_0}\left(e^{-\frac{4\mu k x}{D}}\right) \tag{B.8}$$

If no initial pressure condition exits such at x = 0, which is the case for modelling the PBMR where the pebble density is adapted to account for the helium pressure drop, $P_{V_0} = 0$.

B.2.2 Matlab Code for Janssen's Theory

```
clc
clear all

load Wallpressure
load WallForces

WallForce = Wall_zpos_force(1:372,2);
Wallpressure = Wall_zpos_pressure(1:372,2);
Wallpos = Wall_zpos_pressure(1:372,1);

mu = 0.7;
phi = atan(mu);
%k = (1-sin(phi))/(1+sin(phi))
k = 0.047
c = 20;
rho = 6701;
g = 9.81;
% Do = 1.2;
% Di = 0.25;
Do = 3.7;
Di = 2;
D = (Do^2-Di^2)/(Do + c*Di);
Area = pi*(Do^2 - Di^2)/4;

% x = [0:0.0001:18.65];
x = [0:0.06:11];
x = fliplr(x);

PV = ((rho*g*D)/(4*mu*k)).*(1-exp((-4*mu.*k.*x)./(D)));

PV = fliplr(PV);

PH = PV*k;


%VForce = PV*Area/2460;
%plot (x,VForce)
plot(x,PV,'--')
%plot(x,PH)
%hold
%plot(Wallpos,Wallpressure,'r')
%plot(Wallpos,WallForce)
```

B.3 Matlab Code for Hertz Stress at Contact

In the Matlab-code below the principle stresses are calculated when two graphite pebbles with the correct physical properties are compressed against each other. From these principle stresses the shear stress (t_max) is calculated and the result is shown in Figure 44.

```
clc
clear all
mu1 = 0.2;
mu2 = 0.2;
E1 = 2*(1+mu1)*1.4E9;
E2 = E1;
R1 = 0.03;
R2 = R1;
F = 20;


Estar = ((1-mu1^2)/E1 + (1-mu2^2)/E2)^-1;
Rstar = (1/R1+1/R2)^-1;

a = ((3*F*Rstar)/(4*Estar))^(1/3);

pmax = (3*F)/(2*pi*a^2);

z = [0:0.00005:5*a];

zeta = z./a;

sx = -pmax*((1-abs(zeta).*atan(1./(abs(zeta))))*(1+mu1) -
1./(2*(1+zeta.^2)));
sy = sx;
sz = -pmax./(1+zeta.^2);

s1 = sx./pmax;
s2 = s1;
s3 = sz./pmax;

t_max = (s1-s3)/2;

figure(1)
hold
plot(zeta,abs(s1),'--')
plot(zeta,abs(s3),'.')
plot(zeta,t_max)
```

B.4 Calibration of Sensors

B.4.1 Thermocouple

The thermocouple (type k) was calibrated in an oil bath with a mixer to ensure homogeneous oil mixture and platinum thermocouple. The platinum thermocouple was coupled to an electrical circuit and the resistance. The resistance was converted to actual temperature measurements by means of an existing calibration curve for the circuit. The temperature was measured in equal time intervals and the actual and measured temperature obtained.

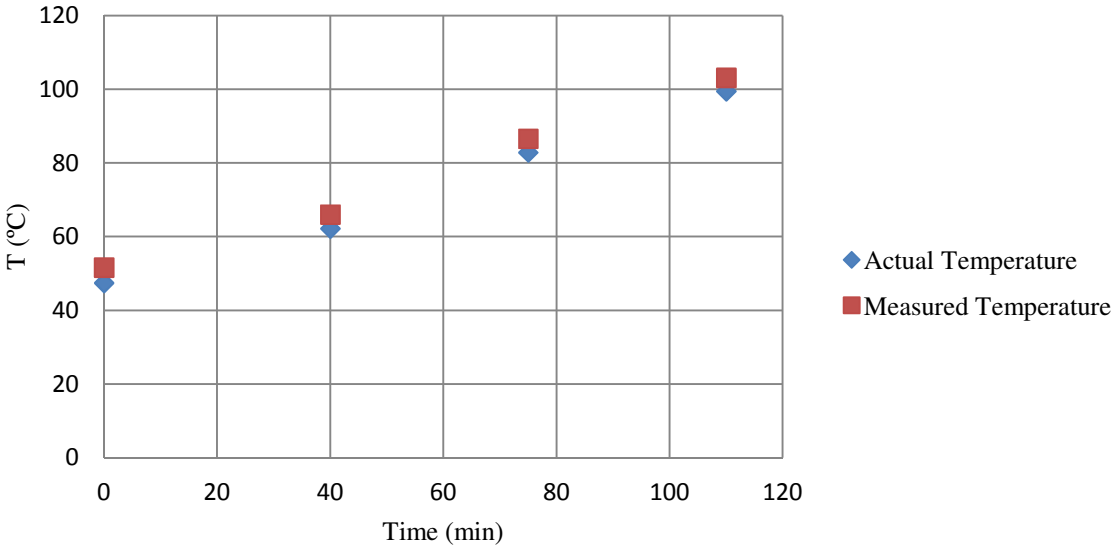

Figure 53: Calibration data for thermocouple

Figure 53 shows the comparison between the actual oil temperature and thermocouple temperature. From Figure 54 the error as a function of thermocouple temperature is obtained. From this data the calibrated thermocouple temperature (T_{cal}) is given as:

$$T_{cal} = T - 7.8306T^{-0.168}\ (°C) \qquad \text{(B.9)}$$

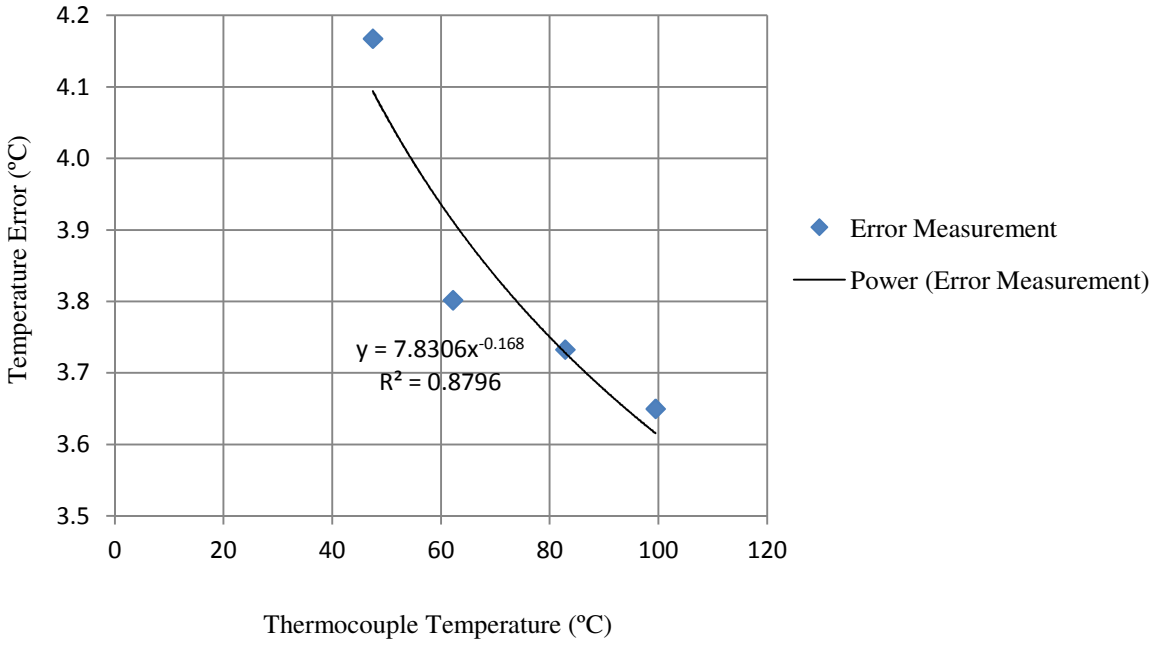

Figure 54: Thermocouple error curve

B.4.2 Torque Transducer

The torque transducer was calibrated using a torque calibration arm that was clamped to the front end of the drive shaft. Calibration weights were suspended from the end of the arm at a known distance from the centre of the drive shaft. The resultant torque value (T_v) was then compared to the voltage read-out to obtain an equation for torque-based transducer voltage (V_{torque}). The following equation was obtained (Conradie, 2010):

$$T_v = 19.9326V_{torque} + 0.790974 \quad \text{(B.10)}$$

The torque is used to obtain the frictional force at the contact between the two graphite specimens.

B.4.3 High Temperature Displacement Transducer

The displacement transducer has been calibrated at room temperature by measuring the worn distance (refer to Figure 55) from the instance the transducer has been zeroed. The rotation graphite specimen was placed inside the chamber with the high temperature bearing on top of the specimen. At this instance the transducer was zeroed electronically. After the specimen has been worn for a few minutes, the weight of the specimen was noted as well as the distance on the transducer electronic display. Once the calibration curve has been fitted to the data, the true wear extent could be measured at any instance during the experiment.

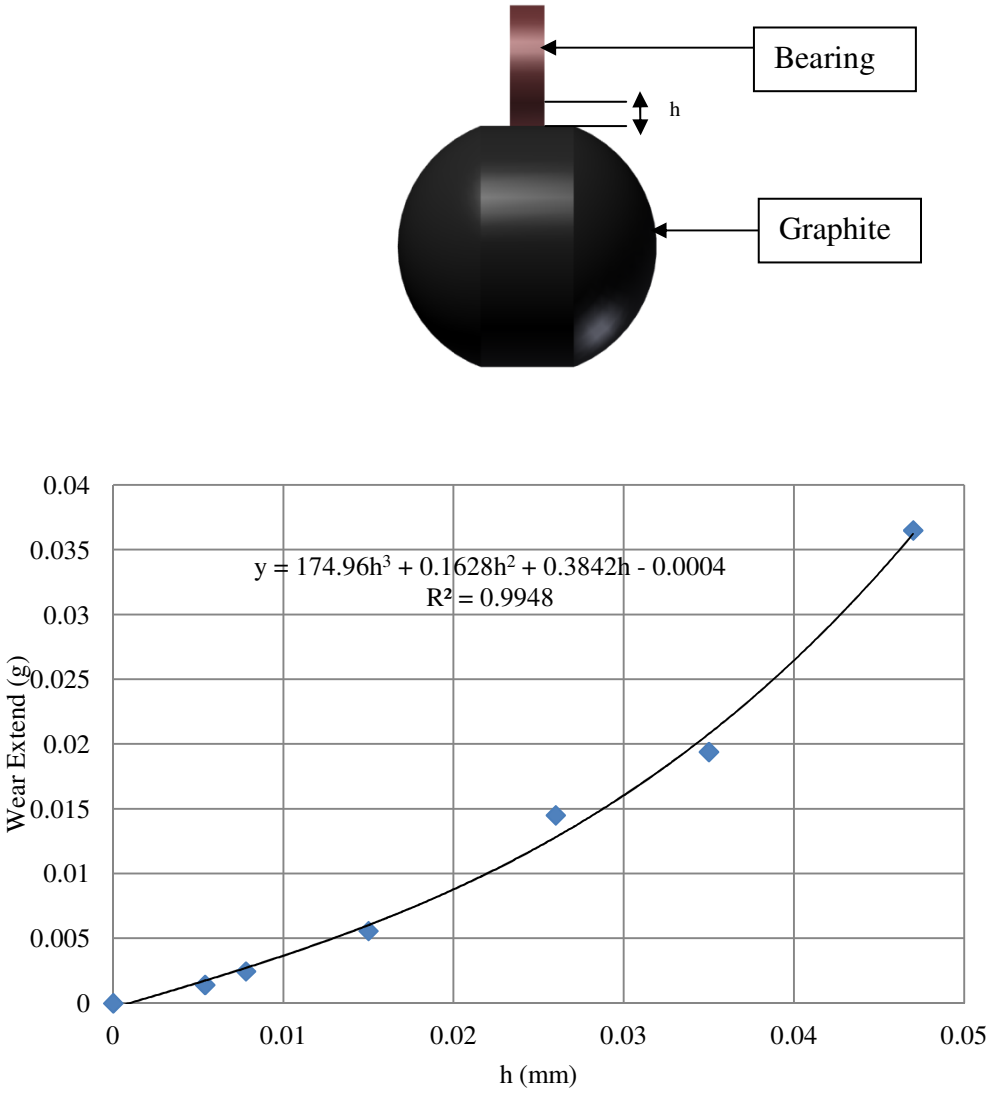

Figure 55: Calibration curve for displacement transducer

B.5 Experimental Setup Sample Pictures

In Figure 56 on the left is a box with the Gefran Temperature controller. Inside the box is the 110 V, 2.3 kW transformer and other electrics. On the right is the general setup as seen from the side.

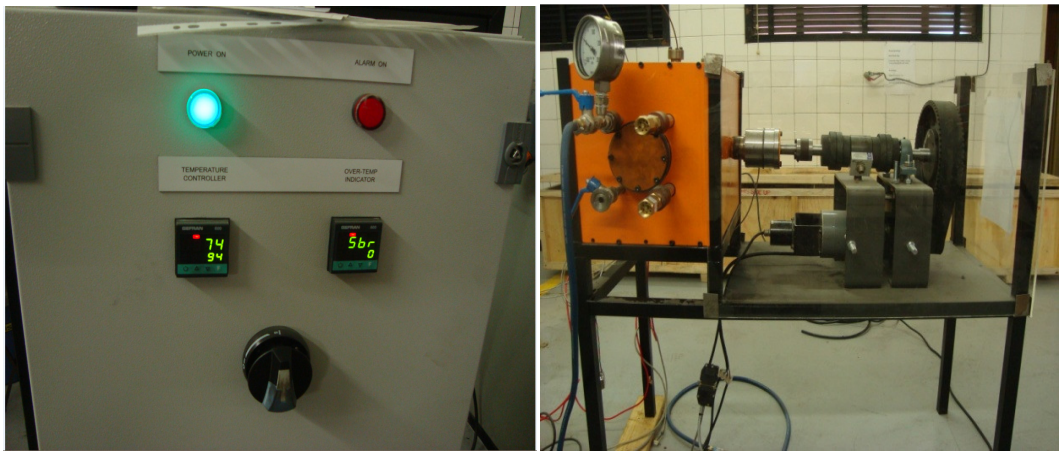

Figure 56: Temperature control system (left) and general setup (right)

In Figure 57 on the left is the HBM (100 Nm) torque transducer with two couplings attached to it to account for misalignment between the shaft and the driver pulley. On the right is the general setup with the computer as seen from the front. The stepper motor was controlled with AX-software. The spider can also be seen on the right bottom and was used to record the normal applied load.

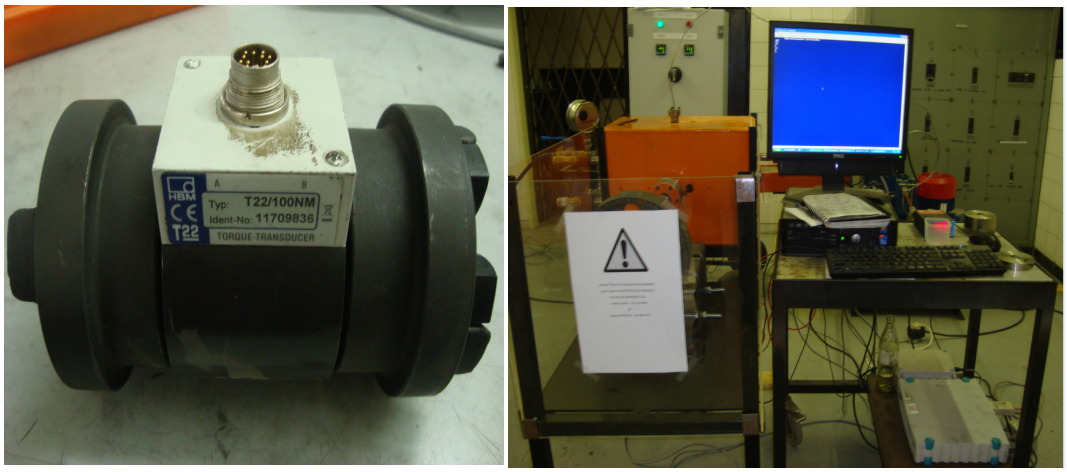

Figure 57: Torque transducer (left) & general setup (right)

In Figure 58 the heating element can be seen inside the stainless steel chamber. The pressure gauge on the outside was used to monitor the helium pressure differential between the chamber and the environment. The 2 bar brass safety valves can also be seen on the left. On the right is the rotational shaft which rotated the graphite specimen. On the shaft is the rotational seal which locates on the shaft and presses with the silicon-carbide face against the stationary seal.

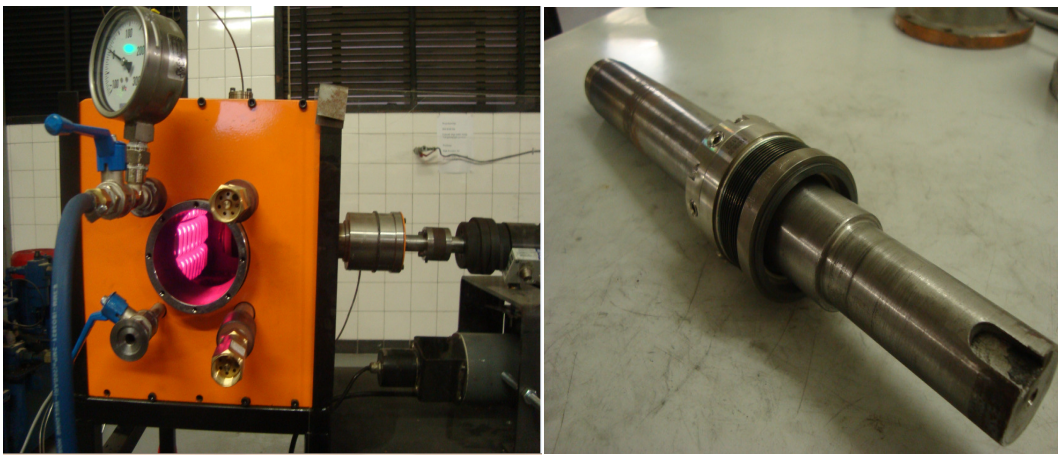

Figure 58: Heating element in chamber (left) & rotational shaft with rotation seal assembly (right)

In Figure 59 on the left is the helium base 5 with the flow meter to supply helium to the pressure vessel. The flow rate to maintain a pressure differential of 50 kPa was between 5 Lpm and 10 Lpm. On the right is the stationary seal which was located inside the rotation pipe.

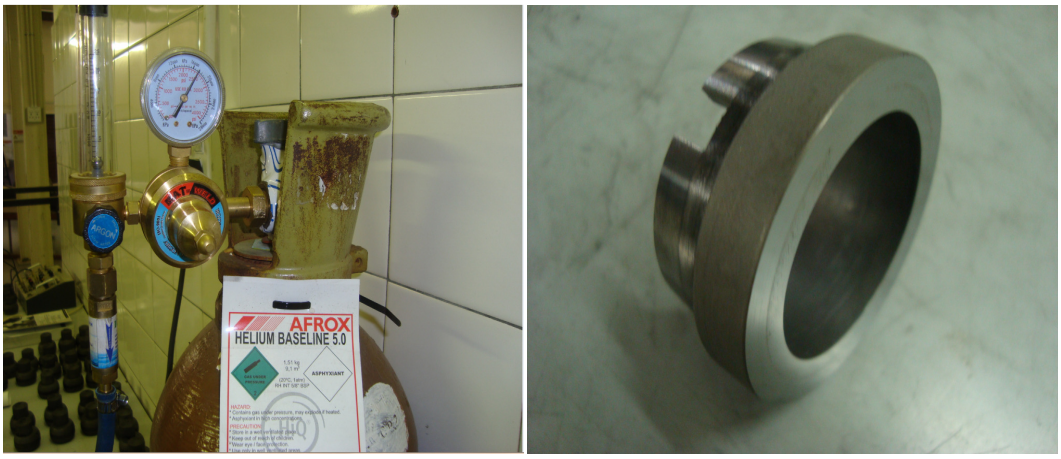

Figure 59: Helium baseline 5 cylinder and flow meter (left) & the stationary seal (right) with one face pressing against the rotational seal

APPENDIX C: DEM CODE

C.1 DEM Code for Annular Reactor Geometry Horizontal Pressure Distribution

In this section the pressure distribution along the vertical height of a reactor annular geometry (see Figure 15) is simulated and illustrated in Figure 16. CreateCylinders in section C.1.1 creates the annular reactor geometry with a base which consists of three outlets spaced at a 120º angle from each other. The function which creates the base is CloseTopBottom. After the reactor geometry is created, the positions of balls are randomly created with function AddFirstBalls. The balls are then allowed to settle to the bottom by activation gravity. The balls are closely packed together and the positions of all the balls are copied to fill the rest of the reactor. This function is called AddBalls. Once all balls have settled, the pressure distribution on the side walls can be calculated in Section C.2.

C.1.1 - Reactor geometry created

```
new
;-----------------------------------------------------------------------------------------------
define Geometry
      ;=== USER INPUT
================================================
         Origin_x = 0.0          ;coordinates of point 1 on box
         Origin_y = 0.0
         Origin_z = 0.0
         BotDist = 0.5
         BotAngle = 0.0                  ;deg
         BotAngle=BotAngle*pi/180.0
         Wallangle = 60.0
         Wallangle1 = (150-Wallangle)*pi/180.0
         Wallangle2 = (150+Wallangle)*pi/180.0
         Lz = 30.0               ;height  Lz_actual = 11.0
         dz = 0.05               ;cylinder incremental height
         Nc = Lz/dz              ;Number of cylinders
         Do = 1.0                ;outer diameter
         Di = 0.25               ;inner diameter
         levelsnr = 129
         NrSeg = 50
         br1 = 0.03              ;ball radii
         br2 = 0.03
         Nb = 500
         ;Nb  = 2000             ;number of balls 30 degrees
         ;Nb  = 2700             ;number of balls 30 degrees
         ;Nb  = 1000             ;number of balls 45 degrees
         ;Nb  = 1400             ;number of balls 60 degrees
```

```
        ;Nb  = 2000              ;number of balls 60 degrees
         ID_start = 1            ;first ID of box walls
        ;specify wall properties
        command
                macro wall_props 'kn = 1e8 ks = 1e8 fric = 0.7'
                macro ball_props 'shear = 1.4e9 poiss = 0.2 fric = 0.7 dens =
                6701.0'
                ;if maxfric "off", it uses the minimum of wall and ball friction,
                otherwise the maximum
                wall property maxfric off
        endcommand

        ;=== END USER INPUT
==========================================
        ;general model settings
        command
        set time = 0.0                  ;reset
        set def_dt = 1e-4               ;timestep size with no balls
        set max_balls = 100000                  ;default = 5000 - reserves memory
        set safety_fac = 0.8            ;time step size safety factor: default = 0.8
        set dtcalc = 1000               ;steps taken before new stable time step is
        calculated: default = 1
        set gravity 0.00  0.00 -9.81    ;gravity components
        wall property maxfric on        ;if "on" uses the maximum friction
        coefficient of ball and wall, otherwise the minimum
        endcommand
        ;=== USER INPUT START ===
        ;solve static equilibrium damping values
        dampG  = 0.7                            ;local mass damping   [-]
        dampn  = 0.0                            ;contact viscous damping  [-]
        damps  = 0.0
        ;final damping values
        dampG_f  = 0.3                                  ;local mass damping   [-]
        dampn_f  = 0.0                                  ;contact viscous damping  [-]
        damps_f  = 0.0
        ;---set damping values---
        command
                damp default local dampG
                damp default viscous normal dampn
                damp default viscous shear  damps
                damp default viscous notension on
                damp local dampG
                damp viscous normal dampn
                damp viscous shear  damps
                damp viscous notension on
        endcommand
```

```
end
;-------------------------------------------------------------------------------------------
define CreateCylinders
        end_x = Origin_x
        end_y = Origin_y
        end1_z = Origin_z
        end2_z = Origin_z + dz
        Rr = Do/2.0
        ID_end = ID_start
        loop a (1,Nc)
                command
                wall id=ID_end wall_props type cylinder
                end1=(Origin_x,Origin_y,end1_z) end2=(end_x,end_y,end2_z)
                rad=(Rr,Rr)
                endcommand
                end1_z = end2_z
                end2_z = end1_z + dz
                ID_end = ID_end + 1
        endloop
        end_z = Origin_z + Lz
        Rr = Di/2.0
        command
wall id=ID_end wall_props type cylinder end1=(Origin_x,Origin_y,Origin_z)
end2=(end_x,end_y,end_z) rad=(Rr,Rr)
        endcommand
end
;-------------------------------------------------------------------------------------------
define filter_creation
        _xpos = fc_arg(1)
        _ypos = fc_arg(2)
        _zpos = fc_arg(3)
        _zlim = Origin_z
        Ballangle = pi + atan(_ypos/_xpos)
        if _zpos > _zlim
                filter_creation = 0 ; accept the ball by default
                if (_xpos^2+_ypos^2)^0.5 < (Di/2.0)
                                filter_creation = 1 ; do not accept the ball
                end_if
                if (_xpos^2+_ypos^2)^0.5 > (Do/2.0)
                        filter_creation = 1 ; do not accept the ball
                end_if
        else
                filter_creation = 1 ; do not accept the ball
        end_if
end
;-------------------------------------------------------------------------------
```

```
define CloseTopBottom
Rr = Do/2.0
x1 = Rr
y1 = 0.0
z1 = 0
dtheta = 2.0*pi/NrSeg
theta = dtheta
x2 = Rr*cos(theta)
y2 = Rr*sin(theta)
loop n (1,NrSeg)
        ID_end = ID_end + 1
                command
                wall ID=ID_end wall_props face (Origin_x,Origin_y,z1)
(x1,y1,z1) (x2,y2,z1)
                endcommand
                z2 = Lz
                ID_end = ID_end + 1
                y1 = -y1
                y2 = -y2
                command
                wall ID=ID_end wall_props face (Origin_x,Origin_y,z2)
(x1,y1,z2) (x2,y2,z2)
                endcommand
                x1 = x2
                y1 = y2
                theta = theta + dtheta
                x2 = Rr*cos(theta)
                y2 = Rr*sin(theta)
        endloop
        ID_end = ID_end + 1
end
;-----------------------------------------------------------------------------------------------
define AddFirstBalls
        xmin = (-Do/2.0)
        xmax = (Do/2.0)
        ymin = (-Do/2.0)
        ymax = ( Do/2.0)
        zmin = 0.0
        zmax = 2.0
        ids = 1
        ide = ids + Nb - 1
        command
generate hertz id ids ide rad br1 br2 x xmin xmax y ymin ymax z zmin zmax &
FILTER filter_creation tries 100000
range name Ballrange1 id ids ide
property ball_props range Ballrange1
```

```
endcommand
end ;AddFirstBalls
;-----------------------------------------------------------------------------------------------
define AddBalls
        MaxBallz = 0
        loop q (1,Nb)
                bp = ball_head
                Ballz = b_z(bp)
                if Ballz > MaxBallz
                        MaxBallz = Ballz
                endif
        bp = b_next(bp)
        endloop
        idd = Nb
        zmin = 0
        loop q (1,levelsnr)      ;levelsnr
                zmin = zmin + MaxBallz + 0.2
                loop qq (1,Nb)
                        bp = find_ball(qq)              ;pointer na bal met id=qq
                        xb = b_x(bp)
                        yb = b_y(bp)
                        zb = zmin + b_z(bp)
                        idd = idd + 1
                        command
                                ball rad 0.03 hertz id=idd  x=xb  y=yb  z=zb
                                property ball_props
                        endcommand
                endloop
        endloop
end ;AddBalls
;-----------------------------------------------------------------------------------------------
define ResetDamping
        ;---set damping values---
        command
        damp default local dampG_f
        damp default viscous normal dampn_f
        damp default viscous shear  damps_f
        damp default viscous notension on
        damp local dampG_f
        damp viscous normal dampn_f
        damp viscous shear  damps_f
        damp viscous notension on
        endcommand
end

;-----------------------------------------------------------------------------------------------
```

```
Geometry
CreateCylinders
CloseTopBottom
AddFirstBalls
range name Cylinder id=ID_start,ID_end
plot add wall blue range Cylinder wireframe on
plot set center 0 0 0
plot set size 7.969
plot set perspective off
plot add axes
plot add ball
step 10000
solve
ResetDamping
save FirstBallsSettled.sav
AddBalls
save AllBallsAdded.sav
step 10000
solve
save AllBallsSettled.sav
```

```
new
restore AllBallsSettled.sav
;-------------------------------------------------------------------------------------------------
define UserParam
        command
        ;initialise the tables for storing data
                table 1 erase   ;wheight wallpressure
                table 2 erase   ;wheight wforce
        endcommand
end
;-------------------------------------------------------------------------------------------------
define StoreBallData

        warea = 3.14*Do*dz
        wheight = 0.0
        loop wcounter (1,Nc)            ;ALL wALL LOOP
                wp = find_wall(wcounter)
                wid = wcounter                  ;ball id
                wforce_x = w_xfob(wp)
                wforce_y = w_yfob(wp)
                wforce = sqrt(wforce_x^2 + wforce_y^2)
                wheight = wheight+dz
                wallpressure = wforce/warea
                command
                        table 1  wheight   wallpressure
```

```
                        table 2  wheight   wforce
                    endcommand
            endloop
end ;StoreBallData
;-------------------------------------------------------------------------------------------
StoreBallData
save WallForces.sav
```

C.2 DEM Code to Validate Pebble Material Properties

1_Janssen:

In this code the force versus displacement graph is obtained when a graphite pebble is compressed between two plates. The result is illustrated in Figure 45.

```
new
;-------------------------------------------------------------------------------------------
;Set Model Properties
;-------------------------------------------------------------------------------------------
set max_balls = 10000
set memory size = 10
set memory add = 10
set safety_fac = 1.0
set dtcalc = 100
set gravity = 0.00  0.0  -9.81
set def_dt = 1e-3
;-------------------------------------------------------------------------------------------
define GenerateBall
;-------------------------------------------------------------------------------------------
command
        macro ball_props 'shear = 1.4e9 poiss = 0.2 fric = 0.7 density = 6701'
        ball hertz rad=0.03 id=1  x=0.0  y=0.0  z=0.0
        property ball_props
endcommand
 end   ;GenerateBall
 ;-------------------------------------------------------------------------------------------
def BoxParameters
;-------------------------------------------------------------------------------------------
FlatPlate = 0.1             ; Length and width of Square Flat Plate (m)
end_point1 = 0.03004
begin_point = -0.03
command
        macro Box_Parameters 'kn=10000000 ks=10000000 friction=0.7'
endcommand
```

```
end BoxParameters
;-------------------------------------------------------------------------------------------------
define MakeBox
;-------------------------------------------------------------------------------------------------
pointC = -FlatPlate
pointD = FlatPlate
command
        wall id 2 Box_Parameters face (pointC pointD begin_point) (pointC
pointC begin_point) (pointD pointC begin_point) (pointD pointD begin_point)
        wall id 1 Box_Parameters face (pointC pointD end_point1) (pointD
pointD end_point1) (pointD pointC end_point1) (pointC pointC end_point1)
endcommand
end ;MakeBox
;-------------------------------------------------------------------------------------------------

define Parameters
;-------------------------------------------------------------------------------------------------
TopWall = 1
LidVelocity1 = -0.00005                 ; m/s
Max_Normal_Load = 960.0       ; N
Data_dt = 0.1
Data_time = Data_dt
  command
        set time = 0.0
        set def_dt = 1e-3
        table 100 erase
        table 200 erase
  endcommand
end ;Parameters
;-------------------------------------------------------------------------------------------------
define Initial_Compress
;-------------------------------------------------------------------------------------------------
current_time = time
wp = find_wall(TopWall)
w_zvel(wp) = LidVelocity1
loop while current_time >= 0.0
        command
        cycle 10
        endcommand
if w_zfob(wp) >= Max_Normal_Load
   w_zvel(wp) = 0.0
   exit
endif
endloop
end ;Initial_Compress
```

```
;-------------------------------------------------------------------------------------------
define Store_Data                       ;writes data to tables
;-------------------------------------------------------------------------------------------
        Acurrent = time
        if Acurrent >= Data_time
                wp = find_wall(TopWall)
                Fn = w_zfob(wp)
                Zdisp = w_z(wp)
                 Zvel = w_zvel(wp)
                command
                        table 100 Acurrent Zvel
                        table 200 Fn  Zdisp
                endcommand
                Data_time = Acurrent + Data_dt
        endif
end ;Store_Data
;-------------------------------------------------------------------------------------------
;MAIN PROGRAM
;-------------------------------------------------------------------------------------------
GenerateBall
BoxParameters
MakeBox
plot create Footing
plot set perspective off
plot add wall
plot add ball red
plot add axes black
plot show
Parameters
set fishcall 12 Store_Data
Initial_Compress
save PBMR_Compress.sav
```

To retrieve the data:

```
;-------------------------------------------------------------------------------------------
; This program retrieves the necessary data from the Initial Compression
Simulations.
;-------------------------------------------------------------------------------------------
; Make sure to restore the correct file and to specify the correct "BasicName"
variable
;-------------------------------------------------------------------------------------------
new
restore PBMR_Compress.sav       ; Make sure to restore the correct file.
;-------------------------------------------------------------------------------------------
define  WriteData
```

```
        BasicName  = 'PBMR_Compression_Data_'       ; Make sure to specify
        the correct variable.
        IO_WRITE = 1
        IO_ASCII = 1
        tL_1  = table_size(100)
        tL_2  = table_size(200)
        Fname_1 = BasicName + 'time_Zvel.dat'
        Fname_2 = BasicName + 'Fn_Zdisp.dat'
        status = open(Fname_1, IO_WRITE, IO_ASCII)
        array A1(1)
        loop counter (1,tL_1)
                x = xtable(100,counter)
                y = ytable(100,counter)
                A1(1) = string(x) + '  '+ string(y)
                status = write(A1,1)
        end_loop
        status = close
        status = open(Fname_2, IO_WRITE, IO_ASCII)
        array A2(1)
        loop counter (1,tL_2)
                x = xtable(200,counter)
                y = ytable(200,counter)
                A2(1) = string(x) + '  ' + string(y)
                status = write(A2,1)
        end_loop
        status = close
end
;-------------------------------------------------------------------------------
WriteData
```

2_Get Data:

```
new
restore AllBallsSettled.sav
;-----------------------------------------------------------------------------------------------
define UserParam
        command
        ;initialise the tables for storing data
                table 1 erase   ;wheight wallpressure
                table 2 erase   ;wheight wforce
        endcommand
end
;-----------------------------------------------------------------------------------------------
define StoreBallData
        warea = 3.14*Do*dz
        wheight = 0.0
        loop wcounter (1,Nc)            ;ALL wALL LOOP
```

```
                wp = find_wall(wcounter)
                wid = wcounter                  ;ball id
                wforce_x = w_xfob(wp)
                wforce_y = w_yfob(wp)
                wforce = sqrt(wforce_x^2 + wforce_y^2)
                wheight = wheight+dz
                wallpressure = wforce/warea
                command
                        table 1  wheight   wallpressure
                        table 2  wheight   wforce
                endcommand
        endloop
end ;StoreBallData
;-------------------------------------------------------------------------------------------
StoreBallData
save WallForces.sav
```

C.3 DEM Code to Simulate Dust Production in PBMR Core

1_ Reactor Geometry:

In this code an annular reactor geometry is created and filled with a number of balls. The balls are then recycled at different rates and for different scale factors after which the amount of dust for the simulated time is recorded. The results are shown in Table 6.

```
new;
;-------------------------------------------------------------------------------------------
define ProgramParameters
;-------------------------------------------------------------------------------------------
ID_start = 1
ID_end = ID_start
command
        macro wall_props 'kn = 1e8 ks = 1e8 fric = 0.7'
        macro ball_props 'shear = 1.4e9 poiss = 0.2 fric = 0.7 dens = 6701.0'
endcommand
;general model settings
      command
        set time = 0.0                  ;reset
                set def_dt = 1e-4               ;timestep size with no balls
                set max_balls = 100000          ;default = 5000 - reserves memory
                set safety_fac = 1      ;time step size safety factor: default = 0.8
                set dtcalc = 1          ;for scale 1.5 and smaller
                set gravity 0.00  0.00 -9.81
        endcommand
end ProgramParameters
```

```
;-------------------------------------------------------------------------------------------------
define Parameters
;-------------------------------------------------------------------------------------------------
scale = 0.6
Do = scale*3.7
Ro = Do/2.0
Di = scale*2.0
Ri = Di/2.0
Doutlet = scale*0.5
SR = Doutlet/2.0
botheight = -0.5*scale
Segnr = 20.0
Nb = 5000  ;scale = 0.6
br1 = 0.03
br2 = 0.03
ReactorHeight = scale*11.0
end ;Parameters
;-------------------------------------------------------------------------------------------------
define CreateCylinders
;-------------------------------------------------------------------------------------------------
end_x = 0.0
end_y = 0.0
end_z = ReactorHeight
        Rr = Do/2.0
        command
                wall id=ID_end wall_props type cylinder end1=(0,0,0)
                end2=(end_x,end_y,end_z) rad=(Rr,Rr)
        endcommand
        ID_end = ID_end + 1
        Rr = Di/2.0
        command
                wall id=ID_end wall_props type cylinder end1=(0,0,0)
                end2=(end_x,end_y,end_z) rad=(Rr,Rr)
        endcommand
end
;-------------------------------------------------------------------------------------------------
define Bottom
;-------------------------------------------------------------------------------------------------
A11 = 150.0*pi/180.0
A12 = 30.0*pi/180.0
Angle1 = pi/2.0
Angle2 = pi
dA1 = (120.0*pi/180.0)/Segnr
dA2 = (180.0/Segnr)*pi/180.0
smallcirclex0 = ((Do-Di)/4.0 + Ri)*cos(Angle1)
smallcircley0 = ((Do-Di)/4.0 + Ri)*sin(Angle1)
```

```
loop a (1,3)
        if a = 3
                Angle2 = -90*pi/180.0
        end_if
        th1 = A11
        th2 = Angle2
                loop n (1,Segnr)
                x1 = Ri*cos(th1)
                y1 = Ri*sin(th1)
                z1 = 0
                th1 = th1 - dA1
                x2 = Ri*cos(th1)
                y2 = Ri*sin(th1)
                z2 = 0
                x3 = smallcirclex0 + SR*cos(th2)
                y3 = smallcircley0 + SR*sin(th2)
                z3 = botheight
                th2 = th2 + dA2
                ID_end = ID_end + 1
                        command
                                wall ID=ID_end wall_props face (x1,y1,z1)
                                        (x2,y2,z2) (x3,y3,z3)
                        endcommand
        endloop
        th2 = Angle2
        th1 = A11
        loop n (1,Segnr)
                th1 = th1 - dA1
                x2 = Ri*cos(th1)
                y2 = Ri*sin(th1)
                z2 = 0
                x1 = smallcirclex0 + SR*cos(th2)
                y1 = smallcircley0 + SR*sin(th2)
                z1 = botheight
                th2 = th2 + dA2
                x3 = smallcirclex0 + SR*cos(th2)
                y3 = smallcircley0 + SR*sin(th2)
                z3 = botheight
                ID_end = ID_end + 1
                        command
                                wall ID=ID_end wall_props face (x1,y1,z1)
                                        (x2,y2,z2) (x3,y3,z3)
                        endcommand
        endloop
        A11 = A12
        A12 = A12 - 120.0*pi/180.0
```

```
        Angle2 = Angle2 - pi/2.0
        Angle1 = Angle1 - 120.0*pi/180.0
        smallcirclex0 = ((Do-Di)/4.0 + Ri)*cos(Angle1)
        smallcircley0 = ((Do-Di)/4.0 + Ri)*sin(Angle1)
endloop
A21 = 150.0*pi/180.0
A22 = 30.0*pi/180.0
Angle1 = pi/2.0
Angle2 = pi
dA1 = (120.0*pi/180.0)/Segnr
dA2 = (180.0/Segnr)*pi/180.0
smallcirclex0 = ((Do-Di)/4.0 + Ri)*cos(Angle1)
smallcircley0 = ((Do-Di)/4.0 + Ri)*sin(Angle1)
loop a (1,3)
        if a = 3
                Angle2 = -90*pi/180.0
        end_if
        th1 = A21
        th2 = Angle2
        loop n (1,Segnr)
                x1 = Ro*cos(th1)
                y1 = Ro*sin(th1)
                z1 = 0
                th1 = th1 - dA1
                x3 = Ro*cos(th1)
                y3 = Ro*sin(th1)
                z3 = 0
                x2 = smallcirclex0 + SR*cos(th2)
                y2 = smallcircley0 + SR*sin(th2)
                z2 = botheight
                th2 = th2 - dA2
                ID_end = ID_end + 1
                command
                        wall ID=ID_end wall_props face (x1,y1,z1) (x2,y2,z2)
                                (x3,y3,z3)
                endcommand
        endloop
        th2 = Angle2
        th1 = A21
        loop n (1,Segnr)
                th1 = th1 - dA1
                x3 = Ro*cos(th1)
                y3 = Ro*sin(th1)
                z3 = 0
                x1 = smallcirclex0 + SR*cos(th2)
                y1 = smallcircley0 + SR*sin(th2)
```

```
                z1 = botheight
                th2 = th2 - dA2
                x2 = smallcirclex0 + SR*cos(th2)
                y2 = smallcircley0 + SR*sin(th2)
                z2 = botheight
                ID_end = ID_end + 1
                command
                        wall ID=ID_end wall_props face (x1,y1,z1) (x2,y2,z2)
                        (x3,y3,z3)
                endcommand
        endloop
        A21 = A22
        A22 = A22 - 120.0*pi/180.0
        Angle2 = Angle2 - pi/2.0
        Angle1 = Angle1 - 120.0*pi/180.0
        smallcirclex0 = ((Do-Di)/4.0 + Ri)*cos(Angle1)
        smallcircley0 = ((Do-Di)/4.0 + Ri)*sin(Angle1)
endloop
;-------------------------------------------------------------------------------------------
;T: Triangle
;-------------------------------------------------------------------------------------------
th1 = 150*pi/180.0
th2 = pi
Angle1 = pi/2.0
smallcirclex0 = ((Do-Di)/4.0 + Ri)*cos(Angle1)
smallcircley0 = ((Do-Di)/4.0 + Ri)*sin(Angle1)
T1x1 = Ri*cos(th1)
T1y1 = Ri*sin(th1)
T1z1 = 0.0
T1x2 = smallcirclex0 + SR*cos(th2)
T1y2 = smallcircley0 + SR*sin(th2)
T1z2 = botheight
T1x3 = Ro*cos(th1)
T1y3 = Ro*sin(th1)
T1z3 = 0.0
th1 = 30*pi/180.0
th2 = 0.0
smallcirclex0 = ((Do-Di)/4.0 + Ri)*cos(Angle1)
smallcircley0 = ((Do-Di)/4.0 + Ri)*sin(Angle1)
T2x1 = Ri*cos(th1)
T2y1 = Ri*sin(th1)
T2z1 = 0.0
T2x3 = smallcirclex0 + SR*cos(th2)
T2y3 = smallcircley0 + SR*sin(th2)
T2z3 = botheight
T2x2 = Ro*cos(th1)
```

```
T2y2 = Ro*sin(th1)
T2z2 = 0.0
th2 = pi/2.0
Angle1 = -30.0*pi/180
smallcirclex0 = ((Do-Di)/4.0 + Ri)*cos(Angle1)
smallcircley0 = ((Do-Di)/4.0 + Ri)*sin(Angle1)
T3x1 = Ri*cos(th1)
T3y1 = Ri*sin(th1)
T3z1 = 0.0
T3x2 = smallcirclex0 + SR*cos(th2)
T3y2 = smallcircley0 + SR*sin(th2)
T3z2 = botheight
T3x3 = Ro*cos(th1)
T3y3 = Ro*sin(th1)
T3z3 = 0.0
th1 = -90*pi/180.0
th2 = 270*pi/180.0
Angle1 = -30.0*pi/180
smallcirclex0 = ((Do-Di)/4.0 + Ri)*cos(Angle1)
smallcircley0 = ((Do-Di)/4.0 + Ri)*sin(Angle1)
T4x1 = Ri*cos(th1)
T4y1 = Ri*sin(th1)
T4z1 = 0.0
T4x3 = smallcirclex0 + SR*cos(th2)
T4y3 = smallcircley0 + SR*sin(th2)
T4z3 = botheight
T4x2 = Ro*cos(th1)
T4y2 = Ro*sin(th1)
T4z2 = 0.0
th1 = -90*pi/180.0
th2 = -90*pi/180.0
Angle1 = -150.0*pi/180
smallcirclex0 = ((Do-Di)/4.0 + Ri)*cos(Angle1)
smallcircley0 = ((Do-Di)/4.0 + Ri)*sin(Angle1)
T5x1 = Ri*cos(th1)
T5y1 = Ri*sin(th1)
T5z1 = 0.0
T5x2 = smallcirclex0 + SR*cos(th2)
T5y2 = smallcircley0 + SR*sin(th2)
T5z2 = botheight
T5x3 = Ro*cos(th1)
T5y3 = Ro*sin(th1)
T5z3 = 0.0
th1 = 150*pi/180.0
th2 = 90*pi/180.0
Angle1 = -150.0*pi/180
```

```
smallcirclex0 = ((Do-Di)/4.0 + Ri)*cos(Angle1)
smallcircley0 = ((Do-Di)/4.0 + Ri)*sin(Angle1)
T6x1 = Ri*cos(th1)
T6y1 = Ri*sin(th1)
T6z1 = 0.0
T6x3 = smallcirclex0 + SR*cos(th2)
T6y3 = smallcircley0 + SR*sin(th2)
T6z3 = botheight
T6x2 = Ro*cos(th1)
T6y2 = Ro*sin(th1)
T6z2 = 0.0
        ID_end = ID_end + 1
        command
                wall ID=ID_end wall_props face (T1x1,T1y1,T1z1)
                        (T1x2,T1y2,T1z2) (T1x3,T1y3,T1z3)
        endcommand
        ID_end = ID_end + 1
        command
                wall ID=ID_end wall_props face (T2x1,T2y1,T2z1)
                        (T2x2,T2y2,T2z2) (T2x3,T2y3,T2z3)
        endcommand
        ID_end = ID_end + 1
        command
                wall ID=ID_end wall_props face (T3x1,T3y1,T3z1)
                        (T3x2,T3y2,T3z2) (T3x3,T3y3,T3z3)
        endcommand
        ID_end = ID_end + 1
                command
                        wall ID=ID_end wall_props face (T4x1,T4y1,T4z1)
                                (T4x2,T4y2,T4z2) (T4x3,T4y3,T4z3)
                endcommand
        ID_end = ID_end + 1
        command
                wall ID=ID_end wall_props face (T5x1,T5y1,T5z1)
                        (T5x2,T5y2,T5z2) (T5x3,T5y3,T5z3)
        endcommand
        ID_end = ID_end + 1
        command
                wall ID=ID_end wall_props face (T6x1,T6y1,T6z1)
                        (T6x2,T6y2,T6z2) (T6x3,T6y3,T6z3)
        endcommand
end ;Bottom
;-------------------------------------------------------------------------------------------
define CloseTopBottom
;-------------------------------------------------------------------------------------------
        Rr = Do/2.0
```

```
        NrSeg = 40.0
        x1 = Rr
        y1 = 0.0
        z1 = botheight
        dtheta = 2.0*pi/NrSeg
        theta = dtheta
        x2 = Rr*cos(theta)
        y2 = Rr*sin(theta)
        z2 = ReactorHeight
        loop n (1,NrSeg)
                ID_end = ID_end + 1
                command
                        wall ID=ID_end wall_props face (0.0,0.0,z1) (x1,y1,z1)
                                (x2,y2,z1)
                endcommand
                ID_end = ID_end + 1
                y11 = -y1
                y22 = -y2
                command
                        wall ID=ID_end wall_props face (0.0,0.0,z2) (x1,y11,z2)
                                (x2,y22,z2)
                endcommand
                x1 = x2
                y1 = y2
                theta = theta + dtheta
                x2 = Rr*cos(theta)
                y2 = Rr*sin(theta)
        endloop
end CloseTopBottom
;-------------------------------------------------------------------------------------------
ProgramParameters
Parameters
CreateCylinders
Bottom
CloseTopBottom
range name Cylinder id=ID_start,ID_end
save ReactorGeometry_0_6.sav
```

2_AddFirstBalls:

```
restore ReactorGeometry_0_6.sav
;-------------------------------------------------------------------------------------------
define AddFirstBalls
;-------------------------------------------------------------------------------------------
        xmin = -Do/2.0 + br1
        xmax =  Do/2.0 - br1
        ymin = -Do/2.0 + br1
```

```
        ymax =  Do/2.0 - br1
        zmin = 0.0
        zmax = ReactorHeight
        ids = 1
        ide = ids + Nb - 1
        command
                generate hertz id ids ide rad br1 br2 x xmin xmax y ymin ymax z
                zmin zmax & FILTER filter_creation tries 100000
                range name Ballrange1 id ids ide
                property ball_props range Ballrange1
        endcommand
end ;AddFirstBalls
;-------------------------------------------------------------------------------------------
define filter_creation
;-------------------------------------------------------------------------------------------
        _xpos = fc_arg(1)
        _ypos = fc_arg(2)
        _zpos = fc_arg(3)
        ;_zlim = Origin_z + Do*tan(BotAngle)
        ;_zlim = Origin_z
        _zlim = 0.0
        Ballangle = pi + atan(_ypos/_xpos)
        if _zpos > _zlim
                filter_creation = 0 ; accept the ball by default
                if (_xpos^2+_ypos^2)^0.5 < (Di/2.0)
                        filter_creation = 1 ; do not accept the ball
                end_if
                if (_xpos^2+_ypos^2)^0.5 > (Do/2.0)
                        filter_creation = 1 ; do not accept the ball
                end_if
        else
                filter_creation = 1 ; do not accept the ball
        end_if
end
;-------------------------------------------------------------------------------------------
AddFirstBalls
step 20000
solve
save AddFirstBalls_0_6.sav
```

3_Prepare:

```
restore AddFirstBalls_0_6.sav
;-------------------------------------------------------------------------------------------
define RunParameters
;-------------------------------------------------------------------------------------------
        ;=== USER INPUT START ===
```

```
        ;solve static equilibrium damping values
        dampG  = 0.7                    ;local mass damping   [-]
        dampn  = 0.0                    ;contact viscous damping  [-]
        damps  = 0.0
        ;final damping values
        dampG_f  = 0.3                          ;local mass damping   [-]
        dampn_f  = 0.0                          ;contact viscous damping  [-]
        damps_f  = 0.0
        ;=== USER INPUT END ===
        ;---set damping values---
        command
        damp default local dampG
        damp default viscous normal dampn
        damp default viscous shear  damps
        damp default viscous notension on
        damp local dampG
        damp viscous normal dampn
        damp viscous shear  damps
        damp viscous notension on
        endcommand
end RunParameters
;-------------------------------------------------------------------------------------------
define ResetDamping
;-------------------------------------------------------------------------------------------
        ;---set damping values---
        command
        damp default local dampG_f
        damp default viscous normal dampn_f
        damp default viscous shear  damps_f
        damp default viscous notension on
        damp local dampG_f
        damp viscous normal dampn_f
        damp viscous shear  damps_f
        damp viscous notension on
        endcommand
end
;-------------------------------------------------------------------------------------------
define MaxHeight
;-------------------------------------------------------------------------------------------
zmax = 0.0
loop a (1,Nb)
        bp = find_ball(a)               ;pointer na bal met id=a
        zpos = b_z(bp)
        if zpos > zmax
                zmax = zpos
        endif
```

```
endloop
end MaxHeight
;-------------------------------------------------------------------------------------------
define AddBalls
;-------------------------------------------------------------------------------------------
idd = Nb
levelnr = ReactorHeight/zmax
loop q (1,levelnr)        ;levelsnr
        loop qq (1,Nb)
                        bp = find_ball(qq)              ;pointer na bal met id=qq
                        if b_z(bp) > 0.0
                                xb = b_x(bp)
                                yb = b_y(bp)
                                zb = q*zmax + b_z(bp)
                                if zb < ReactorHeight
                                        idd = idd + 1
                                                command
                                                        ball rad 0.03 hertz id=idd
                                                        x=xb  y=yb  z=zb
                                                        property ball_props
                                                endcommand
                                endif
                        endif
                endloop
endloop
end ;AddBalls
;-------------------------------------------------------------------------------------------
define AddLastBalls
;-------------------------------------------------------------------------------------------
ids = 1
ide = idd
zmax = 0.0
zmin = 1000000.0
        loop a (ids,ide)
                bp = find_ball(a)               ;pointer na bal met id=a
                zpos = b_z(bp)
                if zpos > zmax
                        zmax = zpos
                endif
                if zpos < zmin
                        zmin = zpos
                endif
        endloop
        loop qq (ids,ide)
                        bp = find_ball(qq)              ;pointer na bal met id=qq
                        xb = b_x(bp)
```

```
                    yb = b_y(bp)
                if b_z(bp) > 0
                    zb = b_z(bp) + zmax
                    if zb < ReactorHeight
                        idd = idd + 1
                        command
                            ball rad 0.03 hertz id=idd  x=xb  y=yb  z=zb
                            property ball_props
                        endcommand
                    endif
                endif
        endloop
end AddLastBalls
;-----------------------------------------------------------------------------------------------
RunParameters
step 500
MaxHeight
AddBalls
ResetDamping
solve
AddLastBalls
step 1000
solve
plot add ball
plot add wall blue range Cylinder wireframe on
plot add axes
plot show
step 10000
save Prepare_0_6.sav
```

4_Get Forces and Velocities

```
restore Prepare_0_2.sav
;-----------------------------------------------------------------------------------------------
define UserParam
;-----------------------------------------------------------------------------------------------
        Ttotal= 7.2         ;total simulation time [sec]
        CircRate = 500.0    ;balls per hour
        dt_data  = 0.1      ;time step to record data
        del_x1 = 0.0        ;the ball closest to these coordinates is deleted
        del_y1 = (Do-Di)/4.0 + Ri
        del_z1 = botheight
        theta2 = -30*pi/180.0
        del_x2 = ((Do-Di)/4.0 + Ri)*cos(theta2)
        del_y2 = ((Do-Di)/4.0 + Ri)*sin(theta2)
```

```
        del_z2 = botheight
        theta3 = 210*pi/180.0
        del_x3 = ((Do-Di)/4.0 + Ri)*cos(theta3)
        del_y3 = ((Do-Di)/4.0 + Ri)*sin(theta3)
        del_z3 = botheight
        Mass = 0.0
        Temp = 1100.0
        Pdt  = 0.1          ;time increment to save picture
        picFileName = 'Run1_'
        pic_index = 100                 ;index used in pic filename
        picTitle  = 'My DEM model...time = '
        ;---END USER PARAM -----------
        dt_delete = 3600.0/CircRate   ;time in seconds to delete a single ball
        command
        set plot jpg quality 2   ; 2-best   255 worst (only version 3)
        ;set plot bmp            ;version 4 0nly
        set time = 0.0
        ;initialise the tables for storing data
        ;table 1 erase   ;time   #balls
        ;table 2 erase   ;var1   var2
        ;table 3 erase   ;var3   var4
        endcommand
        pic_time = Pdt          ;initialise time to take picture
        del_time = dt_delete   ;initialise time to delete ball
end
;-----------------------------------------------------------------
define Simulate
        ;do the time stepping
        current  = time                         ;get current time
        StepNow  = current + dt_data            ;time for next data aquisition

        bp_del1 = ball_near3(del_x1,del_y1,del_z1) ;get the ball closest to the
        coordinates
        bp_del2 = ball_near3(del_x2,del_y2,del_z2)
        bp_del3 = ball_near3(del_x3,del_y3,del_z3)
        dum1 = b_delete(bp_del1)                        ;delete the ball - a dummy
                        variable is returned
        dum2 = b_delete(bp_del2)
        dum3 = b_delete(bp_del3)
        loop while current < Ttotal
                command
                        solve ave 0.00000000000000000000001 max
                                0.00000000000000000000001 step
                                1000000000000000000000000 time StepNow
                endcommand
                current = time
```

```
                StoreBallData           ;function call
                if current >= del_time
                        bp_del1 = ball_near3(del_x1,del_y1,del_z1) ;get the ball
                        closest to the coordinates
                        bp_del2 = ball_near3(del_x2,del_y2,del_z2)
                        bp_del3 = ball_near3(del_x3,del_y3,del_z3)
                        dum1 = b_delete(bp_del1)                    ;delete the ball
                        - a dummy variable is returned
                        dum2 = b_delete(bp_del2)
                        dum3 = b_delete(bp_del3)
                        del_time = del_time + dt_delete             ;increment the
                        time to delete the next ball
                endif
                if current >= pic_time
                        MakePic2                                    ;make a picture
                        pic_time = pic_time + Pdt
                        pic_index = pic_index + 1      ;index picture filename
                endif
                StepNow = current + dt_data                         ;increment
        endloop
end
;-------------------------------------------------------------------------------------------
define MakePic2
        pic_ext = '.jpg'
        picture_open = picFileName + string(pic_index) + pic_ext  ;create
filename
        tt = time
        picTitle2 = picTitle + string(tt) + ' s'                    ;create title
        command
                plot set title text picTitle2                       ;set the title
plot hardcopy file picture_open                                     ;save picture file
        endcommand
end
;-------------------------------------------------------------------------------------------
define StoreBallData
        bp = ball_head
        wp = wall_head
        current = time
        bcounter = 0
        zpos = 0.0
        act_wall = 0
        loop while bp # null            ;ALL BALL LOOP
                bcounter = bcounter + 1
                bid = b_id(bp)          ;ball id
                ;--------------------------
                ;reset contact data for this ball
```

```
                avg_cnf = 0.0
                avg_vel = 0.0
                zpos = b_z(bp)
                contact_counter = 0
                cp = b_clist(bp)        ;header of linked-list of contacts around bp
                loop while cp # null    ;BALL CONTACT LOOP
                        contact_counter = contact_counter + 1
                        ;FIND POINTER TO THE OTHER BALL IN THIS
                        CONTACT
                        if c_ball1(cp) = bp then ; find bp_other, the adjoining ball
                                bp_other = c_ball2(cp)
                        else
                                bp_other = c_ball1(cp)
                        endif
                        ;GET CONTACT DATA
                        cnf = c_nforce(cp)
                        wp = wall_head
                        loop while wp # null ;CHECK IF POINTER TO WALL
                                if bp_other = wp then
                                        act_wall = 1
                                        rz0 = c_z(cp) - b_z(bp)
                                        ry0 = c_y(cp) - b_y(bp)
                                        rx0 = c_x(cp) - b_x(bp)
                                        wy0 = b_ryvel(bp)
                                        wx0 = b_rxvel(bp)
                                        wz0 = b_rzvel(bp)
                                        vx0 = b_xvel(bp)
                                        vy0 = b_yvel(bp)
                                        zy0 = b_zvel(bp)
                                        relvx0 = vx0 + wy0*rz0 - wz0*ry0
                                        relvy0 = vy0 - (wx0*rz0-wz0*rx0)
                                        relvz0 = vz0 + wx0*ry0-wy0*rx0
                                        cnx0 = c_xun(cp)
                                        cny0 = c_yun(cp)
                                        cnz0 = c_zun(cp)
relvnx0 = (relvx0*cnx0 + relvy0*cny0 + relvz*cnz0)*(cnx0)
relvny0 = (relvx0*cnx0 + relvy0*cny0 + relvz*cnz0)*(cny0)
relvnz0 = (relvx0*cnx0 + relvy0*cny0 + relvz*cnz0)*(cnz0)
                                        relvtx0 = relvx0 - relvnx0
                                        relvty0 = relvy0 - relvny0
                                        relvtz0 = relvz0 - relvnz0
relvt = sqrt(relvtx0^2 + relvty0^2 + relvtz0^2)
avg_vel = avg_vel + relvt
Mass = Mass  +
2*(0.0000000025511*(relvt^0.402471)*(cnf^1.9681)*(dt_data^0.74923)/(Temp^
0.12884))
```

```
                endif
                wp = w_next(wp)
            endloop
            if cnf > 0.0 then
                if act_wall = 0 then
                    ;relxvel = vx + (wyrz - wzry)
                    ;relyvel = vy - (wxrz - wzrx)
                    ;relzvel = vz + (wxry - wyrx)
                    rz1 = c_z(cp) - b_z(bp)
                    ry1 = c_y(cp) - b_y(bp)
                    rx1 = c_x(cp) - b_x(bp)
                    rz2 = c_z(cp) - b_z(bp_other)
                    ry2 = c_y(cp) - b_y(bp_other)
                    rx2 = c_x(cp) - b_x(bp_other)
                    wy1 = b_ryvel(bp)
                    wx1 = b_rxvel(bp)
                    wz1 = b_rzvel(bp)
                    wy2 = b_ryvel(bp_other)
                    wx2 = b_rxvel(bp_other)
                    wz2 = b_rzvel(bp_other)
                    vx1 = b_xvel(bp)
                    vy1 = b_yvel(bp)
                    zy1 = b_zvel(bp)
                    vx2 = b_xvel(bp_other)
                    vy2 = b_yvel(bp_other)
                    zy2 = b_zvel(bp_other)
                    relvx1 = vx1 + wy1*rz1 - wz1*ry1
                    relvy1 = vy1 - (wx1*rz1-wz1*rx1)
                    relvz1 = vz1 + wx1*ry1-wy1*rx1
                    relvx2= vx2 + wy2*rz2 - wz2*ry2
                    relvy2 = vy2 - (wx2*rz2-wz2*rx2)
                    relvz2 = vz2 + wx2*ry2-wy2*rx2
                    cnx1 = c_xun(cp)
                    cny1 = c_yun(cp)
                    cnz1 = c_zun(cp)
                    cnx2 = -c_xun(cp)
                    cny2 = -c_yun(cp)
                    cnz2 = -c_zun(cp)

relvnx1 = (relvx1*cnx1 + relvy1*cny1 + relvz1*cnz1)*(cnx1)
relvny1 = (relvx1*cnx1 + relvy1*cny1 + relvz1*cnz1)*(cny1)
relvnz1 = (relvx1*cnx1 + relvy1*cny1 + relvz1*cnz1)*(cnz1)
relvnx2 = (relvx2*cnx2 + relvy2*cny2 + relvz2*cnz2)*(cnx2)
relvny2 = (relvx2*cnx2 + relvy2*cny2 + relvz2*cnz2)*(cny2)
relvnz2 = (relvx2*cnx2 + relvy2*cny2 + relvz2*cnz2)*(cnz2)
```

```
relvtx1 = relvx1 - relvnx1
relvty1 = relvy1 - relvny1
relvtz1 = relvz1 - relvnz1
relvtx2 = relvx2 - relvnx2
relvty2 = relvy2 - relvny2
relvtz2 = relvz2 - relvnz2

relvt = sqrt((relvtx1- relvtx2)^2+( relvty1- relvty2)^2+( relvtz1- relvtz2)^2)
Mass = Mass  +
0.0000000025511*(relvt^0.402471)*(cnf^1.9681)*(dt_data^0.74923)/(Temp^0.1
2884)
                                                avg_cnf = avg_cnf + cnf
                                                avg_vel = avg_vel + relvt
                                    endif
                            endif
;FIND NEXT CONTACT POINTER FOR BALL WE ARE LOOKING ATif
        c_ball1(cp) = bp then ; determine which linked-list to follow
        cp = c_b1clist(cp) ; choose the one that surrounds bp
        else
                cp = c_b2clist(cp)
                        endif
                        act_wall = 0
                endloop
                avg_cnf = avg_cnf/contact_counter
                avg_vel = avg_vel/contact_counter
                command
                        table 2  bid        Mass
                        table 3  avg_cnf    avg_vel
                endcommand
                bp = b_next(bp)
        endloop
        command
                table 1 current bcounter
        endcommand
end
;-------------------------------------------------------------------------------------------
UserParam
Simulate
Save End_0_2_Circrate_500.sav
```

6_Data to File:

```
;=========================================================
;Data2File.txt
;=========================================================
new;
restore End_0_2_Circrate_500.sav
```

```
;-------------------------------------------------------------------------------------------
define  WriteData
        IO_WRITE = 1                    ;standard settings
        IO_ASCII = 1
        FName  = 'Results_0_2_Circrate_500.dat'     ;filename
        tL_1  = table_size(1)  ;table 1's length
        tL_2  = table_size(2)  ;table 2's length (and table 3 and 4, .....)
        status = open(Fname,IO_WRITE,IO_ASCII)
        ;create new file
        array A1(1)                                                     ;define array
        A1(1) = '%time  number_of_balls'                                ;header 1
        status = write(A1,1)                                            ;write the
        header to the file
        A1(1) = '%ball_ID  zpos  avg_cnf  avg_vel'; avg_csf  SlipWork'    ;header
        2
        status = write(A1,1)    ;write the header to the file
        ne = 0  ;initialise
        ns = 1
        loop counter (1,tL_1)  ;loop through table 1 (one line per data collection)
                tt = xtable(1,counter)          ;get time from table
                Num_Balls = ytable(1,counter)       ;number of balls at this time
                ;create array entry using data from the table
                A1(1) = string(tt) + '  '+ string(Num_Balls) + '  ' + '0' + '  ' + '0' + '  '
                + '0' + '  ' + '0'
                status = write(A1,1)            ;write array entry to file
                ns = ne + 1                     ;the row index should start here
                ne = ns + Num_Balls - 1         ;the row index should end here
        loop nn (ns,ne)                 ;loop through the other tables and string the
                                        data together in a single row for each ball
                        bid     = xtable(2,nn)
                        zpos    = ytable(2,nn)
                        avg_cnf = xtable(3,nn)
                        avg_vel = ytable(3,nn)
                        A1(1) = string(bid) + '  '+ string(Mass) + '  '+
                        string(avg_cnf) + '  '+ string(avg_vel)
                        status = write(A1,1)            ;write array entry to file
                end_loop
        end_loop
        status = close          ;close file
end
WriteData
```

REFERENCES

Bayer, RG 1994, *Mechanical Wear Prediction and Prevention*, Marcel Dekker, New York, USA

Bhushan, B 2000, *Modern Tribology Hand-book*, CRC Press, Boca Raton, Florida, USA

Becker,T 2011, *Understanding and Modelling Damage and Fracture in Nuclear Grade Graphite*, Ph.D thesis, University of Cape Town

Cachon, L & Falcand, C 2008, *Raphael Eurocourse: Tribology and Corrosion,* 18 November. Aix-en Provence, France

Conradie, PJF 2010, *Edge fan performance in air cooled condensers*, M.Sc. Eng. Thesis, Department of Mechanical and Mechatronic Engineering, University of Stellenbosch, South Africa

Driesner, AR & Wagener, P 1958, 'Friction coefficients of graphite over the temperature interval 25°C to 2450°C', *Journal of Applied Physics*, Vol. 29, no 6, p901-903

Hayworth, L 2009, 'Graphite Dust Generation Analysis', Unpublished dissertation, University of Stellenbosch, Stellenbosch, South Africa

Hrovat, M & Grosse, K 2006, 'Manufacture of high corrosion resistant fuel spheres for high temperature pebble bed modular reactors', Paper B00000281, *Third international topical meeting on high temperature reactor technology*, Johannesburg, South Africa

Itasca Consulting Group, Inc, 2003, '*PFC3D (Particle Flow Code in 3D) Theory and Background Manual*', Version 3.0, ICG, Minneapolis

Johnson, KL 1985, *Contact Mechanics*, Cambridge University Press, Cambridge

Kaczorowski, D & Vernot, JP 2004, 'Wear problems in nuclear power plant, environment effect', *The Annals of University "Dunărea de Jos" of Galaţi*, Fascicle VIII, ISSN 1221-4590, Tribology

Kichuki, K & Kawaguchi, K & Nemoto, M & Sanokawa, K & Watanabe, S 1984, 'Impurity gas effects on friction and wear of high temperature materials for VHTRs', *Nuclear Technology*, Vol.66, p491-502

Lancaster, JK 1980, Pritchard JR, 'On the 'dusting' wear regime of graphite sliding against carbon', *Journal of Physics D: Applied Physics*, Vol. 13, p1151-1164

Lancaster, JK & Pritchard, JR 1981, 'The influence of environment and pressure on the transition to dusting wear of graphite', *Journal of Physics D: Applied Physics*, Vol. 14, p747-762

Li, CC & Sheehan, JE 1981, 'Friction and wear characteristics of graphite and carbon-carbon composite in air and in helium', *International Conference on Wear of Materials*, 31 March, San Francisco, CA

Luo, X & Zhang, L & Yu, S 2004, 'The wear properties of nuclear grade graphite IG-11 under different loads', *International Journal of Nuclear Energy Science and Technology*, Vol. 1, no 1, p33-43

Luo, X & Yu,S & Sheng, X & He, S 2005, 'Temperature effect on IG-11 graphite wear performance', *Nuclear Engineering and Design*, Vol. 235, p2261-2274

Mitchell, M & Polson, A 2005, 'Assessment of the loads on a solid centre reflector of a pebble bed reactor using DEM techniques', *18th International Conference on Structural Mechanics in Reactor Technologies (SMiRT18)*, Beijing, China

Nightingale, RE 1966, *Graphite: Advantages, Limitations and Applications*, Batelle Memorial Institute, Pacific Northwest Laboratories, Richland, Washington, USA

Rabinowicz, E 1995, *Friction and Wear of Materials,* Second Edition, Wiley & Sons, New York, USA

Ramadanoff, D and Glass, SW 1944, High-Altitude Brush Problem, *Trans. AIEE*,Vol. 63, p825-830

Robert,F & Paulmier, D & Zaidi, H & Scholler, E 1995, 'Combined influence of an inert gas environment and a mechanical action on a graphite surface', *Wear*, Vol. 181-183, p687-690

SABS, 2010, 'South African National Standard: Categorization and conformity assessment criteria for all pressure equipment', Edition 1.1, SABS Standards Division, Pretoria, South Africa

Semenov, AP 2005, 'Tribology at high temperatures', *Tribology International*, Vol. 28, no 1, p45-50

Sheng, X & Yu, S & Luo, X & He, S 2003, 'Wear behaviour of graphite studies in an air conditioned environment', *Nuclear Engineering and Design,* Vol. 223, p109-115

Slabber, J 2006, 'Technical Description of the PBMR Demonstration Power Plant', PBMR, Pretoria, South Africa

Sperl, M 2005, 'Experiments on corn pressure in silo cells - translation and comment of Janssen's paper from 1895', *Grannular Matter*, Vol 8, p59-65

Stansfield, OM 1969, 'Friction and wear of graphite in dry helium at 25, 400 and 800 ºC', *Nuclear Applications*, Vol. 6, p313-320

UCAR Carbon Company, Inc 2001, *Industrial Graphite Engineering Handbook*, Clarksburg

Ullman, DG 2003, *The Mechanical Design Process*, Third Edition, McGraw Hill, New York, USA

Wahsweiler, HG 1989, *Bisherige erkentnisse zum graphitstaub*, HRB BF3535

Yu, S & Sheng, X 2004, 'Theoretical analysis of the tribological properties of HTGR-10 graphite', Paper E17, *Second International Meeting on High Temperature Reactor Technology*, Beijing, China

Zaidi, H & Paulmier, D & Lepage, J 1990, 'The influence of the environment on the friction and wear of graphite carbons', *Applied Surface Sciences*, Vol. 44, p221-233

Zaidi, H, & Robert, F & Paulmier, D 1995, 'Influence of absorbed gases on the surface energy of graphite: Consequences on the friction behaviour', *Thin Solid Films*, Vol. 264, p46-51